Ministère de l'Enseignement Supérieur et de la Recherche Scientifique
Université Hassiba Benbouali de Chlef
Faculté de Technologie
Département d'Électrotechnique

THÈSE

Présentée pour l'obtention du diplôme de

DOCTORAT LMD

Filière : Électrotechnique

Spécialité : Reseaux Electriques et Haute Tension

Par

LAHOUEL MOHAMMED HABIB ALLAH

Thème :

MODÉLISATION ET SIMULATION D'UNE DÉCHARGE À BARRIÈRES DIÉLECTRIQUES DANS UN MÉLANGE GAZEUX À LA PRESSION ATMOSPHÉRIQUE

Soutenue le 24/11/2021, devant le jury composé de :

Mohammed BOUNADJA	MCA	Université Hassiba Ben bouali -Chlef-	Président
Djilali BENYOUCEF	Professeur	Université Hassiba Ben bouali -Chlef-	Rapporteur
Hocine TEBANI	MCA	Université Hassiba Ben bouali -Chlef-	Co-Rapporteur
Bachir BELMADANI	Professeur	Université Hassiba Ben bouali -Chlef-	Examinateur
Driss RAOUTI	MCA	Université de Saida	Examinateur
Mohamed MANKOUR	MCA	Université de Saida	Examinateur
Mohamed MOSTEFAOUI	MCA	Université Hassiba Ben bouali -Chlef-	Invité

In the name of Allah, the Beneficent, the Merciful

ACKNOWLEDGEMENTS

Although only one author's name appears on the cover of a thesis, it is important to note that such an endeavor is above all a collective effort. This is why I would like to thank directly and indirectly the people who have participated in the advancement and completion of this work.

First of all, I thank ALLAH for my life and for all the blessings I have experienced during my Ph.D., especially my intellectual and spiritual growth.

I would like to thank ***Pr. Djillali BENYOUCEF****, my thesis director for his guidance and encouragement, and patience throughout this thesis, without his support and knowledge this thesis would not have been completed, especially during some of the most challenging moments of the doctorate.*

Also, I would like to express my deepest gratitude to ***Dr. Houcine TEBANI****, my thesis co-director for his valuable help and advices, for pushing me to go beyond my comfort zone and self-impose limitations to complete my article.*

I extend my thanks to ***Dr. Mohammed Bounadja*** *MCA at CHLEF University for giving me the honor of chairing my jury for this thesis and for evaluating this work. My thanks also go to* ***Pr. Bachir BELMADANI****, professor at the University of CHELF for showing great interest in the subject by accepting to be members of the jury I would also like to thank the rest of my committee:*

Also, we thank the other members of the jury ***Dr. Dris RAOUTI*** *and* ***Dr. Mohamed MANKOUR,*** *MCA at the University of SAIDA for the relevance of their wise remarks, which will allow the improvement of the quality of the manuscript and the development towards new perspectives.*

I would also like to thank ***Dr. Mohamed MESTEFAOUI****, MCB at the University of CHLEF, for participating in the jury for this thesis, for his experimental skills, his advice and his fruitful discussions.*

In addition, I feel deeply grateful to my senior lab mate, ***Dr. Abdelatif GADOUM****, who helped and guided me during my first years.*

Last but not the least, I would like to thank my family members, especially my wife, for her unlimited support and love. Million thanks to my father, without his encouragement, I would not have finished this degree, to my mother, my brothers, Hichem and Abdallah and all my five sisters for their support and encouragement to pursue this degree.

اليك أبي . . . إليك أمي

فضلكم يا والدي عمني حتى اللجم

كل هم قد أصابني زادكم بالطبع هم

إن كل ما جنيت من جهودكم نجم

أبي يا خير عون كنت لي عند المحن

أمي يا من تملكين جنة تحت القدم

كل ألفاظ لساني كل شكر قد رهن

اجمعوا كل المعاني من عراب او عجم

Abstract

The subject of this thesis is in the field of electric discharge at atmospheric pressure, especially dielectric barrier discharges in a gas mixture, and also the characteristics of this type of discharge. The mixture chosen is oxygen and nitrogen; these two gases represent approximately 99% of the air.

The discharge in this mixture allow to produce ozone, where the Ozone is a powerful disinfecting and oxidizing agent, and for this reason, it is used in a wide range of applications such as treatment of municipal and wastewater, food processing, fire restoration, restoration of buildings and other objects after floods, etc. When ozone exposed to organic compounds or bacteria, the extra atom of oxygen destroys the contaminant by oxidation. Thus, ozone will neutralize virtually all organic odors, specifically those containing carbons as their base element. This will include all bacteria as well as smoke, decay and cooking odors.

To facilitate the understanding of this work research work, we devised the manuscript in five chapters;

The first chapter gave the description of the context which is accompanied by information on the main mechanisms of discharges in a gas, as well as a summary of current knowledge on the generation of ozone by non-thermal plasmas.

In the second chapter we in details the determination and validation of the basic data, which will be inserted in the model for the dielectric barrier discharge simulation.

Third and fourth chapters are devoted to the development of the dielectric barrier discharge models in nitrogen and oxygen respectively, and also the simulation results.

Finally, the model proposed in the last chapter is the main objective of this thesis, which is a modeling of dielectric barrier discharge in gas mixture at atmospheric pressure (dry air 20% oxygen and 80% nitrogen) with a parametric study.

The results of this thesis are shown in the form of curves. These results are clear and satisfactory to justify the validity and reliability of the dielectric barrier discharge model used in this thesis. This method makes it possible to obtain a large amount of operating information and parametric study.

الملخص

موضوع هذه الأطروحة هو في مجال التفريغ الكهربائي عند الضغط الجوي ، وخاصة التفريغ الكهربائي في وجود عازل كهربائي في خليط الغاز ، وكذلك خصائص هذا النوع من التفريغ. الخليط المختار هو الأكسجين والنيتروجين. يمثل هذان الغازان حوالي 99٪ تركيب من الهواء من الغازات .

يسمح التفريغ في هذا الخليط الغازيال بإنتاج الأوزون ، حيث يعتبر الأوزون عامل تطهير وأكسدة قوي ، ولهذا السبب ، يتم استخدامه في مجموعة واسعة من التطبيقات مثل معالجة مياه الصرف الصحي ، وتجهيز الأغذية ، واستعادة الحرائق ، والترميم من المباني والأشياء الأخرى بعد الفيضانات ، وما إلى ذلك. عندما يتعرض الأوزون لمركبات عضوية أو بكتيريا ، فإن ذرة الأكسجين الزائدة تدمر الملوثات عن طريق الأكسدة. وبالتالي ، فإن الأوزون سيعادل فعليًا جميع الروائح العضوية ، خاصة تلك التي تحتوي على الكربون كعنصر أساسي لها. و يشمل ذلك جميع البكتيريا بالإضافة إلى الدخان والتسوس ورائحة الطهي.

لتسهيل فهم هذا العمل البحثي ، قمنا بتجزئة المخطوطة إلى خمسة فصول ؛

الفصل الأول يقدم وصفًا للسياق مصحوبًا بمعلومات عن الآليات الرئيسية للتصريفات في الغاز ، بالإضافة إلى ملخص للمعرفة الحالية حول توليد الأوزون بالبلازما غير الحرارية.

في الفصل الثاني قمنا بالتفصيل في تحديد والتحقق من صحة البيانات الأساسية ، والتي سيتم إدراجها في النموذج لمحاكاة التفريغ الكهربائي في وجود عازل كهربائي.

تم تخصيص الفصلين الثالث والرابع لتطوير نماذج التفريغ الكهربائي في وجود عازل كهربائي في النيتروجين والأكسجين على التوالي ، وكذلك نتائج المحاكاة.

أخيرًا ، النموذج المقترح في الفصل الأخير هو الهدف الرئيسي لهذه الأطروحة ، وهو نمذجة تصريف الحاجز العازل في خليط الغاز عند الضغط الجوي (الهواء الجاف 20٪ أكسجين و 80٪ نيتروجين) مع دراسة بارامترية.

تظهر نتائج هذه الأطروحة في شكل منحنيات. هذه النتائج واضحة ومرضية لتبرير صحة وموثوقية نموذج تفريغ الحاجز العازل المستخدم في هذه الأطروحة. تتيح هذه الطريقة الحصول على كمية كبيرة من معلومات التشغيل والدراسة البارامترية.

Table of contents:

Figures list

Table's list

General Introduction

General Introduction

In the last years, plasma takes a place in lot of scientific domains as industry, medical therapy and electronic components production. Creation of plasma take the attention of scientific society for optimize their parameters and reactors to get the perfect ignition point. Plasma experiences have an expensive cost; therefore, it is indispensable to use information systems for modeling because of their quick development and high preferment with a short time of simulation. Cold Plasma at atmospheric technology already used in many industrial applications such as surface treatment and air pollutant removal.

The pollution in drinking water and air cause serious health problems such diarrhea, cholera, dysentery, typhoid, and polio. Even Viruses that transmitted through the air contaminates drinking water, is estimated to cause 485 000 diarrheal deaths each year (Organisation, 2019). Therefore, it is important to make a way to avoid disease transmission by air or water. The scientific society takes place of this subject in research as sterilization and disinfection of air and water by ozone. Ozone is gas neutrally exist in the air, and its can be generated industrially by a various method, because of high effectiveness to eliminate virus and bacteria and other numerous advantages, used for water and air treatment (sterilization and disinfection).

Ozone is a powerful disinfecting and oxidizing agent, and for this reason, it is used in a wide range of applications such as treatment of municipal and wastewater, food processing, fire restoration, restoration of buildings and other objects after floods, etc. When ozone exposed to organic compounds or bacteria, the extra atom of oxygen destroys the contaminant by oxidation. Thus, ozone will neutralize virtually all organic odors, specifically those containing carbons as their base element. This will include all bacteria as well as smoke, decay and cooking odors. However, due its oxidizing nature ozone attacks and degrades, is usually generated in one of three ways:

- Electrochemical generation: an electric current pass through the liquid electrolyte and produces gases, containing ozone.
- Generation of ozone by ultraviolet rays.
- Generation of ozone in non-thermal plasma (electrical discharges) (Pekárek, 2003).

Most of the ozone for practical applications is produced in non-thermal plasma generated by electrical discharges specifically by a dielectric barrier discharge DBD reactors, because it is most ecological and economical method. DBDs at atmospheric pressure produced by applied

voltage at low frequency in gaseous gaps on the order of a few millimeters are mainly constituted of unstably triggered non-equilibrium transient plasma filaments. Dielectric presence prevents the formation of the arc that located in one place and causes an augmentation of temperature. A DBD is made up of a multitude of micro-discharges being established perpendicular to the electrodes, that means, the scientific researches should be directed firstly, to gain a better understanding of interactions between plasma filaments. Secondly is to control the energy of each micro discharge and localize it.

Siemens reported first experimental investigations on DBD in 1857. They based on the generation of ozone. This was achieved by subjecting a flow of oxygen or air to the influence of a dielectric-barrier discharge (DBD) maintained in a narrow annular gap between two coaxial glass tubes by an alternating electric field of sufficient amplitude. An important step in characterizing the discharge was made by the electrical engineer K. Buss, who found out that breakdown of atmospheric-pressure air between planar parallel electrodes covered by dielectrics, which always occurs in a large number of tiny short-lived current filaments. Extensive research activities employing modern diagnostic and modeling tools started around 1970, originally aimed at a better understanding of the plasma physical and plasma chemical processes in ozonizers. These research efforts resulted not only in improved ozone generators, but also in a number of additional applications of dielectric-barrier discharges: surface modification, plasma chemical vapor deposition, pollution control, excitation of CO_2 lasers and excimer lamps and, flat plasma display panels used in televisions.

The objective of the work carried out in our thesis is to simulate a dielectric barrier discharge (DBD) at atmospheric pressure in the Nitrogen/Oxygen (N_2/O_2) gas mixture. The thesis will be presented as follows:

In the first chapter, the description of the context will be accompanied by information on the main mechanisms of discharges in a gas, as well as a summary of current knowledge in the generation of ozone by non-thermal plasmas.

The second chapter will be devoted to the determination and validation of the basic data, which will be inserted in the model for the dielectric barrier discharge simulation.

The development of the simulation model of nitrogen DBD and oxygen DBD will be the objective of the third and the fourth chapter respectively.

The model proposed in the last chapter is the main objective of this thesis, which is a modeling a DBD in gas mixture at atmospheric pressure with a parametric study.

Bibliography:

Organisation, W. H. (2019, june 14). *world health organisation.* Récupéré sur Drinking Water: https://www.who.int/news-room/fact-sheets/detail/drinking-water

Pekárek, S. (2003). Non-Thermal Plasma Ozone Generation. *Acta Polytechnica Vol. 43 No. 6*.

Chapter I :

Discharge mechanisms in gases and dielectric barrier discharges

1. Introduction

Non-thermal plasmas are generated by electrical discharges. The voltage source can be DC, pulse or AC. Ions and electrons are accelerated under the influence of the electric field, and collide with other species of gas. The chemical changes created by these collisions in a discharge are more or less important depending on the energies associated with them.

This chapter devoted to the state of art aims to introduce the essential concepts allowing an understanding of the discharge phenomena occurring in the gas of a DBD device. It begins by explaining the different discharge regimes that can develop in a gas. A classification of plasma, according to the temperature of gas also proposed. Then, we explain the specific elements of Dielectric Barrier Discharges (DBDs); also, we explain the fundamental concepts of dielectric barrier discharges, their different possible physical configurations and their most common applications. Moreover, what are the fields of application in which this device is suitable. Some applications of DBDs presented in this chapter, as ozone generation, which used in disinfection and sterilization of air and water.

2. Electrical discharges gases

2.1. Plasma and ionized gases

If we take an element of matter in its solid state and start heating it, we will find that, this element gradually passes from its liquid state, then to the gaseous state, then to plasma. For this reason, plasma is often referred to as "the fourth state of matter" (A.M. POINTU, 2007). Experimenting with the transformation between these four states is very difficult, if not impossible, because of the enormous difference in temperature required to pass from the solid state to plasma. As a result, practically, plasmas are generated from a gas, subjecting it to an electric shock (discharge plasmas) or a magnetic field (RF plasmas). In this thesis, we only consider the discharge plasmas. Langmuir, in his works initiated in the twenties to develop valves that allowed the passage of high currents, introduced in 1929 the word plasma to describe ionized gases. Everything seems to indicate that 99% of the visible matter of Universe is in plasma state. He described the plasma he observed as follows: “Except near the electrodes, where there are sheaths containing very few electrons, the ionized gas contains ions and electrons in about equal numbers so that the resultant space charge is very small. We shall use the name plasma to describe this region containing balanced charges of ions and electrons. (Langmuir, 1928). So, plasma is an ionized gas substance becomes highly electrically conductive to the point that long-range electric and magnetic fields dominate the behavior of the matter

(Chen, 1984) (Freidberg, 2008). Most of matter in the visible Universe is in a plasma state; unlike other states of matter, plasma is rare on the Earth's surface under normal conditions, and is mostly artificially generated from neutral gases. The ionization rate τ_i represents the ratio of the number of free electrons n_e divided by the number of total particles $n_e + N$, N is the number of neutral particles per unit volume. The ionization rate is given by the relation:

$$\tau_i = \frac{n_e}{n_e + N} \tag{I-1}$$

Through ionization rate τ_i, we can classify plasmas in two main categories: thermal and cold plasmas (Kogelschatz, Silent discharges for the generation of ultraviolet and vacuum, 1990).

- If $\tau_i < 10^{-3} \rightarrow 10^{-4}$ is defined as a non equilibrium cold plasma out of
- If $\tau_i > 10^{-3} \rightarrow 10^{-4}$ is defined as a thermal plasma in thermodynamic equilibrium.

2.2. Thermal classification of plasma

Within the plasma, there is not always thermodynamic equilibrium between species, but a stationary state in which each species of particle has an energy characterized by a temperature T_j. Heavy species have average kinetic energies comparable to each other and represented by the macroscopic temperature T_g. On the other hand, the energy of the electrons (represented by T_e) can be much higher (Hammami, 2008). From the diagram, we can distinguish two main types of plasma: thermal plasma at high pressure and nonequilibrium cold plasma at low temperature.

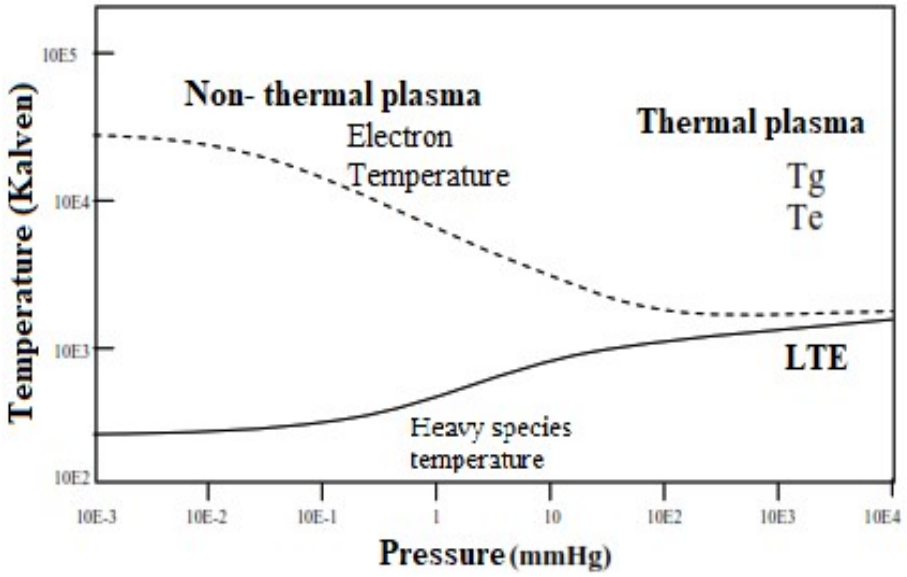

Fig. I-1: Evolution of the temperature as a function of the pressure of heavy species (Tg) and electrons (Te) (D, 1999.)

2.2.1. Thermal plasmas:

They are defined at high pressures (P≥1atm). They are characterized by a local thermodynamic equilibrium (LTE) achieved between electrons and heavy species ($T_e \approx T_g \approx 10^4\ K$). Plasma torches and electric arc usually generate this type of plasma. However, thermal plasmas have drawbacks such as:

- The need to use expensive refractory materials resistant to the working temperature range.
- Quick wear of the arc plasma electrodes.
- The complexity and cost of the installations.

Arc discharge is a high-power thermal discharge of very high temperature (~10,000 K). It can be generated using various power supplies. It is commonly used in metallurgical processes

2.2.2. Non-thermal plasmas:

These plasmas characterized by their state out of thermodynamic equilibrium. The temperature of the gas T_g is in this case close to room temperature, while that of the electrons (up to 10^4K) is sufficient to allow a high rate of inelastic collisions. Most of the injected energy is then converted into chemical reactivity, not thermal energy. In most cases, especially due to economic considerations, a plasma process must be non-thermal. This plasma should be directly produced in the gas to be treated. Artificially discharges can be divided into two types, low-pressure discharges and atmospheric pressure discharges.

Glow discharge plasmas: "These are the non-thermal plasmas generated by DC or low frequency RF (<100 kHz) electric field, in the gap between two metal electrodes. This type of plasmas can be mostly generated within fluorescent light tubes" (Stern, 2010).

Capacitively coupled plasma (CCP): "Capacitively coupled plasmas are generated with high frequency RF electric fields, typically 13.56 MHz. These differ from glow discharges in that the sheaths are much less intense. These are widely used in the microfabrication and integrated circuit manufacturing industries for plasma etching, and plasma enhanced chemical vapor deposition" (Plasma (physics), 2021) (Sobolewski & Langan & Felker, 1997).

Inductively coupled plasma (ICP): Inductively coupled plasmas are similar to CCP but the electrode consists of a coil wrapped around the discharge volume that inductively excites the plasma (Plasma (physics), 2021).

Wave heated plasma: are similar to capacitively coupled and inductively coupled plasmas. Wave heated plasmas are heated by both electrostatic and electromagnetic filed (Plasma (physics), 2021).

Corona discharge: Corona discharge is a non-thermal discharge generated by the application of high voltage to sharp electrode tips. It is commonly used in ozone generators and particle precipitators.

Capacitive discharge: Capacitive discharge is a non-thermal plasma generated by the application of RF power to a powered electrode, with a grounded electrode held at a small separation distance in the order of 1 cm. Such discharges are commonly stabilized using a noble gas such as helium or argon. The following organigram classified the above definitions.

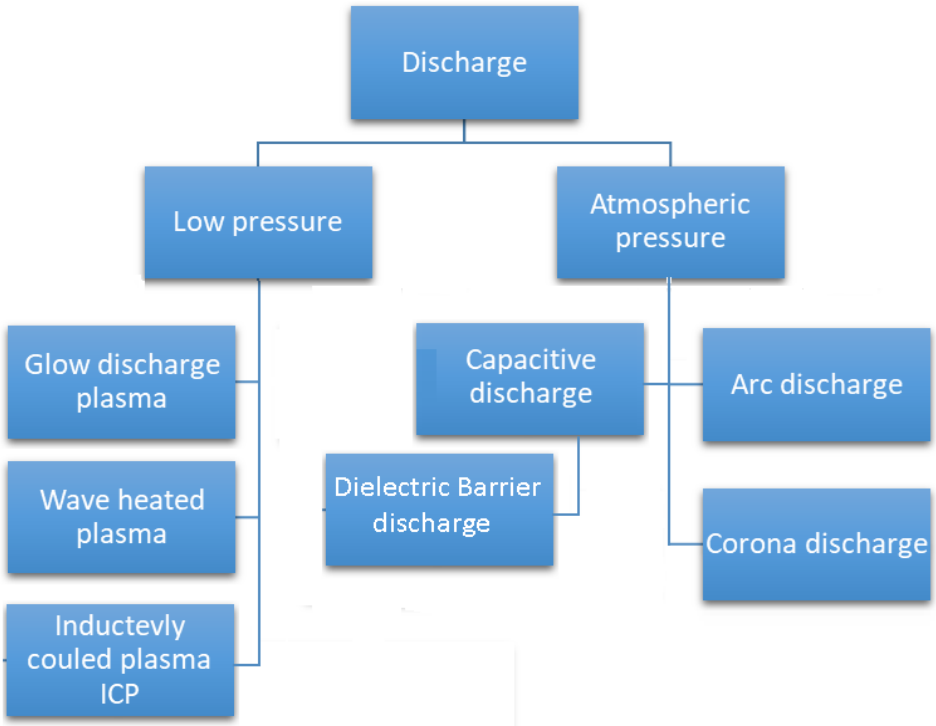

Fig. I-2: Organigram of the classification of discharge

2.3. Discharge Mechanisms at low pressure:

This section exposes the mechanism and Basic aspects of discharges, to understand the operation of the plasma flow controller generated by gas discharge.

A gas subjected under electric discharge, can be in different operating regimes. S. Flügge consider the case where the electrodes are parallel metal plates; thus, he obtains the complete "supply-discharge" system illustrated in Figure 0-1 (S. Flügge, 1956). He measures, the applied voltage between the electrodes V and currant discharge I. First investigations on discharges in

gases were mainly concentrated in low-pressure discharge tubes. Unlike them, plasma controllers are devices that work with alternating current, AC, and in a range of frequencies between 50Hz and 30 kHz, with an inhomogeneous and at least two-dimensional electric field. This implies more complexity in the corresponding download mechanisms and therefore does not allow an exact definition of the properties of the download. Despite this difference, some aspects of the direct current case DC discharge mechanism can also be used for a description of the fundamental aspects of the AC case (Roth R. G., 1998).

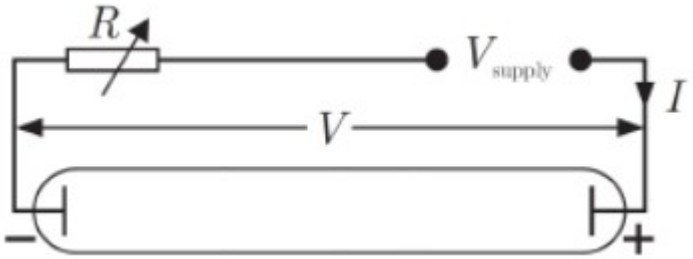

Fig. I-3: Discharge tube (S. Flügge, 1956)

The increase in voltage between the two electrodes in a low-pressure discharge tube leads to a non-linear voltage-current relationship, as it's described in figure I-4. There are three types of discharge regimes: Dark Discharge, Glow Discharge and Arc Discharges (Thornhill, 2007).

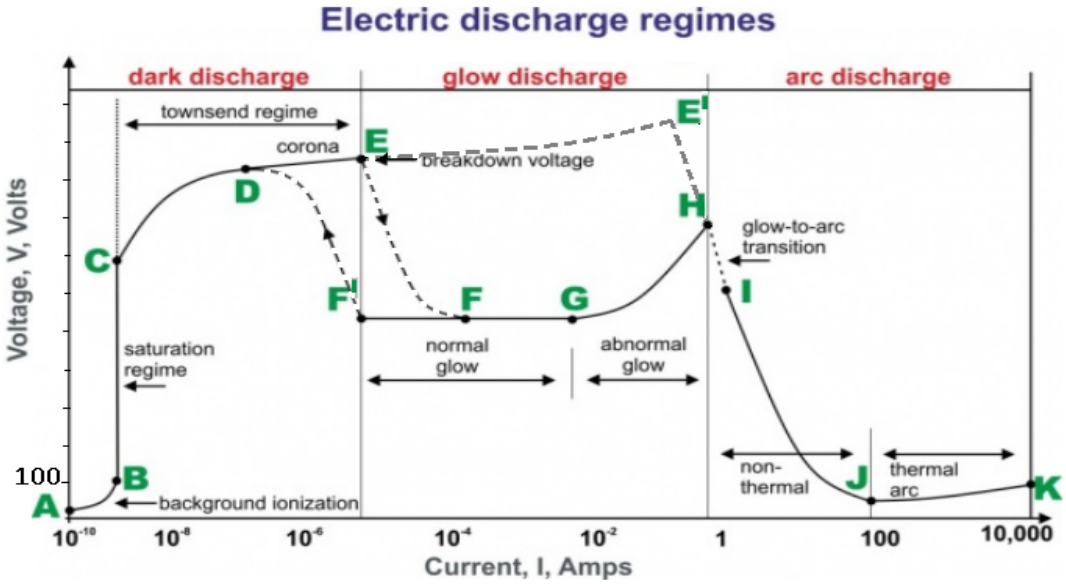

Fig. I-4: voltage-current characteristics (Sozer, 2008)

A. Dark discharge:

The invisibility of this discharge regime to naked eyes is the reason to named it dark discharge.

Background ionization: If we adjust the output voltage V_{supply} at a very low value above 0 V, the anode collects the free electrons that are present in the atmosphere; these are produced by cosmic radiation. A weak current produced in the discharge; this current increases with the increase in the applied voltage. This is zone **A-B** of the static characteristic in figure I-4

Saturation regime: If we continue to gradually, increase the applied voltage V_{supply} at some point all free electrons and ions will disappear, collected by the anode and cathode respectively. If the applied electric field V_{supply}/d is not sufficient to ionize the gas, the current depends only on the ability of cosmic radiation to ionize the gas. This produces a certain number of electrons (or ions) in the discharge volume per unit of time; As a result, the current will be constant for all voltage values.

Townsend discharge: If the applied electric field increase, the electrons circulate with a higher energy (higher speed at the moment of impact at the anode). If this energy is sufficient, the electrons that collide with the neutral species of the gas produce additional electrons; these electrons increase electric field, which in turn accelerates the electrons even more thus generating an electronic multiplication process called electronic avalanche figure I-5. As shown in Fig. the current increases exponentially with the voltage applied in this zone **C-D.**

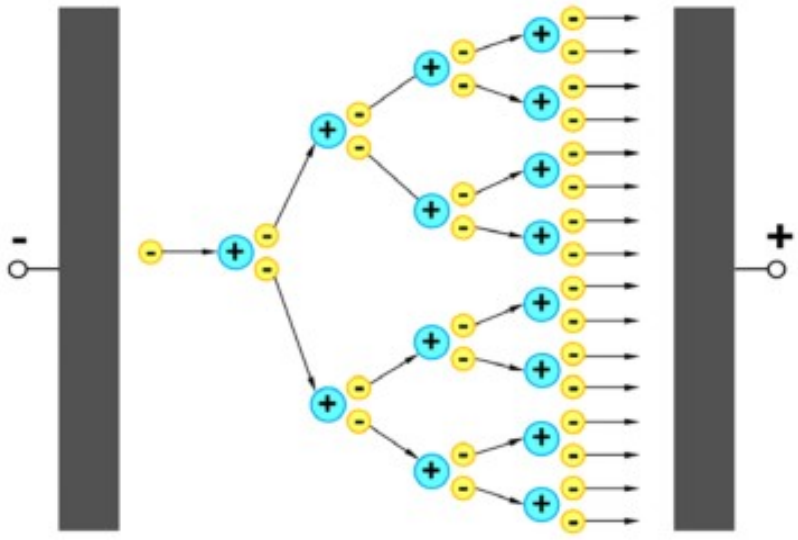

Fig. I-5: Concept of electronic avalanche

B. Glow discharge:

If the electric field get increase further more and becomes sufficiently strong, the cathode, due to the bombardment of the positive ions, emits secondary electrons. These secondary electrons increase the current and drop the voltage across the gas, causing a discontinuous transition

between the Townsend regime and the luminescent regime. This is region **E-D** in the static characteristic of the discharge (figure I-4). The voltage corresponding to the breakdown electric field is called “breakdown voltage” or “disruptive potential” V_{bd}; according to the "Paschen law", it depends only on the multiplication between the gas pressure p_{gas} and inter-electrode distance d_{disch}.

$$V_{bd} = C.p_{gas}.d_{disch} \Big/ \ln\left[A.p_{gas}.d_{disch} \Big/ \ln\left[1+\frac{1}{\gamma}\right]\right] \quad \text{(I-2)}$$

In equation (I.2), **A** and **C** are constants specific to each gas, γ is the secondary electron emission coefficient, which represents the ratio between the number of secondary electrons emitted by the cathode and the sum of the ions and photons that strike it, this coefficient depends on the material of the cathode.

Normal glow: Once the breakdown voltage is reached at point **E**, an electrical break occurs followed by a discontinuous transition from **E** to **F** to the glow discharge regime. The large potential difference between the electrodes drops due to the significant increase in the current flow, and therefore the plasma becomes visible. After reaching point **F**, the gas enters the normal glow/luminescent region, in which the voltage is almost independent of the current over several orders of magnitude in the discharge current and current increases. The electrode current density is independent of total current in this regime. This means that the plasma is in contact with only a small part of the cathode surface at low currents. As the current is increased from **F** to **G**, the fraction of the cathode occupied by the plasma increases, until plasma covers the entire cathode surface at point **G**.

Abnormal glow: In the abnormal glow regime above point **G**, the voltage increases significantly with the increasing total current in order to force the cathode current density above its natural value and provide the desired current, because once the cathode is completely covered, a considerably high voltage rise is needed to achieve an abnormally high current density (this is achieved in electrodes heated in succession and in an incandescent cathode at point **H**). Go on from **C** and moving to the left to lower currents, a form of hysteresis-cycle is observed in the voltage-current characteristic curve. The discharge maintains itself at considerably lower currents and current densities than at point **F** and only then makes a transition back to Townsend regime; it means, the luminescent discharge is maintained below **F**, once it has been established. At point **F’** the transition back to the Townsend regime occurs without going through the Townsend discharge or crown again.

C. Arc discharge:

Glow to arc transition: The electrodes at point H become sufficiently hot that the cathode emits electrons thermionically. In consequence, if the DC power supply has a sufficiently low internal resistance, the discharge will undergo a glow-to-arc transition (H-I).

Non- thermal arc: The transition is followed by a regime of non-thermal arcs (I-J). Where the voltage required for the discharge decays rapidly due to the additional loads of the thermionic emission. The arc regime, from I through K is one where the discharge voltage decreases as the current increases, until large currents are achieved at point J, and after that, the voltage increases slowly as the current increases.

Thermal arc: Since this influence grows with the heating of the electrons, the effect corresponds to a characteristic negative resistance. Beyond the local voltage minimum at point J, the voltage-intensity curve again reaches the thermal arc regime (**J-K**) towards thermal equilibrium at point **K**.

2.4. Paschen Law:

Paschen's law is an equation that gives the breakdown voltage, that is, the voltage necessary to start a discharge or electric arc, between two electrodes in a gas as a function of pressure and gap length. (Wadhwa, 2007). According to this law, the breakdown voltage, for a given gas, depends only on the multiplication between the pressure (p) and the inter-electrode space (d), $V_{bd} = f(p \times d)$. Fig. show the representation of the breakdown voltage as a function of the value $p \times d$ for different gas, commonly called the "Paschen curve".

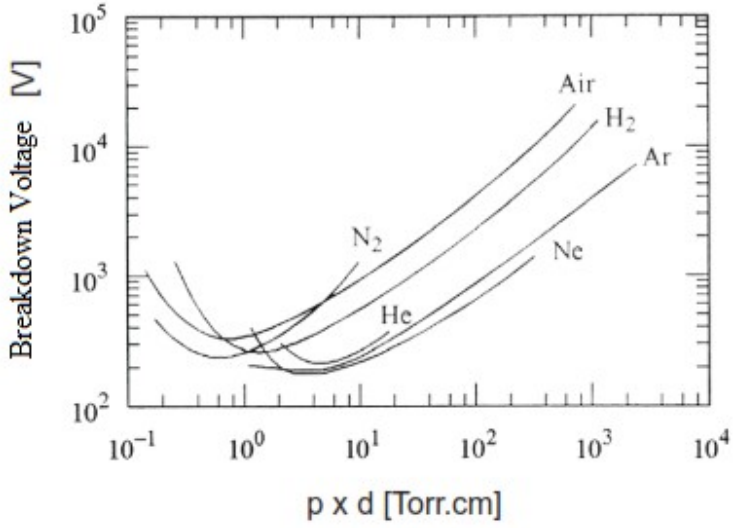

Fig. I-6 :Paschen curves for breakdowns in air, N2, H2, He, Ne, Ar (Thome, 1967)

2.5. Discharge Mechanisms at atmospheric pressure:

Most of the discharges at atmospheric pressure (corona, arc) are initiated by a "streamer" breakdown. In the air, when the value "inter-electrode distance×pressure" becomes greater than 1000 Torr. cm we can expect a "streamer" breakdown. Too much over-voltage also results in "streamer" type breakdown.

The curve in figure I-7 shows a limit between these two types of breakdown in air as a function of the applied over-voltage percentage and of the value p × d (Torr.cm).

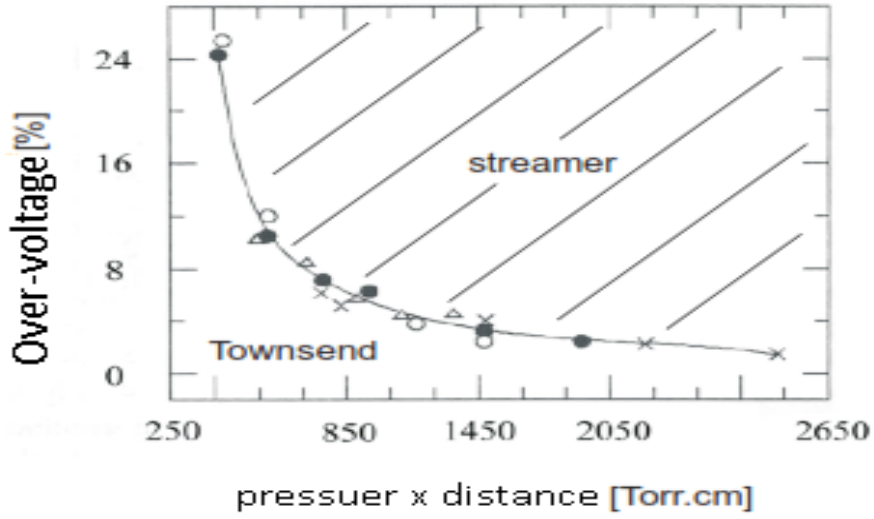

Fig. I-7: Curve separating a Townsend breakdown from a streamer breakdown

When gas at atmospheric pressure is under a sufficiently intense electric field, ionization occurs by collisions between electrons and neutral molecules. New electrons are produced from these collisions and lead to a Townsend avalanche-type process (Y. H. Choi, 2006).

At atmospheric pressure, the luminescent discharges are abnormal (filamentary), Micro-discharges and streamers which are plasma channels from a few mm to hundreds of mm in diameter. Certain fundamental processes, in particular when the field is very divergent, are established over very short time intervals of the order of ms or even ns.

Another fundamental deference with a Townsend breakdown is the fact that the resulting electron avalanche is so strong, it causes an exceeding of the critical number of free electrons in the electrode gap. The critical number refers to the upper limit of free electrons, beyond which a space charge is induced that distorts the local electric field (Craggs, 1953). What then happens is the following:

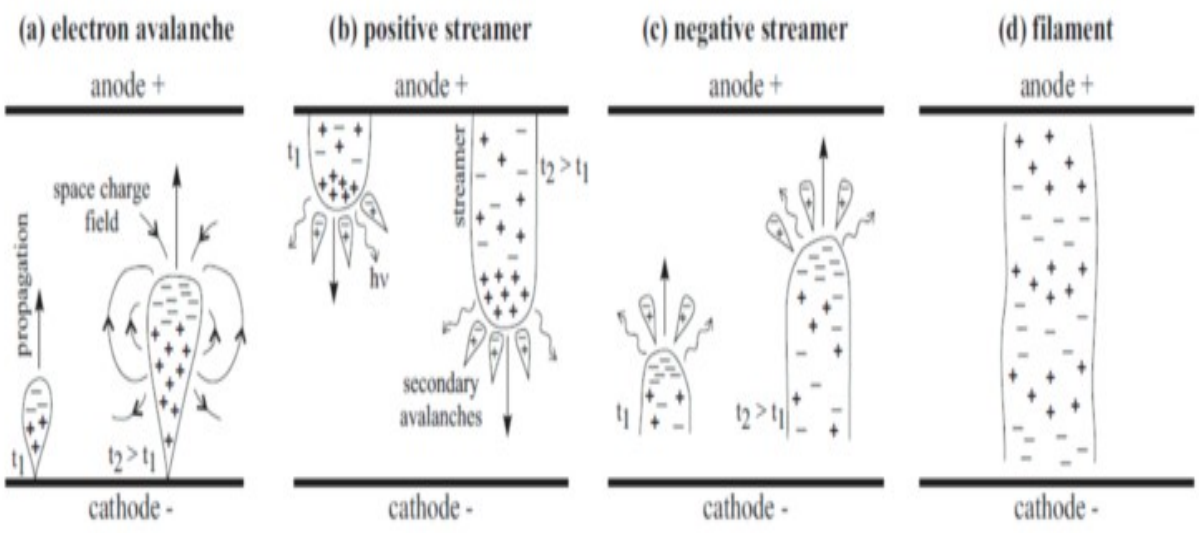

Fig. I-8: Formation of a streamer

a. Similarly, to the Townsend breakdown, an electron avalanche is formed initiated by free electrons, as illustrated in

b. . The electrons released by impact ionization accumulate at the front of the avalanche, polarizing the avalanche. The critical number of free electrons is exceeded and a local electric field, stronger than the applied electric field, is induced due to the accumulated space charge. This is an important aspect, as the local induced electric field ionizes the surrounding neutral particles, which facilitates growth and propagation of the streamer. This process is the formation of the streamer head.

c. For moderate gaps and voltages, the initial avalanche has reached the anode before the streamer head has been formed. The electrons are absorbed by the anode, leaving a cloud of positively charged ions behind, which then forms the streamer head. This induces a positive local electric field. Secondary avalanches are initiated by photoionization, which feed the required electrons. The transported electrons again leave behind positive ions, and the streamer propagates towards the cathode. A current has formed inside the streamer, feeding electrons collected at the streamer head towards the anode. This is called a positive streamer, corresponding to the charge of the streamer head.

d. For large gaps and high voltages, the initial avalanche has not reached the anode yet, but exceeds the critical number of free electrons in the electrode gap. Similarly, though, a streamer head is formed consisting of accumulated particles, this time the negatively charged electrons. The streamer head propagates towards the anode, while an electron current is induced by the idle positive ions, following the streamer head and feeding the streamer. This is called a negative streamer.

e. Regardless of the direction, a significant amount of charged particles is transported resulting in a discharge current. The streamer is characterized by its slim, filament shape between the electrodes. This type of discharge is therefore also called filamentary discharge.

2.6. Cold Plasma reactors:

We will present here the discharges and the reactors used to produce cold plasma at atmospheric pressure. We will be particularly interested in applications aimed at sterilization and decontamination of water treatments. For this category of treatments can be used reactors which are using Corona, DBD or GlidArc electrical discharges which are supplied in direct current, alternative current having the industrial frequency or pulsed current. The main requirement of this category of treatments is that the cold plasma action desired to be as intense as possible so the time treatment to be as short as possible. This demand of the treatments has placed as the first option the GlidArc discharges, characterized by high values of the specific energy and also high values (up to 3 kW) of the discharge useful power for each module.

2.6.1. Gliding arc discharge reactor:

Mehrnaz Gharagozalian on 2017 studied the gliding arc (G Arc) plasma treatment reactor. They reported that G Arc plasma was very efficient to decontaminate wastewater. The schematic diagram of a GlidArc reactor is shown in

Fig. Figure I-9 and is emphasizes two metallic electrodes having a divergent shape, 1, place inside an electro-insulating enclosure 2, shaped like a cylinder or like parallelepiped, the gas nozzle,3, and the discharge, 4. The discharge is igniting in the smallest gap between the two electrodes when they are connected to a high voltage power supply, HV. After the ignition the discharge is gliding along the electrodes and vanish, which allow the cycle resumption with the ignition of another discharge.

The gas can be air, oxygen, nitrogen or inert gas and is assuring deionization phenomena, which allow the maintaining of the cold plasma character for the electrical discharge, and by choosing in a right mode the optimum gas allows even the adaptation of the intended treatments.

The GlidArc reactors are benefiting also by the command and the control possibility of the discharge useful power by using an auxiliary discharge between two auxiliary electrodes conveniently placed; this auxiliary discharge allows the adaptation of this sort of reactors to different working conditions imposed by the treatment.

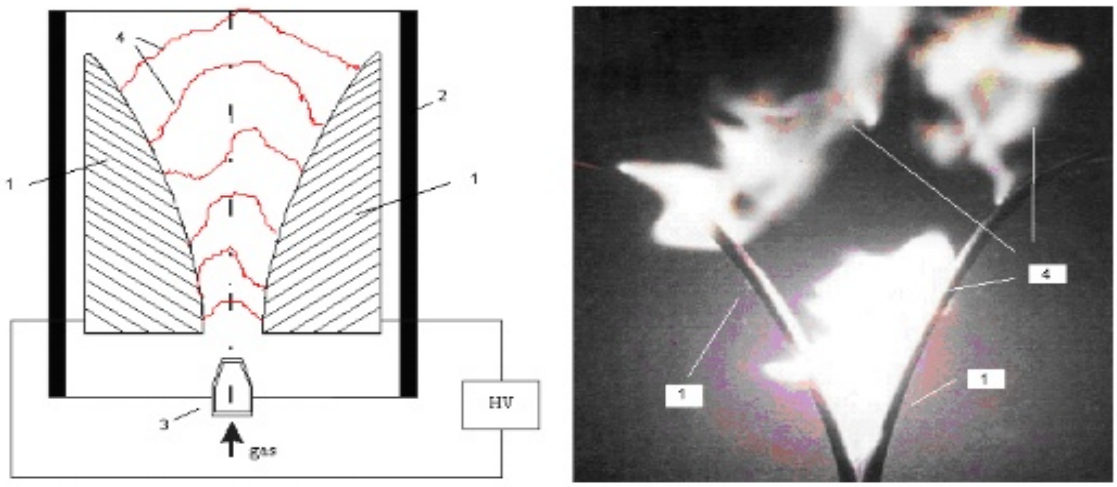

Fig. I-9: Schematic diagram and photo of a DC GlidArc reactor.

2.6.2. Dielectric barrier discharge:

Dielectric barrier discharge is a non-thermal or non-equilibrium plasma and can be generated at atmospheric pressure (Abdul SYAKUR Badrus ZAMAN, 2017). It is known that the typical DBD plasma is generated between two electrodes (plate type and coaxial cylinder type). Dielectric barrier is generally quartz glass, ceramics or Teflon and so on.

There are also some specially configured DBD devices, such as sliding discharge and asymmetric surface DBD, DBD with the dielectric is perforated, micro cavity plasma devices, Resistive Barrier Discharge (RBD) with a highly resistive sheet (Ronny, 2017). When DBD plasma is applied in water treatment, a large number of active species are emerged.

2.6.3. Other representative types of discharge reactors:

Other types of discharge reactors were also designed in recent years for waste water treatment. Selma Mededovic Thagard et al. (Mededovic Thagard Selma, 2017) evaluated plasma-based water treatment for the Treating 23 types of environmental contaminants by enhanced-contact reactor in argon bubbling (Fig. I-10 a). The multiple mobile iron (Fe) based electrodes reactor (Fig. I-10 b) (Meirovich Ariel, 2016), discharge propagating in a bubble in water reactor (Fig. I-10 c) (Iwabuchi Masashi, 2016), and gas-phase pulsed corona discharge reactor (Fig. I-10 d) (Ajo Petri, 2015) were also using in the waste water treatments. All these plasma devices could produce sufficient species, such as H_2O_2, OH, ultraviolet radiations, atomic nitrogen, and atomic oxygen which are efficient for decomposing waste water.

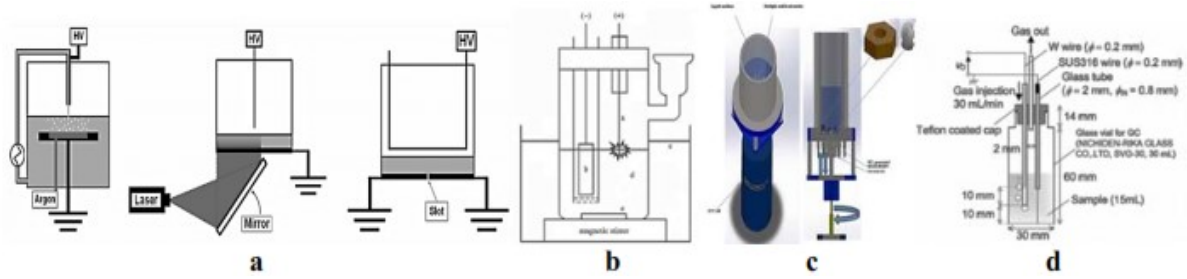

Fig. I-10 : Diagrammatic sketches of other types of discharge reactors. A: enhanced-contact reactor. B: multiple mobile iron (Fe) based electrodes reactor. C: bubble spread reactor. D: gas phase pulsed corona discharge reactor

3. How to avoid the transition to arc at atmospheric pressure:

The main drawback of plasmas at atmospheric pressure is the transition to arc. When applying a potential difference between two metal electrodes, a very localized plasma is obtained which quickly tends towards thermodynamic equilibrium. We are then in the presence of an electric arc, whose temperature can exceed 20,000 K (Reynard, 2006), which can lead to the destruction of the material. However, there are solutions to avoid the transition to the arc and keep the temperature of the electric discharge close to room temperature. In the following paragraphs, we will describe the main solutions

3.1. Decrease the value $p \times d$:

For values of the value $p \times d$ lower than a few tens of Torr.cm, generally the breakdown is of the Townsend type, which can lead to a homogeneous discharge of large radius (Raizer, 1991). Thus, at atmospheric pressure, reducing the inter-electrode distance can help prevent the transition to the arc. This is the technique used in the case of Micro Hollow Cathode Discharges (MHCD), the diameter of which is typically around a hundred μm, which leads to a $p \times d$ value similar to those obtained at low pressure and therefore Townsend-type breakdown as conventionally observed at low pressure.

3.2. Using of corona effect:

The use of an electrode having a small radius makes it possible to obtain a non-homogeneous distribution of the electric field applied to the gas. Thus, depending on the amplitude of the applied voltage, the radius, and the distance between the electrodes, it is possible in this configuration to locate the discharge near the electrode of small radius of curvature, in the area where the electric field is greater than the gas rupture field. This prevents the formation of a

conductive channel between the two electrodes and therefore the transition to the arc. (Plasmas Froids : Génération, caractérisation et technologies., 2004).

3.3. Insertion of a dielectric barrier

The most robust and widely used solution to avoid the atmospheric pressure arc transition is to insert at least one solid dielectric between the two electrodes. We will speak of Dielectric Barrier Discharge (DBD) with large details in the next section.

4. Dielectric barrier discharge

4.1. Histories

The history of DBDs began in 1839 when Schönbein identified the odor appearing around the anode during the electrolysis of water, as the attribute of a new chemical compound, which he called ozone. (U. Kogelschatz, 1999). It was not until 1857 to arrive at the first known experiments on dielectric barrier discharges or barrier discharges (often referred to as silent discharges) carried out by Von Siemens; this one patented the ozonator device, the design of which has not fundamentally changed since.

The main applications were the production of ozone or nitrogen oxide. The system designed by this German engineer consisted of two concentric tubes (Fig. I-11) between which was injected a flow of oxygen. One electrode lined the inside of the inner tube while another covered the outside of the outer tube and the assembly was subjected to a high potential difference via a battery and a coil. The remarkable property of the discharges then produced in the space delimited by the two tubes, called silent discharges, was to produce a large quantity of ozone, whereas an arc discharge would have harmed the creation of this unstable molecule.

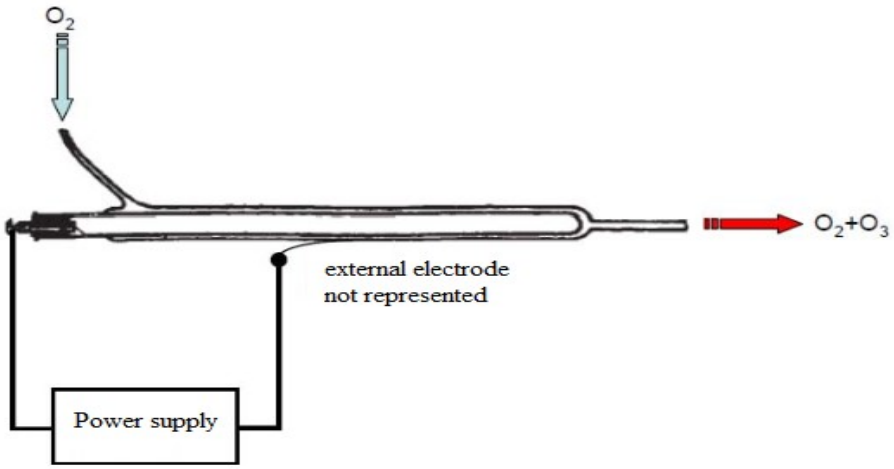

Fig. I-11: Discharge tube of Werner Von Siemens

In 1932, Buss described the filamentary nature of this discharge in the air through the first photographic device and oscilloscope measurements made on DBDs. In the seventies, the first simulations and research on DBDs made it possible to broaden the field of application of these discharges to surface treatments, to layer deposits, and later to lasers, flat screens, laser treatments. gaseous effluents ...

In 1988, Japanese researchers discovered the existence of a homogeneous DBD regime at atmospheric pressure (S. Kanazawa, 1988). Since then, much research has been carried out to understand the physical phenomena governing DBDs.

The establishment of a conductive channel between the two metal electrodes can lead to the formation of an arc. The electron density then increases to $10^{17}\ cm^{-3}$ (Raizer, 1991). If we want to avoid the passage to the arc, we can interpose at least one dielectric barrier between the metal electrodes. When the head has finished propagating, a conductive channel is established between the two electrodes. The current through the channel causes a buildup of charges on the dielectric. When the field induced by these charges screening the applied field, the discharge is extinguished.

The term dielectric barrier discharge (DBD) groups together the discharge configurations for which a current pass between two metal electrodes separated by a gas and by at least one dielectric layer. To carry any current other than the displacement current (current flowing through the capacitor) through the discharge space, the electric field must be strong enough to cause the gas breakdown. For high values of pressure (and inter-electrode distance), the increase in current between two metal electrodes generally results a transition to an arc regime, synonymous with high temperature plasma and damage to the surface.

Therefore, by definition, the role of the dielectric is to somehow constitute a capacitance in series with the gas space. Then its charge will limit the voltage applied to the gas, which helps prevent the transition to an arc. The accumulation of charges from the plasma on the solid dielectric cause a lead down of applied electric field and potential, leading to the discharge being extinguished.

4.2. Dielectric materials:

Insulators are substances, which permit very less current flow through them. Substance such as porcelain, wood are examples. Dielectrics are also insulators. But, more specifically, they are

materials which can be polarized. In dielectric materials, the electrons are bound to the nucleus and have limited movement. When an external voltage is applied to the dielectric, the nucleus of the atoms is attracted to the negative side and the electros are attracted to the positive side. This creates an internal electric field that reduces the overall field within the dielectric itself. If a dielectric is composed of weakly bonded molecules, those molecules not only become polarized, but also reorient so that their symmetry axes align to the field (Kao, 2004). The concept of polarizability is expressed through the magnitude: relative permittivity ε_r , also is called as dielectric constant (Fig. I-12).

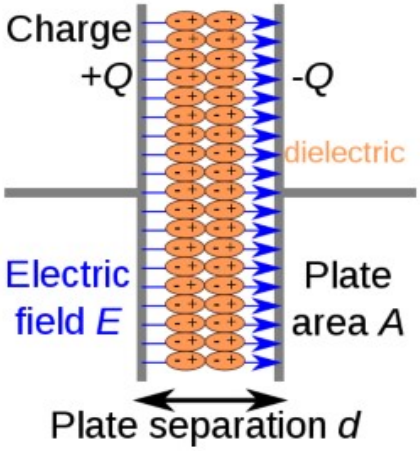

Fig. I-12: Capacitor schematic with dielectric (https://en.wikipedia.org/wiki/Dielectric, 2021)

Thus, a dielectric can be defined as an insulator that can be polarized. Therefore, all dielectrics are insulators, but all insulators are not dielectrics. This characteristic makes it very useful in the form of capacitors. Dielectrics are used to store the electric charges, while insulators are used to block the flow of electric charges (they more or less act like a wall).

4.3. Power supplies for DBD reactors:

Since the dielectric is an insulator, its dielectric constant and its thickness, in combination with the time derivative of the applied voltage dv/dt determines the displacement current that can pass through the dielectric. It does not pass direct current and DBD discharges are therefore necessarily requiring the use of alternating or pulsed voltage to operate (Kogelschatz U. , 2003).

4.3.1. Alternating voltage

Alternating power supplies allow frequency and voltage amplitude to be adjusted (Fig. I-13). Typically, with this power supply, the current flows in the gas only instantaneously, at times of gas breakdown (these are the peaks that can be observed on the current supplied).

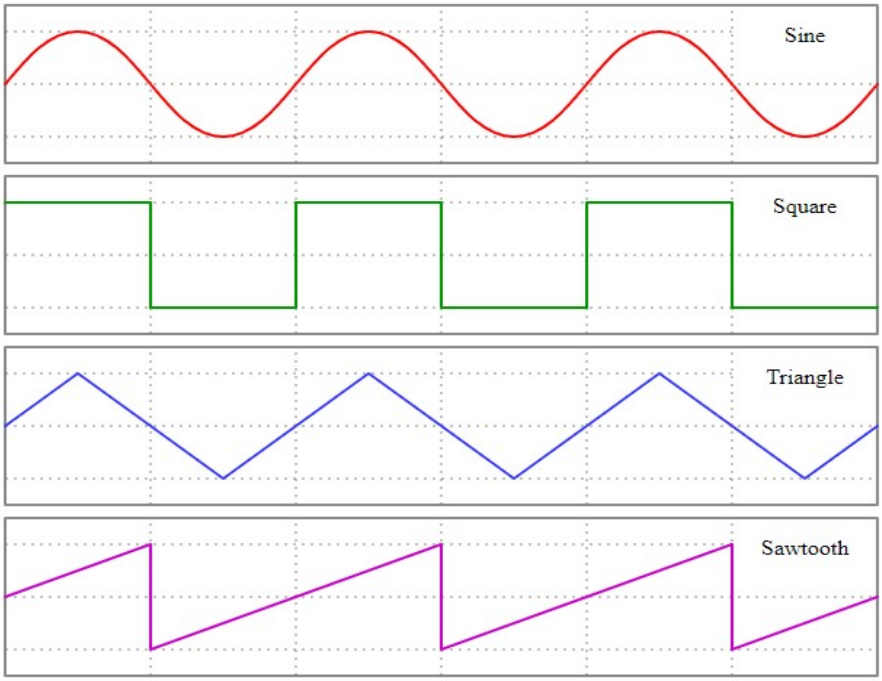

Fig I-13: Altering Voltage (Sine, square, triangle, and sawtooth waveforms)

4.3.2. Impulse voltage

Pulse power supplies for DBDs generally exhibit an amplitude in the order of $10kV$, front times T_1 in the order of one hundred ns and an operating frequency in the order of several tens of kHw (Eun Ha Choi, 2002).

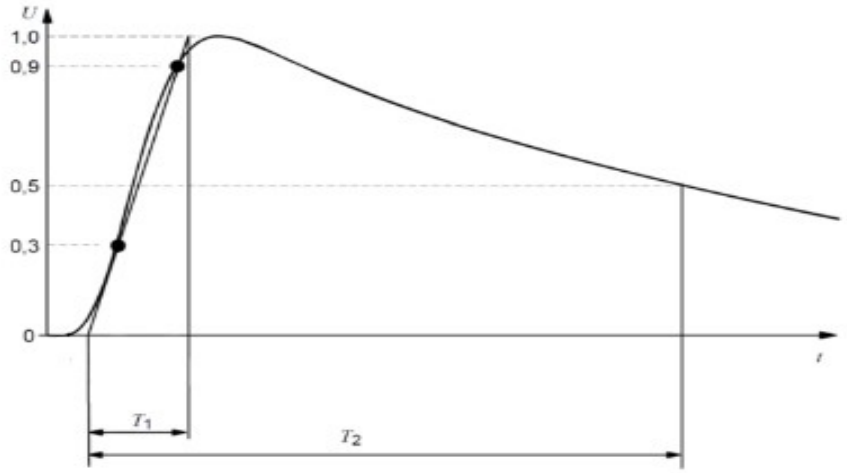

Fig. I-14 : Lightning impulse voltage (Božidar Filipović-Grčić, 2015)

These voltage sources are currently used in some applications due to their superior efficiency in terms of radiated power, compared to sinusoidal power supplies. The time parameters of lightning impulse voltage are shown in figure I-14, with T_2 is the half time**.**

4.4. Current configurations of DBDs

Cold plasmas can be generated by electric fields. To stabilize the discharge and maintain the thermal imbalance (avoid transition to arc), it is firstly important to control the geometry of electric discharge reactors. Thus, geometry is very important for the discharge. Indeed, the geometry can modify the establishment of micro-discharges in the inter-electrode zone. DBD can be declined in various geometric forms. Typical cylindrical or planar configurations of dielectric barrier discharge electrodes are shown in the figure below (Fig.I-15). Two types of configurations are presented: the planar configuration (with one or two dielectrics with different positions and the cylindrical configuration (Falkenstein, 1998).

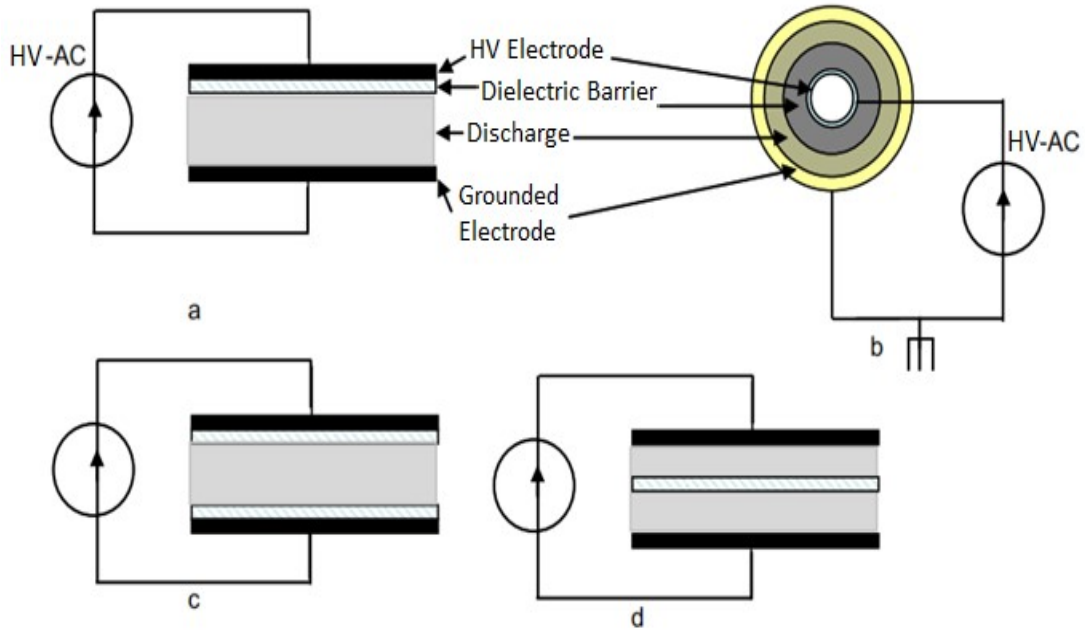

Fig. I-15 Typical geometric configuration of DBD in volume (VDBD)

There are two class types Volume Discharge (VDBD) (Fig.) and Surface Discharge (SD) (Fig I-15). The main difference between these two configurations is that in the VD discharge the rupture occurs through the gas in the space between electrodes, while in the SD discharge the rupture grows periodically on the dielectric. Note that the presence of a dielectric layer is essential for the formation of a surface discharge, since the insulation prevents the flow of current. (Pietsch, 2000). Our work is based on volume discharges. The plan-to-plan configuration (a) and (c) in figure I-15 has the advantage of avoiding any contact between the plasma and the electrodes, a condition that is sometimes useful when using corrosive plasma for example. Configuration (d) allows two discharges to be obtained simultaneously on either side of the dielectric, which may even be the material to be treated. Finally, the cylindrical configuration (b) is particularly suitable for gas treatment or for the generation of Ultraviolet.

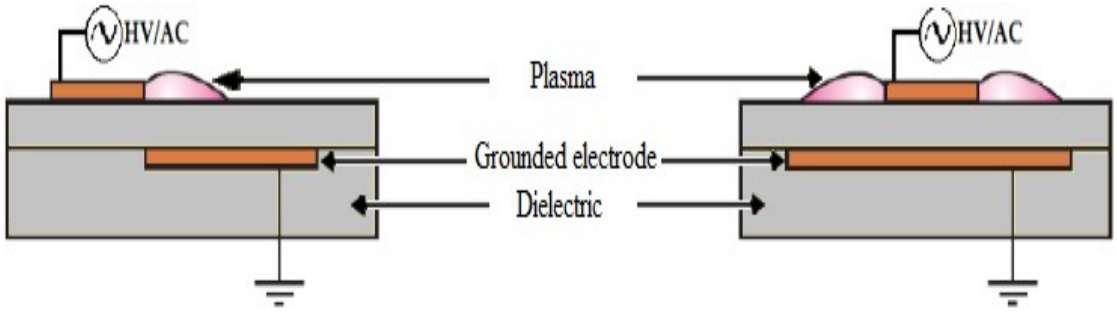

Fig. I-16: Typical geometric configurations of DBD in surface (SDBD)

4.5. Operation principle of DBDs

When a sufficiently high voltage applied on the electrodes, the breakdown of the gas leads to the formation of a conductive channel called micro-discharge (Fig I-17 .a). The diagram of Fig I-17.d can represent this micro-discharge. The dielectric behaves like the insulator of a capacitor, C_{ds}, whose armatures are on one side the discharge and on the other the electrode. Note that this equivalent diagram only makes sense if we consider only a single micro-discharge or a homogeneous discharge over the electrodes surface. Subsequently, we will denote V_a the voltage applied to the discharge gap, V_g that on the gas, and finally V_{ds} that on the dielectric. The passage of the current induces an accumulation of charges on the dielectric surface opposite the discharge channel, which results in an increase in the voltage V_{ds}. If the increase in this voltage as the discharge develops is faster than the increase in voltage, V_a, it causes a decreasing of applied voltage to the gas,V_a, which leads to discharge extinction. Thus, the micro-discharge is blocked long before it has reached a sufficient degree of ionization to pass through an arc regime. As the applied voltage increases, micro-discharges initiate at new positions because the presence of residual charges on the dielectric decreases the electric field applied to the gas at positions where micro-discharges have already developed (Fig I-17.b).

At the change of polarity (Fig I-17.c), the charges previously deposited on the dielectric allow a gas breakdown under a weaker electric field than during the first half-wave: $V_g = V_a - V_{ds}$ (with V_a and V_{ds} have an opposite sign during the change of polarity). The primary function of the dielectric is to limit the charge deposited on the electrodes and thereby the current passing through the channel so that the discharge does not become an arc as can happen between two metal electrodes at atmospheric pressure. In addition, the use of the dielectric also has the consequence of tending towards more uniform distribution of the micro-discharges over the dielectric surface (Lin, 1980).

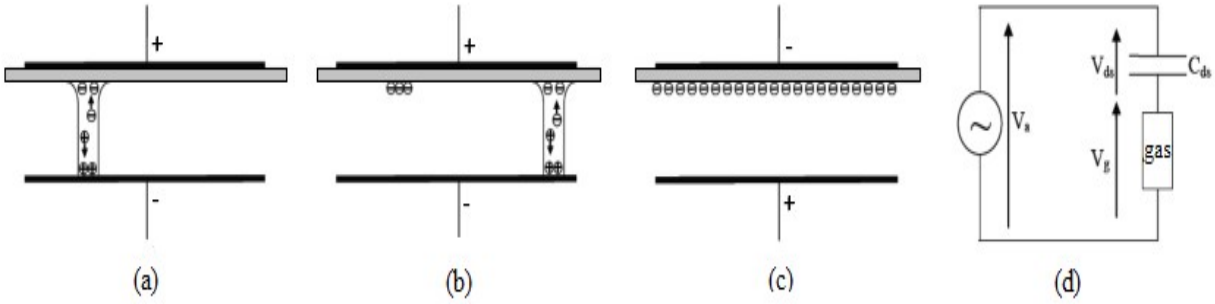

Fig. I-17: Operation principle of DBD

4.6. Types of DBD in volume:

Depending on the type of gas breakdown and the value $p \times d$, two types of discharge can be distinguished: filamentary discharge and homogeneous discharge (G. Bauville, 2003).

4.6.1. Filamentary discharge:

Filament discharge is the first dielectric barrier discharge mode discovered and the easiest to obtain (Bournet, 2007), This type of discharge is composed of a multitude of filaments initiated by a steamer breakdown (Fig I-18, b) (Alban.Sublet, 2007).

When the voltage applied to the electrodes is high enough, ionization phenomena by avalanche effect appear. The charges appearing modify the electric field locally. These charges, by propagating along the field lines, leave a streamer, which corresponds to the channel of a micro-discharge with a radius of approximately 100 µm. (Jean-marie cormiers Ahmed Khacef, 2002) When an ionized channel is established between the electrode and the dielectric, the charges, which decreases the electric field causes the extinction of the micro-discharge. After the extinction of the streamer and the recombination of the charges, the different neutral species created (molecules and radicals) react in a medium whose temperature is close to ambient temperature (Jean-marie cormiers Ahmed Khacef, 2002).

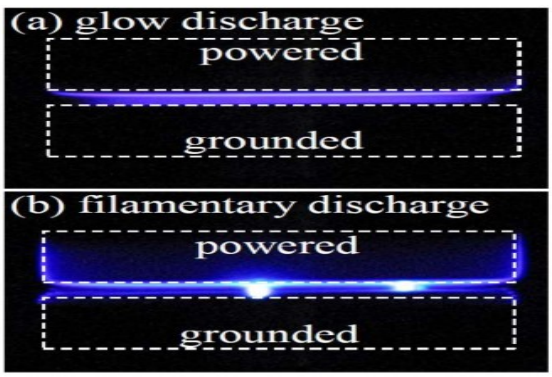

Fig. I-18: Photograph of a filamentary (a) and Glow discharge (b) (K Koga, 2014)

4.6.2. Homogeneous discharge:

It is however possible to obtain luminous and homogeneous discharges (without filaments) in air at atmospheric pressure by applying electric fields of a few tens of kV/cm at frequencies of the order of kHz and with distances between electrodes from 0.5 to $3cm$ (Labergue, 2005). This discharge is characterized by a spatial distribution of light that is radially homogeneous but localized near an electrode when the discharge is established (Fig. I-18.a). It therefore does not correspond to a filamentary discharge.

The term "glow discharge" is used because of the similarities observed between the apparently homogeneous DBD regime and the true glow discharge obtained at a low pressure-distance product (Bournet, 2007).

5. DBD applications

The industrial applications of electric discharges are very varied and affect quite different fields of application, affecting scientific and industrial fields, ranging from surface treatment (thin film) to the reduction of pollutants through the production of UV radiation. In this section, we will discuss some uses of DBD, starting with the oldest: ozone production.

The great diversity of applications offered by DBDs is a motivating point, which opens the spectrum of perspectives to the results obtained in this thesis.

5.1. Ozone generation:

Ozone is an allotropic form of oxygen formed from three atoms of this element. In its ground state, the ozone molecule has two oxygen-oxygen bonds with a length of 1.278 ± 0.003 Å and an angle of $116,45$ °. It has a low dipole moment of 0.53 $Debye$, the best-known function of which is protection against dangerous ultraviolet radiation from the sun, but it is also a powerful oxidant and a powerful disinfectant having a wide variety of uses, the most remarkable is water disinfection.

Under normal temperature and pressure conditions, ozone is thirteen times more soluble in water than oxygen. It is, after fluorine, the most oxidizing compound thanks to its ability to capture electrons, of rapid decomposition and, under the same conditions, it is more stable in water than in air. It is a pale blue, unstable gas, which at room temperature is characterized by a pungent odor (Fridman, 2007) (Kogelschatz U. , 2003).

5.1.1. Ozone instability

Ozone has a maximum half-life of half an hour. This half-life means that after half an hour, half of the residual ozone will have been degraded. In practice, the half-life is less than 30 minutes, due to the presence of bacteria and other contaminants in the air. Ozone is therefore a very powerful compound, but with a short lifespan. (Renate Viebahn-Hänsler, 2012).

5.1.2. Ozone behavior with bacteria, viruses and germs

Ozone is primarily used for disinfection against bacteria, viruses, germs and odors. Bacteria are microscopic, single-celled creatures with a primitive structure. The bacteria are covered with a relatively strong membrane. Ozone collides with the bacteria wall; sufficient ozone passes through the cell membrane and this leads to the destruction of bacteria. Figure I-19 shows the oxidation steps of bacteria by ozone.

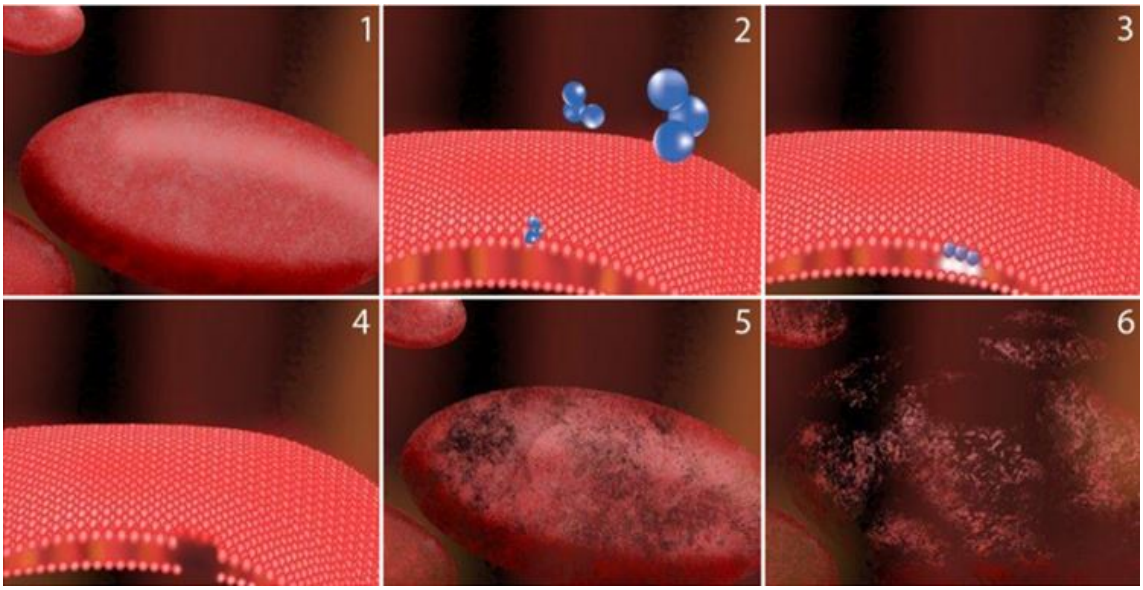

Fig. I-19 : Effect of Ozone on Bacteria (INC, 2017)

1. A healthy bacillus bacterial cell
2. Ozone molecules come in contact with the cell wall
3. A reaction called an oxidative burst occurs which creates a hole in the cell wall
4. A hole in the cell wall has injured the bacterium
5. The bacterium loses its shape while ozone molecules continue creating holes
6. Thousands of ozone collisions occur in only a few seconds. The bacterial wall can no longer hold its shape and the cell dies

5.1.3. Ozone generation:

Ozone is used primarily for treating water, removing bacteria, viruses and unpleasant odors. The production of ozone O_3 at atmospheric pressure, is carried out from air, oxygen O_2, or other gas mixtures composed of oxygen and nitrogen N_2. Figure I-20 shows the block diagram of an ozonier supplied with oxygen. Here the DBD consists of two coaxial dielectric barriers; the discharge is carried out in the volume through which the gas circulates. The electric current will convert some of the incoming gas into ozone.

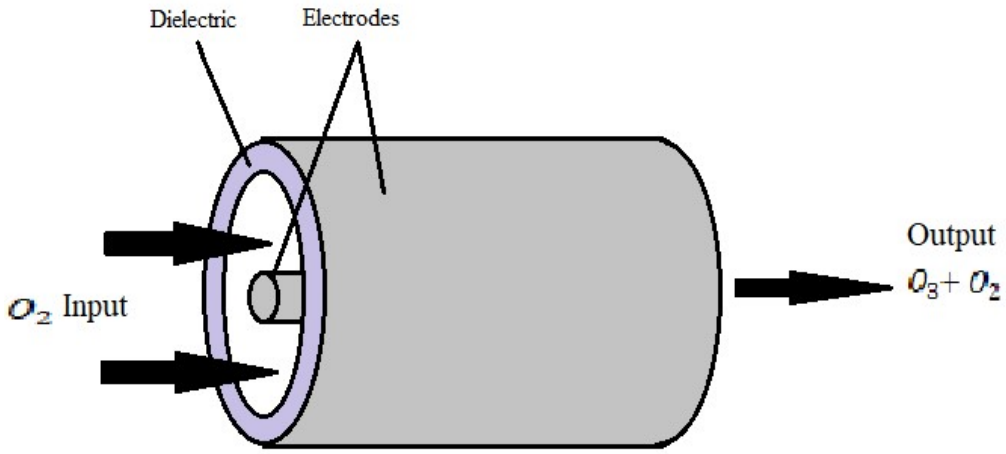

Fig. I-20: Schematic diagram of an ozoniser

Initially, oxygen in its ground state is dissociated, by an electronic collision (a consequence of the electric field) producing two atoms of oxygen. An oxygen atom O associates in an excited state with an O_2 molecule with the help of a third species M; this third component can be, for example, O_2, O_3, O or N_2. The excited state generated O_3^*, returns to the closest stable state, corresponding to ozone O_3.

$$O + O_2 + M \rightarrow O_3^* + M \rightarrow O_3 + M \qquad (0\text{-}3)$$

Today, a few thousand ozone generation factories are in operation. The larger ones reach power levels of several MW and produce a few tones of ozone per day. Although the purification of drinking water is still the most important ozone market, other applications have emerged.

5.1.4. Advantage of ozone over other disinfection methods:

The reasons for using ozone disinfection appear when compared with other disinfection methods. It has a number of advantages over chlorine. It is used despite the often-significant cost of a water ozonization system. These advantages are as follows:

- it does not remain in the water;

- it does not cause the appearance of organochlorines, which can be carcinogenic;
- it does not leave a bad taste that is not appreciated by drinking water consumers.
- Ozone destroys bacteria 3,500 times faster than chlorine.

5.2. Oxygen generation:

In 2004, LPGP launched a new study theme on micro-discharges (LeannePitchford, 2005), which have remarkable stability properties, allowing the generation of stable plasmas at high pressure and at high density of injected power. From a fundamental point of view, the study of these non-equilibrium micro-discharges opens a new field of research in plasma physics. From the point of view of applications, these high-pressure micro-plasmas can allow the development of micro-reactors showing new and very promising potentials, in particular for the production of large fluxes of reactive species or UV photons. The "MicroPlasRé" project aims to use high-pressure plasmas out of thermodynamic equilibrium created in micro-discharges to produce large fluxes of radicals and metastable.

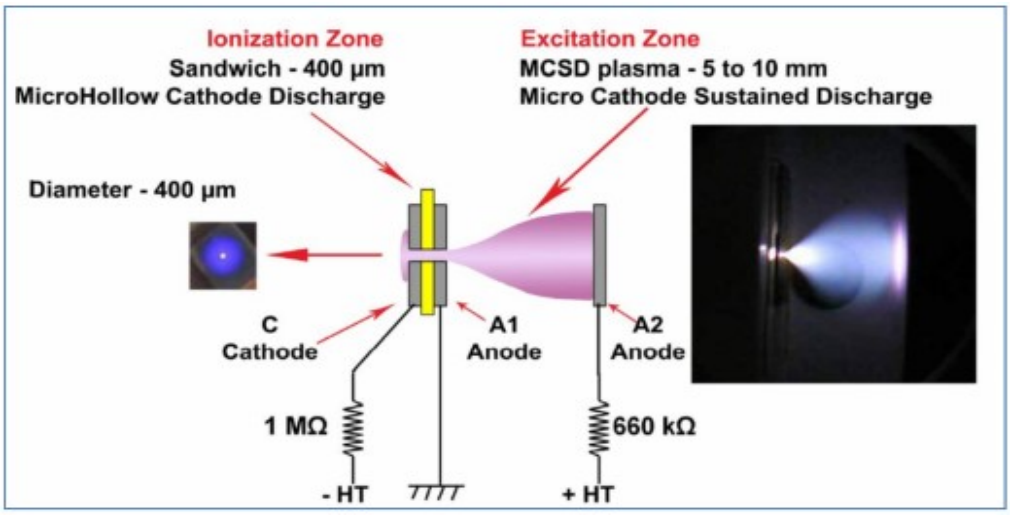

Fig. I-21: Schematic diagram of a "Micro-Cathode Sustained Discharge" produced in oxygen (LeannePitchford, 2005)

5.3. Surface treatment:

The use of DBDs for surface treatments covers a wide spectrum. We can cite among others the following applications Modification of the surface properties of a material; Improvement of adhesion properties, wettability; Textile treatment; Polymer treatment, deposit of SiO_2; Cleaning of surfaces (silicon, steels, etc.); Disinfection, sterilization. One of the main properties of DBDs is that they can operate in a filamentary or homogeneous regime. The "homogeneous" characteristic gives them the property of being able to act for a uniform modification of the

treated surfaces. For example, the processing of plastics, to allow them to stick easily or be receptive to printing ink (F. MASSINES, 2001). DBD can be easily introduced into the industrial papermaking process, by discharging between a roller that turns the paper and an electrode (sometimes several) covered by a dielectric (Fig. I-22).

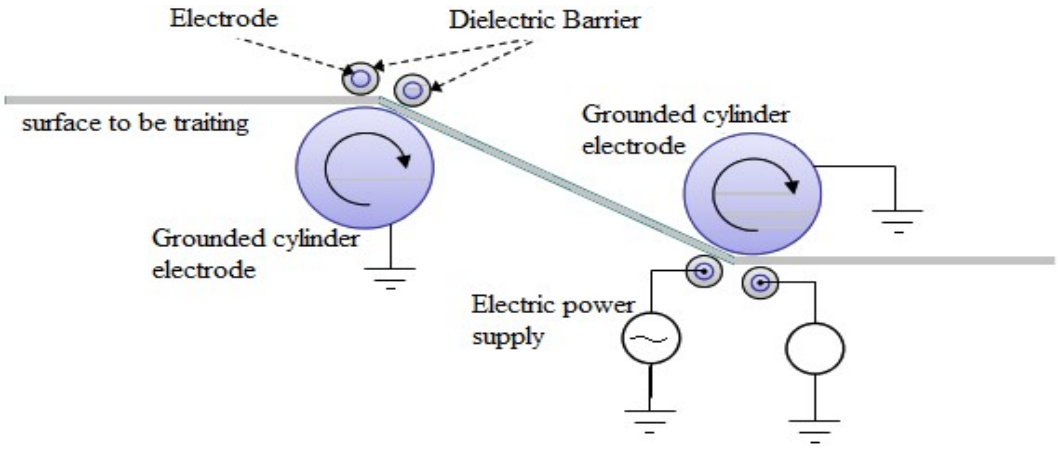

Fig. I-22: Using DBD for surface treatment (Kogelschatz, 2003)

5.4. Treatment of gaseous pollutants:

Few tens of years ago, the scientific society, had the possibility of using cold plasmas for the depollution of gaseous effluents. The basic idea is to harness the chemical reactivity of radicals and species generated in the plasma to transform polluting molecules into harmless molecules, the reaction taking place in air at ordinary pressure and without heat loss. The residues obtained can also sometimes be recoverable. The pollutants targeted in current developments are essentially sulfur and nitrogen oxides (VOCs or volatile organic compounds) and malodorous molecules.

Today, DBD is being studied in the destruction of toxic exhaust gases, such as CO, NOx and in the reduction of greenhouse emissions, such as carbon dioxide. CO_2, responsible for global warming (T. Ikematsu, 2004). In addition, DBD is also used to produce Hydrogen from hydrocarbons or, in order to facilitate their transport; to synthesize liquid fuels, such as methanol, from gases produced in oil extraction (K. Okazaki, 2002).

5.5. Treatment of liquid pollutants:

DBD has been widely used for the treatment of various liquid pollutants. Indeed, it was recently the subject of a study on the treatment of endocrine disruptors (EDCs). Three molecules have been studied: clofibric acid, carbamazepine and iopromide. The experimental results show

that for a 30-minute treatment, there is a degradation rate greater than 98% for carbamazepine, 99% for iopromide and below the detection limit for clofibric acid (Holger Krause, 2009).

There are also several applications of DBD on the treatment of Diur. During these studies the effect of pH and that of Fe was discussed to improve the performance of this technique. Indeed, by decreasing the pH and by increasing the concentration of Fe^{+2}, Cu^{+2} the degradation of diuron becomes more efficient (Jingwei. F Z. Z., 2008), (Jingwei. F Z. Z., 2009). DBD has also been used for the treatment of aqueous solutions containing dyes. It is noted that for Indigo Carmine, a discoloration rate of 95% is reached after only 18 minutes of treatment (Zanhua. S, 2008). For Orange, there is a reduction in Total Organic Carbon (TOC) of 44% for an initial concentration of 25mg / L (Young. S. M, 2008).

5.6. Lighting:

Contact between the electrode and the gas in the lamps is the main source of gas contamination and electrode erosion; DBD is a good solution to this problem, and helps increase the life of new generation lamps (.Y. ZHANG, 2000). With regard to lighting, DBD lamps also have the advantage of being able to produce homogeneous radiation across the surface of the electrodes (N.N. GUIVAN, 2005).

Lamps with excited species, excimers or exciplexes, have advantages over conventional UV production techniques (E.A. SOSNIN, 2005), (U. KOGELSCHATZ, 2000).

* They do not use mercury in the gas mixture, avoiding serious consequences for health and the environment;

* They do not need a gas (mercury) heating system and can be used in low temperature applications (luminescent regime instead of arc regime);

* Their emission spectrum can be adjusted with the gas mixture, with multiple choices, with a linewidth of the order of ten nanometers.

5.7. Plasma Display Panels (PDP):

AC plasma displays using xenon VUV radiation to excite phosphorus are recent innovations in the wide range of DBD applications. This idea is the work of two professors at the University of Illinois, Bitzer and Slottow, and was invented in 1964 (Kogelschatz U. , 2003). A plasma

screen display consists of two flat glasses separated by a gap of approximately 100 µm filled with a mixture of rare gases (generally Xe-Ne or Xe-Ne-He) capable of emitting UV radiation. An array of electrodes is placed on each glass slide. Thin layers of dielectric 20 µm to 40µm thick cover these electrodes. The standard geometry of commercially available electrodes is coplanar (ACC) (Fig. I-23).

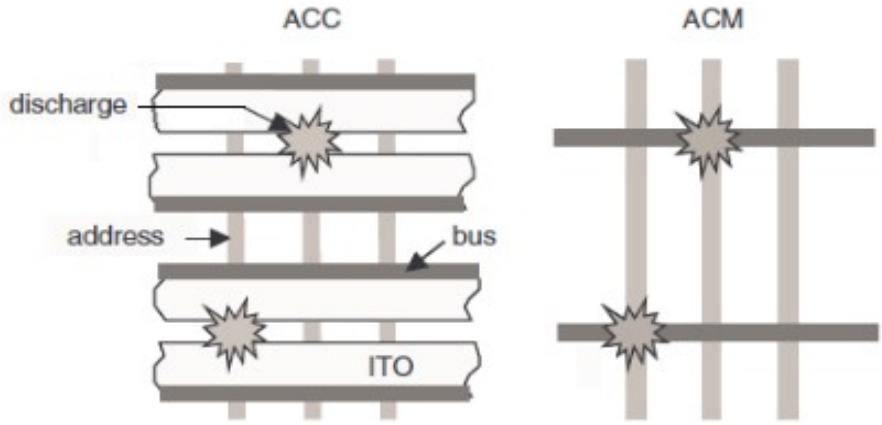

Fig. I-23: Coplanar Electrode (ACC) and Matrix (ACM) Plasma Display Configurations

Although the ACC electrode structure is the most developed nowadays, the ACM electrode structure is however considered to be the best because the properties of the discharges as well as the addressing scheme are very simple.

A flat screen is made up of a large number of cells or "pixels", each made up of three phosphorescent mini-lamps, one radiating in red, the other in green and the third in blue. The configuration of the cell can be with parallel or coplanar electrodes (Fig. I-24).

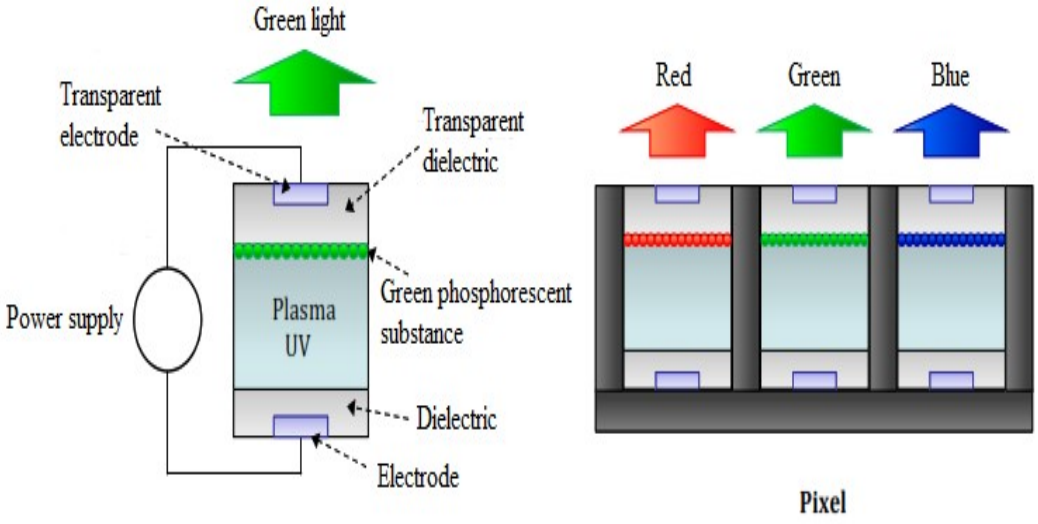

Fig. I-24 : DBD in plasma flat screens

6. Conclusion

This chapter was devoted to an outline on the electric discharge and the cold plasmas out of thermal equilibrium and its difference between thermal plasma, and we have given a classification of the types of the discharges by a flow chart. In particular, it contains the detailed explanation for the processes of low-pressure discharges (Townsend discharge) and atmospheric pressure discharges (streamer type discharge) according to the current-voltage breakdown characteristics. There is also an overview of the different cold plasma reactors to characterize these unbalanced discharges and their field of use.

Therefore, we have introduced the concept of dielectric barrier discharge and the physical elements that characterize it. We started with the general principles of DBDs, their current configurations and the various industrial applications.

Given the orientation chosen for this thesis, we have insisted on the basic principle governing ozone generators and have drawn up a non-exhaustive overview of their applications.

Bibliographie

I. Langmuir, "Oscillations in Ionized Gases," *Proceedings of the National Academy of Sciences .14 (8),* p. 627–637, 1928.

F. F. Chen, «Introduction to Plasma Physics and controlled fusion,» *Springer International Publishing,* pp. 2-3, 1984.

J. P. Freidberg, «Plasma Physics and Fusion Energy,» *Cambridge University Press,* p. 121, 2008.

J. R. Roth, «Industrial Plasma Engineering : Principles,» *Institute of Physics Publishing,* Publishing.

U. Kogelschatz, « Silent discharges for the generation of ultraviolet and vacuum,» *Pure & Appl. Chem., Vol. 62, No. 9,* pp. 1667-1674, 1990.

J. Roth, «Glow discharge-like characteristics of a oaugdp revealed by computer modeling,» *IEEE International on Plasma Science,* p. 288, 1998.

G. F. S. Flügge, «The glow discharge at low pressure,» *Encyclopedia of Physics, volume Volume 22:,* pp. 53-61, 1956.

W. Thornhill, «The Z-Pinch Morphology of Supernova 1987A and Electric Stars.,» *IEEE Transactions on Plasma Science, vol. 35, issue 4,* pp. 832-844, 2007.

E. Sozer, Gaseous Discharges and Their Applications as High Power Plasma Switches, 2008.

D. D. P. Stern, «The Fluorescent Lamp: A plasma you can use,» *Retrieved ,* pp. 5-19, 2010.

«Plasma (physics),» 15 January 2021. [En ligne]. Available: http://en.wikipedia.org/wiki/Plasma_(physics).

M. Sobolewski et J. &. B. Langan & Felker, «Electrical optimization of plasma - enhanced chemical vapor deposition chamber cleaning plasmas,» *16. J. Vac. Sci. Technol,* pp. 173-182, 1997.

J. Lichtenberg, Principles of Plasma Discharges and Materials Processing, Second Edition, John Wiley & Sons, Inc., 2005.

C. Wadhwa, High Voltage Engineering 2nd edition, New Age International., 2007.

Y. A. Trishin, «Acceleration of rigid bodies by coherent jets,» *Journal of Applied Mechanics and Technical Physics 21,* p. 696–699, 1980.

G. Thome, «Kurzzeitphysik,» *Springer Berlin,* p. 8, 1967.

Y. H. Choi, «One-dimensional discharge simulation of nitrogen DBD atmospheric pressure plasma,» *Thin Solid Films, vol. 506,* p. 389–395, 2006.

J. D. Craggs, «Electrical breakdown of gases,» *Oxford (Clarendon Press),* pp. vii, 507, 1953.

Gharagozalian Mehrnaz, «Water treatment by the AC gliding arc air plasma,» *Journal of Theoretical and Applied Physics,* pp. 171-180, 2017.

Y. J. Du ChangMing, «Degradation and Discoloration of Textile Dyes Using Gliding Arc Plasma Combined with Fenton Catalysis,» pp. 21-39, Plasma Combined with Fenton Catalysis.

Abdul SYAKUR Badrus ZAMAN, «International Conference on Information Technology,» chez *Application of dielectric barrier discharge plasma forreducing Chemical Oxygen Demand (COD) on industrial rubber wastewater*, 2017.

B. Ronny, «Dielectric barrier discharges: progress on plasma sources and on the understanding of regimes and single filaments,» *Plasma Sources Science and Technology,* p. 053001, 2017.

Mededovic Thagard Selma, «lasma-based water treatment:development of a general mechanistic model to estimate the treatability of different types of contaminants,» *Journal of Physics D: Applied Physics,,50(1),* p. 014003, 2017.

Meirovich Ariel, «Treatment of Methylene Blue water solution by submerged pulse arc in multielectrode reactor,» *Journal of Water Process Engineering,13,* pp. 53-60, 2016.

Iwabuchi Masashi, «Simultaneous Decomposition of Phenol and Sodium Formate by Discharge Inside Bubble in Water,» *Transactions of the Materials Research Society of Japan,41(2),* pp. 183-187, 2016.

S. Ajo Petri, «Pulsed Corona Discharge in Water Treatment: The Effect of Hydrodynamic Conditions on Oxidation Energy Efficiency,» *Industrial & Engineering Chemistry Research,* pp. 7452-7458., 2015.

U. Kogelschatz, «From ozone generators to flat television screens: history and future potential of dielectric-barrier discharges,» *Pure Appl.Chem., Vol. 71, No. 10,* pp. 1819-1828, 1999.

S. Kanazawa, «Stable glow plasma at atmospheric pressure,» *J. Phys. D: Appl. Phys. 21,* p. 838, 1988.

A. Raghu. S, «Evaluation of electrochemical oxidation techniques for degradation of dye effluents—A comparative approach,» *Journal of Hazardous Materials 171,* pp. 748-754, 2009.

M. D, PHD Thesis .Destruction du tributylphosphate par effluvage électrique. Utilisation d'un réacteur à décharges glissantes, Université de Rouen., 1999..

S. Hammami, PHD thesis. Étude de dégradation des colorants de textile par les procédés d'oxydation avancée. Application à la dépollution des rejets industriels, l'Université Paris-Est et Tunis El Manar, 2008.

Y. P. Raizer, Gas Discharge Physics, Allen, John E. (Ed.), 1991.

K. C. Kao, Dielectric Phenomena in Solids, London: Elsevier Academic Press, 2004.

https://en.wikipedia.org/wiki/Dielectric, «Dielectric,» 30 January 2021. [En ligne]. Available: https://en.wikipedia.org/wiki/Dielectric.

L. Reynard, Thèse de doctorat, Modélisation tridimensionnelle de l'amorcage de l'arc électrique dans un disjoncteur basse-tension, Lyon: Ecole Centrale de Lyon, 2006.

«Plasmas Froids : Génération, caractérisation et technologies.,» *Publications de l'Université de Saint Etienne, . ,* 2004.

M. K. Eun Ha Choi, «Vacuum ultraviolet luminous efficiency and plasma ion density in alternating current plasma display panels,» *Applied Physics Letters 81,* p. 3341, 2002.

Z. Falkenstein, «Applications of dielectric barrier discharges,» chez *in High-Power Particle Beams*, BEAMS '98. Proceedings of the 12th International , 1998.

G. J. Pietsch, «The Development of Dielectric Barrier Discharges in Gas Gaps and on Surfaces,» *Journal of Physics D: Applied Physics. 33(20),* p. 2618, 2000.

Božidar Filipović-Grčić, «Estimation of Load Capacitance and Stray Inductance in Lightning Impulse Voltage Test Circuits,» *Electric Power Systems Research, Volume 119,* pp. 439-446, 2015.

S.-C. Lin, «Necessary conditions for the homogeneous formation of pulsed avalanche discharges at high gas pressures,» *J. Appl. Phys., 51,* pp. 210-222, 1980.

G. Bauville, «Proceeding des résumés du 8eme congrès "Plasma" de la société Française de physique 5-7 Mai,» chez *Traitement de tôles métalliques par décharge à barrière diélectrique monopolaire fonctionnant à pression atmosphérique*, Cadarache- St Paul Lez Durance., 2003.

C. S. Bournet, PhD Thesis, Design et réalisation d'un réacteur plasma à pression atmosphérique pour des traitements de surface dans le domaine des biomatériaux, Université de Laval , 2007.

Alban.Sublet, PhD thesis, Caractérisation de décharges à barrière diélectriques atmosphériques et sub-atmosphériques et application à la déposition de couches d'oxyde de silicium, Ecole polytechnique fédérale de Lausanne, 2007.

O. M. Jean-marie cormiers Ahmed Khacef, «Dépollution des effluents gazeux par plasma; A la pointe de l'instrumentation et de la technologie,» *Centre National de la Recherche Scientifique:(CNRS) France. n.d.,* 2002.

U. Kogelschatz, «Filamentary and diffuse barrier discharges,» *J. Phys. D: Appl. Phys vol. 20, ,* p. 1421, 1987.

K Koga, «Formation of carbon nanoparticle using Ar+CH4 high pressure nanosecond discharges,» *Journal of Physics: Conference Series 518 ,* p. 012020, 2014.

A. Labergue, PhD thesis. Etude de décharges électriques dans l'air pour le développement d'actionneurs plasmas– Application au contrôle de décollements d'écoulements, université de Poitiers, 2005 .

F. MASSINES, «The Role of Dielectric Barrier Discharge Atmosphere and Physics on Polypropylene Surface Treatment,» *Plasmas and Polymers, Vol. 6, ,* 2001.

Leanne Pitchford, «ProjectsANR (Microplasré, 2005) Microdéchargeset jets de plasma,» Toulouse, 2005.

N. H. S. I. S. S. C. Y. T. IKEMATSU, «Advanced oxidation Advanced oxidation,» *Vacuum 73 ,* p. 579–582, 2004.

T. K. K. O. T. N. K. OKAZAKI, «Direct conversion from methane to methanol for high efficiency energy system with exergy regeneration,» *Energy Conversion and Management 43 ,* p. 1459–1468, 2002.

B. S. J. S. S. S. U. S. Holger Krause, «Degradation of the endocrine disrupting chemicals (EDCs) carbamazepine, clofibric acid, and iopromide by corona discharge over water,» *Chemosphere,* pp. 163-168, 2009.

Z. Z. Y. S. J. L. Z. W. L. W. J. F. Jingwei. F, «Degradation of diuron in aqueous solution by dielectric barrier discharge,» *Journal of Hazardous Materials Volume 154, Issues 1–3,* pp. 1081-1089, 2008.

Z. Z. J. L. K. L. L. W. J. F. Jingwei. F, «Gas–liquid hybrid discharge-induced degradation of diuron in aqueous solution,» *Journal of Hazardous Materials Volume 164, ,* pp. 838-846, 2009.

D. X. Y. C. C. H. X. Zanhua. S, «Plasma decoloration of dye using dielectric barrier discharges with earthed spraying water electrodes,» *Journal of Electrostatics vol 66,* pp. 476-481, 2008.

J. O. W. J. C. Young. S. M, «Degradation of an azo dye Orange II using a gas phase dielectric barrier discharge reactor submerged in water,» *Chemical Engineering Journal, Volume 142,,* pp. 56-64, 2008.

I. B. .Y. ZHANG, « Lifetime investigation of excimer UV sources,» *Applied Surface Science 168 ,* pp. 296-299, 2000.

J. J. A. B. P. S. P. S. L. S. N.N. GUIVAN, «Planar UV excilamp excited by a surface barrier discharge,» *J. Phys. D: Appl. Phys. 38,* p. 3188–3193, 2005.

M. E. V. T. E.A. SOSNIN, « Capacitive discharge exciplex lamps,» *J.Phys. D: Appl. Phys. 38 ,* p. 3194–3201, 2005.

H. E. J. Z. I. B. U. KOGELSCHATZ, «High-intensity sources of incoherent UV and VUV excimer radiation for low-temperature materials processing,» *Applied Surface Science 168,* pp. 29-36, 2000.

G. S. A. J. M. M. B. A. .. &. F. G. Fridman, «Floating electrode dielectric barrier discharge plasma in air promoting apoptotic behavior in melanoma skin cancer cell lines,» *Plasma Chemistry and Plasma Processing, 27(2),* pp. 163-176, 2007.

O. S. L. F. e. Z. F. Renate Viebahn-Hänsler, «Ozone in Medicine: The Low-Dose Ozone Concept—Guidelines and Treatment Strategies,» *Ozone: Science Engineering, Volume 34, Issue 6, ,* pp. 408-424, 2012.

C. M. W. INC, «OZONE PROCESSING,» 2017. [En ligne]. Available: https://www.coloradomedicalwaste.com/ozone-technology/.

U. Kogelschatz, «Dielectric-barrier Discharges: Their History, Discharge Physics, and Industrial Applications,» *Plasma Chemistry and Plasma Processing, Vol. 23,* 2003.

A.M. POINTU, "Plasmas froids de décharge : Propriétés électriques" Les techniques de l'ingénieur, 2007.

H.C. Thejaswini, «Deposition of functional films by atmospheric Pressure Discharge,» chez *Poster presented in SFB - TR24 workshop*, Potsdam, Germany, September 26-28, 2011.

Chapter II:

Model parameters and solving methods

1. Introduction:

This chapter is devoted to a presentation of the research tools that we have developed and used for the study of a dielectric barrier discharge. The operation of this discharge, like that of all discharges in gases, is governed by a multitude of physical phenomena, which are different from each other but strongly coupled. The modeling of electric discharge plasmas is today considered a very complementary tool to experimental analysis for the design and optimization of the plasma reactor for such or such application.

The modeling and numerical simulation of the plasma reactor allows us, for a precise dimensioning of the reactor, to have the optimal operating parameters with regard in particular to the composition of the gas, its pressure and its flow rate, the configuration of the electrodes, the characteristics of the gas, power supply. Indeed, by the simulation one obtains fast answers concerning the effects of all these different operating parameters (pressure, power, gas flow ...) on the general performance of the system. For a given reactor, the most precise models of the discharge must be used to study the transport of charged particles, the deposition rate, the thicknesses of the cladding, the spatial distribution of radicals, and the dynamics of the dielectric...

The mathematical modeling of an electric discharge is relatively complex because of the many phenomena involved and their strong coupling, for example that between the variation of the densities of charged particles and that of the electric field.

In this chapter, we will present the characteristic quantities of plasma, particles types and the chemical reactions between these species. Then, we describe the physical model used for a dielectric barrier discharge and the basic data used. In addition, the numerical model associated with this physical model used in this thesis will be described.

2. Physical characteristics of the DBD model

2.1. Characteristic quantities of plasma:

2.1.1. Species densities:

The density of a given species represents the number of particles contained on average per unit volume around a given point in space and at a given time. Densities are often expressed in cm^{-3} or m^{-3}. For our model, the densities to be determined are the electrons density n_e, the ion density n_i, the neutrals density n_o.

2.1.2. Ionization rate:

The ionization rate τ_i represents the ratio of the number of free electrons n_e divided by the number of total particles $n_e + N$, N is the number of neutral particles per unit volume. The ionization rate is given by the relation:

$$\tau_i = \frac{n_e}{n_e + N} \quad \text{(II-1)}$$

2.1.3. Plasma potential:

The average electrostatic potential in the plasma is well defined, it is approximately constant in the volume of the plasma in the case of a plane-plane geometry. It can be defined from the energy required to transport a charged particle from the plasma to where the potential is zero. In general, the plasma potential is greater compared to the walls that surround it.

2.1.4. Plasma frequency:

If an elementary volume of the plasma is deviated from its local electrical neutrality (for example displacement of electrons from one elementary volume to another), this elementary volume returns to its neutrality by oscillating near the plasma frequency.

$$f_p = \frac{\omega_p}{2\pi} \quad \text{(II-2)}$$

and $\omega_p^2 = e^2 n_e / \varepsilon_0 m_e$ with: f_p plasma frequency ω_p: plasma pulsation e: elementary charge, m_e: electron mass, n_e: electrons density and ε_0: the permittivity of vacuum.

2.1.5. Debye length:

Debye length λ_D is the distance traveled by a thermal electron during a cycle of the plasma pulsation:

$$\lambda_D = \frac{V_e}{\sqrt{2}\omega_p} \quad \text{(II-3)}$$

$\lambda_D{}^2 = \varepsilon_0 k_B T_e / e^2 n_e$ with: k_B: is the Boltzmann constant and T_e : is the electronic temperature.

Debye's length gives the scale of the typical distances over which an electrostatic disturbance extends in a plasma before being screened by the response of plasma charges.

2.1.6. Landau Length:

The length of "Landau" λ_L is the distance for which the potential energy of interaction between two electrons is equal to their kinetic energy of thermal agitation. This distance is therefore such that:

$$\lambda_L = \frac{e^2}{4\pi\varepsilon_0 k_B T_e} \quad \text{(II-4)}$$

2.2. Description of the particles present in plasma

2.2.1. Electron

Free electrons are the real engine of electric discharges. Due to their very low relative mass, they move much faster than other species and are therefore the first to store the energy of the electric field that will then allow them to excite, dissociate and ionize the gaseous medium. Electrons actually respond to electromagnetic disturbances on time scales 100 to 1000 times shorter than ions. It is also the electrons, which, due to their high mobility, are primarily responsible for the electrical conductivity of plasmas.

2.2.2. Heavy species:

A. Positive and negative ions:

Unlike electrons, which are all identical, the nature of ionic species in an out of equilibrium discharge can be very varied. In the electric discharges that interest us, the ions generally formed by ionization are mono-charged but can be mono or polyatomic. In the presence of electronegative gases (halogen, oxygen, nitrogen oxides, etc.), there are also negative ions. These ions are usually formed by the attachment, dissociative or not, of a free electron to an electronegative molecule.

B. Molecular fragments:

The plasma can contain a large number of dissociation products which, after a relatively short time, will react either with another molecule or with the wall. They can be either simple atoms (H, N, O, etc.), or more complex molecular structures, including radicals from traditional chemistry (NO_2, NO, O_3 …).

The term radical designates a molecular fragment with an odd peripheral electron number (for example NO, CH_3, OH, etc.) with dangling bonds which make it very reactive in collisions with other species.

C. Excited states:

During the impact of energetic particles with atoms and molecules of the gaseous medium can find themselves in an excited state, energetically higher than the ground level. Internal energy can be stored in different ways:

Rotational energy: Molecular species can acquire rotational energy. This energy is quantified, the energy jump between levels is small, of the order of 0.01 eV.

Vibrating energy: This type of excitation corresponds to a periodic deformation of the molecular structure. In a simplistic way, we can distinguish between the elongation vibration of one chemical bond and the angular torsional vibration of two bonds. Here again the molecule can only pass from one energy state to another state by a quantum leap. The order of magnitude of these energy jumps is 0.1 eV.

Electronic energy: An atom or a molecule can see, as a result of an excitation, one of its electrons placed on a more energetic orbital. The species is then electronically excited and the electronic energy levels are quantified. The energy levels is several in electronvolts (eV). An electronically excited species can go from one lower level to another higher absorbing energy. Conversely, the optically permissible passage from the upper level to the lower level is a de-excitation that allows the emission of a photon whose energy corresponds to the energy difference between the two levels.

The excited species can be: in a radiative state, which disappears by spontaneous emission in a few hundred nanoseconds or in a metastable excited state having a much longer lifespan and generally disappears by collisions, which often play an important role in the maintenance of the discharge as by example stepwise ionization or Penning ionization…

D. Photons:

Photons are most often emitted by de-excitation of electronic states, so they are energies or well-defined line spectra. Our electric discharges can emit photons in a wide spectral band ranging from Ultraviolet UV to infrared IR.

The number of photons emitted by the plasma can represent a significant part of the energy dissipated in the discharge. Photons can also influence on the discharge chemistry by gas or surfaces irradiation for photochemical or photobiology or photo-catalytic applications. This is particularly true for the VUV component.

2.3. Description of reactions types between species in plasma

The following table (Table II-1) summarize the collisions produced by electrons impact in an electric discharge

Table II-1: Collisions produced by electrons

Elastic collision	$e + A \rightarrow e + A$
Ionization	$e + A \rightarrow 2e + A^+$
Excitation	$e + A \rightarrow e + A^*$
Ionization (Penning)	$e + A^* \rightarrow 2e + A^*$
Dissociation	$e + AB \rightarrow e + A + B$
Dissociative ionization	$e + AB \rightarrow 2e + A^+ + B$
Dissociative attachment	$e + AB \rightarrow A^- + B$
Recombination	$e + A^+ + B \rightarrow A + B$

2.3.1. Inelastic collisions:

The inelastic collisions happened between electrons and neutrals in the ground state, because electron is the first to store energy by the electric field Among the many possibilities of reactions:

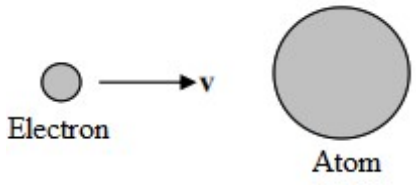

Fig. II-1: Electron acceleration toward heavy species

A. Ionization:

Under the action of an electric field, the electron which moves with kinetic energy $W=mv/2$ collides with the atom; with m is particle mass and v is particle velocity. If $W_c \geq W_i \rightarrow$ atom

ionization: $e+A \rightarrow 2e + A^+ + \Delta W$, with $\Delta W = W_c - W_i$: extra energy given to the released electron as kinetic energy. It is the most common ionization process in gases (Tilmatine, 2012).

B. Dissociative ionization:

Example: $e + N_2 \rightarrow 2e + N + N^+$

C. Excitation:

An excited atom A^* is an atom which has absorbed and stored energy. This happens when the kinetic energy is slightly less than ionization W_i.

If W_c is slightly less than $W_i \rightarrow$ excitation of the atom, and each gas has its value of energy excitation W_{ex}: $W_{ex} = eV_{ex}$ with: V_{ex} is excitation potential.

D. Dissociative attachment:

Example: $e + O_2 \rightarrow e + O^- + O$

All these inelastic collisions have an energy threshold; the electrons must have an energy greater than this threshold to give rise to the reaction. After the collision, the electron loses the threshold energy. To maintain the electric shock, these energy losses are compensated for by the action of the electric field, which constantly transfers energy to the electrons

2.3.2. Heavy species reactions:

The reactions between heavy species are more diverse and have a longer timescale than electronic reactions. They include all the reactions between an unstable species resulting more or less directly from a primary reaction and the gas.

These reactions types are implanted in the following table II-2 with examples:

Table II-2: Heavy species reactions types

Reactions types	**Examples**
Ion - molecule	$N_2^+ + N \rightarrow N^+ + N_2$
Radical - molecule	$O + O_3 \rightarrow O_2 + O_2$
Associative collision detachment	$O^- + O_2^* \rightarrow O_3 + e$

Dissociative recombination	$e + N_4^+ \rightarrow N_2^* + N_2$
Detachment by electronic impact	$e + O^- \rightarrow O + 2e$
Radical - radical	$NO + NO_3 \rightarrow NO_2 + NO_2$
Super-elastic collision	$e + N(D) \rightarrow e + N$
Radical excitation	$e + O(^1D) \rightarrow e + O$

2.3.3. Wall reaction:

Walls and surfaces can be subjected to a flow of particles and various chemical species. In this case, they are the site of a large number of reactions which can result either in a chemical modification of the surface (recombination, passivation, oxidation, nitriding, etc.), or in an erosion of the wall (etching), or finally in thin film formation (deposit).

3. DBD modeling:

Due to the complexity of the systems, simplified models with many approximations exist in the literature like the models (0D, 1D). These approaches make it possible to quantitatively estimate the fundamental characteristics of the plasma in a DBD reactor (electron density, temperature, etc.) with reasonable calculation times. Such models can be used in a first approach to select certain reactions and the associated basic data but cannot be used as a predictive tool.

It is obviously impossible to describe the movement of each particle in the plasma. To avoid this, we introduce the notion of distribution function for each species, this one being obtained by solving the Boltzmann equation:

3.1. Distribution function:

Each particle of the gas is defined by a position vector r which goes from the origin of the coordinate system to its center of gravity and by a speed vector v. We associate with the position vector and the speed vector two spaces of coordinates that we group together to form the phase space. At a time t, the probable number of particles $dN(r,v,t)$ located in the volume element dr^3 located around the point d^3r and animated with a speed v varying in the speed element dv^3 is defined by:

$$dN(r,v,t) = dr^3 dv^3 f(r,v,t) \quad \text{(II-5)}$$

With $f\left(t,r,v\right)$ the particle density distribution function. The density of particles at a point in the plasma at an instant *t*:

$$N\left(r,t\right)=\int f\left(r,v,t\right)dv^3 \tag{II-6}$$

We can define the average speed of a particle:

$$v=\frac{1}{N\left(r,t\right)}\int v\,f\left(r,v,t\right)dv^3 \tag{II-7}$$

3.2. Boltzmann equation:

The transport of a set of charged particles is statistically described by the Boltzmann equation:

$$\frac{\partial f_i}{\partial t}+\vec{v}_i.\overrightarrow{\nabla}_r.f_i+\frac{\vec{f}_i}{m_i}.\overrightarrow{\nabla}_v f_i=\left(\frac{\partial f_i}{\partial t}\right)_{col} \tag{II-8}$$

Its resolution makes it possible to know the distribution function fi of particle i at each point and at each instant. In our case, the external forces are those generated by the electric field, which consequently has an influence on the distribution functions. However, the electric field itself depends on the charge densities via the Poisson equation:

$$\nabla\vec{E}=\frac{e}{\varepsilon_o}\left(n^+-n^-\right) \tag{II-9}$$

Solving Boltzmann's equations is not an easy task, and coupling with electrical phenomena only increases the difficulty. We can distinguish three different approaches to model an electric discharge. The simplest, the fluid model responds to many approximations, but under certain conditions to have reliable results and quite quickly. In contrast, a so-called microscopic or particulate approach deals directly with the Boltzmann equation. Hybrid methods halfway between the previous two extremes have also been developed. The foundations of these three approaches will now be expressed.

3.3. Fluid model

The fluid model describes plasma based on the density, average velocity and average energy of species. The values of these macroscopic quantities are obtained by solving the continuity, flux and energy equations for each species in the plasma. These fluid equations are obtained by taking the velocity moments of Boltzmann's equation. Maxwell's (or Poisson's) equations are

coupled with the fluid equations to obtain the self-coherent electric and magnetic fields. The continuity equation is given in the form:

$$\frac{\partial n}{\partial t} + \overrightarrow{\nabla_r} n\vec{v} = \int_v \left(\frac{\partial f}{\partial t}\right)_{col} = S = n_e\left(\nu_i(r,t) - \nu_a(r,t)\right) - r(r,t)\, n_e n_p \qquad \text{(II-10)}$$

The two left terms of equation *(II-10)* correspond respectively to the time derivative of the density and to the divergence of the flux. The term on the right corresponds to the source term; it characterizes all the collisional processes of the creation and loss of the species considered. Charged particle creation and loss frequencies are then defined, which are a function of the nature of the gas considered, of the species distribution function and of pressure.

Fluid simulations are more appropriate for high-pressure discharges where non-local effects tend to be less important due to the very frequent collisions between particles. However, the non-local phenomenon can occur even in atmospheric pressure discharges, if the electric field is strong.

Fluid models are widely used because of their advantage in computing speed. In addition, a large number of species can be modeled allowing the study of complex chemistry with many reactions. These problems are more difficult to deal using PIC codes.

The basis of fluid models requires two main hypotheses to limit the number of equations and close the system of equations obtained.

- The first assumption concerns the physical order to limit the number of hydrodynamic equations generated by the Boltzmann equation. For example, we can go up to the second moment of the Boltzmann equation (order 1) or up to the third moment (order 2). In order 1, we consider the conservation equation of density and momentum while in order 2; we add the conservation equation of energy density.
- The second assumption concerns the condition of closing the system, which requires additional assumptions. At the first order, the system is closed by adopting the local field hypothesis where the transport and reaction parameters are assumed to depend directly on the electric field prevailing locally at a given instant in the electric discharge. Pre-tabulated basic data are therefore used as a function of the reduced electric field E / N. At the second order, the system is closed using the local energy hypothesis where the transport and reaction parameters are assumed to depend directly on the average energy of the charged particles.

3.4. Particle-in-cell PIC model:

PIC Simulations take advantage of the collective behavior of charged particles in plasmas to model the kinetics of various species by simulating a reduced number of digital particles (also called super - particles or macro particles). Since super - particles are tracked by solving the fundamental equations (Newton - Lorentz equation for the motion of charged particles coupled with Maxwell equations for the self-consistent calculation of electric and magnetic fields) without making any assumption on their speed distribution, the kinetics of each species is simulated with very few approximations. Typically, electrons and ions are simulated. Neutrals are assumed to be evenly distributed in space.

3.5. Hybrid model:

The term hybrid model is used to denote another simulation by considering two groups of electrons. These two electronic population groups are relatively independent. The first includes the majority of low energy electrons. The second group is made up of energetic electrons accelerated in the presence of the electric field. In order to optimize the computation time, the electrons of the first group are processed using the fluid model. On the other hand, the fast electrons are treated by adopting a Monte Carlo (MC) type method.

In this model, the ionization source term and the electron impact excitation source term will not appear in the hydrodynamic equations because the electrons responsible for these two phenomena are the most energetic electrons. So, only the terms of low energy reactions (recombination, attachment, etc.) remain as the source term in the transport equations.

This model also allows a description of anisotropic regions (sheaths) with a reasonable computation time, as it allows describing the particle-surface interactions, which adjusted between the complete physical description, the computation time and the precision.

4. Physical model

In this section, we describe the physical discharge model we used, the approximations it involves, and the basic data it uses. The one-dimensional model used in our work, is based on the fluid description of the three moments of the Boltzmann equation for the transport of electrons, ions coupled with the Poisson equation, and with the kinetic equations characterizing the evolution of the population of excited states.

4.1. Transport equation:

From the distribution function, we can have access to all the macroscopic quantities such as density, average velocity, average energy. The average density of particles is written as:

$$N(r,t) = \int f(r,v,t)\,dv^3 \tag{II-11}$$

The average value χ:

$$\chi(r,t) = \frac{1}{n_s(r,t)} \int \chi_s f_s(r,v,t)\,dv^3 \tag{II-12}$$

It is therefore possible to obtain the macroscopic equations by integrating the Boltzmann equation multiplied by the value χ

For such a description, the Boltzmann equation is replaced by three equations that describe these mean values. They are the continuity equation for the densities, the momentum equation for the average speeds, and the energy equation for the average energy of electrons. These equations called moments of the Boltzmann equation are the results of integrating the Boltzmann equation multiplied by the physical macroscopic quantities $\chi(v)$ varying as polynomials of the speed over the speed space.

A. Continuity equation:

When $\chi(v)$ equals 1, we get the first moment of the Boltzmann equation, which is the continuity equation:

$$\frac{\partial n_{e,p}}{\partial t} + \nabla_{\vec{r}} . n_{e,p} = S_{e,p} \tag{II-13}$$

This equation represents the conservation of charge, n represents the density of charged particles (e refer to electrons, and p refer to positive or negative ions). S is the source term of the continuity equation, it accounts for the creations (ionizations) and losses (attachments, recombination) of charged particles. It is written as follows:

$$S_{e,p} = n_e\left(\nu_i(r,t) - \nu_a(r,t)\right) - r(r,t)\,n_e n_p \tag{II-14}$$

ν_i is the ionization frequency and ν_a is the attachment frequency. $r\,(r,t)$ is the electron-ion recombination (loss) coefficient. This term takes into account collisions between charged particles: it is small compared to the ionization term during the current pulse. The ionization and

attachment frequencies are dependent on the electronic distribution function (which is unknown and about which one has to make assumptions).

B. Momentum transfer equation

When $\chi(v)$ equals $m\,v$, the momentum with a few simplifications, the following momentum transfer equation:

$$n_{e,p}\bar{v}_{e,p} = a\,n_{e,p}\,\mu_{e,p}E - \nabla\left(D_{e,p}N_{e,p}\right) \tag{II-15}$$

$\bar{v}_{e,p}$is the mean velocity, E is the electric field, μ and D are the mobility and the diffusion coefficient respectively, 'a' is –1 for electrons and negative ions and +1 for positive ions. In this equation, the flow of charged particles is the sum of a derivative term reflecting the influence of external forces (here, only the electric field) and a diffusion term reflecting the effect of the density gradient.

C. Energy equation:

By replacing $\chi(v)$ in the Boltzmann equation by $mv^2/2$, we get the scalar energy equation which is the third moment of the Boltzmann equation:

$$\frac{\partial n_e\bar{\varepsilon}_e}{\partial t} + \frac{5}{3}\nabla\left[n_e\bar{\varepsilon}_e\bar{V}_e\right] + \nabla.q - n_e\,e\bar{V}_e\,E = -n_e\bar{\varepsilon}_e\nu_\varepsilon \tag{II-16}$$

where ∇q is the change in thermal energy, ν_ε is the energy exchange frequency, $\bar{\varepsilon}_e$ is the average energy.

The space charges due to the presence of ions and electrons are sufficient to distort the electric field. These modifications in the electric field cause evolve of the distribution function by the term which take account the action of external forces. To correctly describe the discharge, it is therefore necessary to couple the resolution of this system of equations with that of the Poisson's equation because this equation gives the variations of the electric field as a function of the space charge. The Poisson equation is written:

$$\nabla E = \frac{|e|}{\varepsilon_0}\left(n_p - n_e\right) \tag{II-17}$$

with: ε_0 is the permittivity of vacuum.

The system formed by the three equations coupled to Poisson's equations describes the discharge, however the system is not closed (there are no solutions). It is then necessary to perform approximations on the energy distribution function of the charged particles to close the system.

5. Description of the mathematical model used in our calculations

To describe the kinetics of the particles in the DBD dischqrge, we used the fluid model which consists in replacing the Boltzmann equation by these moments using the drift diffusion approximation (Prevosto L, 2016), these equations are described below (Gadkari S, 2017).

5.1. Basic equation:

The particle continuity equation is given by:

$$\frac{\partial n_{e,i,n}}{\partial t} + \nabla.\Gamma_{e,i,n} = S_{e,i,n} \quad \text{(II-18)}$$

$$S_{e,i,n} = \sum_{j=1}^{M} c_{j,e} R_j \quad \text{(II-19)}$$

$$\Gamma_{e,i} = \mu_{e,i} E n_{e,i} - D_{e,i} \nabla n_{e,i} \quad \text{(II-20)}$$

$$\Gamma_n = -D_n \nabla n_n \quad \text{(II-21)}$$

where, the indicators e, i and n refer to electrons, ions and neutrals respectively. With n_e, n_i and n_n are the number densities. Γ_e, Γ_i and Γ_n are the particles flux of electron, ion, and neutrals respectively. $S_{e,i,n}$ is the production or loss rate for every species in each chemical interaction occur in discharge. $c_{j,e}$ represent stoichiometric number of electrons j, R_j the reaction rate and M is the number of electron reactions. E is the electric field, $D_{e,i}$ and $\mu_{e,i}$ are the diffusion coefficient and mobility of electron and ions respectively.

The electron energy equation is given by:

$$\frac{\partial n_\varepsilon}{\partial t} + \nabla.\Gamma_\varepsilon + E.\Gamma_e = S_\varepsilon \quad \text{(II-22)}$$

The flux including source expression settled as (Hagelaar GJM, 2005):

$$\Gamma_\varepsilon = -\mu_e E n_\varepsilon - D_e \nabla n_\varepsilon \quad \text{(II-23)}$$

Where ε refers to energy, with n_ε is the electron energy density, S_ε : Energy loss or production by inelastic collisions.

$$S_\varepsilon = -e\Gamma_e.E - \sum_{j=1}^{P} c_{(j,e)} R_j \varepsilon_j \quad \text{(II-24)}$$

P is the number of inelastic collisions, the energy lost or produced in a collision represented by ε_j which is considered similar to the threshold of a reaction. In the previous expressions, the source coefficients specified through the system stoichiometry, using rate coefficients (Ghassemi M, 2011).

$$-\nabla.\varepsilon_0.\varepsilon_r \nabla V = \rho_q \quad \text{(II-25)}$$

with ε_0 is the vacuum permittivity and ε_r is the relative permittivity. ρ_q is the space charge density

$$\rho_q = e\left(\sum_{k=1}^{N} Z_k n_k - n_e\right) \quad \text{(II-26)}$$

e: is the absolute value of electronic charge, Z_k is the electric charge, E is the electric field and V is the electric potential.

The properties of the dielectric are described by the following relation:

$$D = \varepsilon_0 \varepsilon_r E \quad \text{(II-27)}$$

5.2. Boundary conditions:

The impact of heavy species on the surface of the dielectric barrier represents the most important parameter governing the behavior of the discharge.

- The accumulation of charges on the surface of the dielectric, resulting from variations in the flows of electrons and ions is described as follows (Gadkari S, 2017):

$$-n.\left(D_1 - D_2\right) = \rho_s \quad \text{(II-28)}$$

$$\frac{d\rho_s}{dt} = J_i + J_e \quad \text{(II-29)}$$

with ρ_s is the density of surface charge. On the boundaries, the electric fields displacement is defined by D_1 and D_2. J_i : the total current density of ion, and J_e the total current density of electron.

- At electrode surface, the electron energy is written as (Boeuf JP, 1995):

$$\Gamma_\varepsilon.\mathbf{n} = \frac{1}{3} v_{e,th} \bar{\varepsilon} n_e \tag{II-30}$$

where **n**: boundary normal vector and $v_{e,th}$: electron thermal. $\bar{\varepsilon}$: is the mean energy of electron.

- For electron, electron energy, and heavy species beside to both sides of the gap, the boundaries conditions are written as (Wei LS, 2016):

$$\begin{cases} -\mathbf{n}.\Gamma_e = 0 \\ -\mathbf{n}.\Gamma_\varepsilon = 0 \\ -\mathbf{n}.\Gamma_k = 0 \end{cases} \tag{II-31}$$

Surface reactions neutralize ions, at the scale of dielectric surfaces, the surface interaction coefficient is used, specifying the perspective of a species that will react on the surface [16], this is described mathematically by the relation below:

$$\Gamma_k = \frac{\beta_k}{4} \sqrt{\frac{8 k_B T_k}{\pi m_k}} n_k \tag{II-32}$$

where k refer to heavy species, β_k is the surface interaction coefficient, k_B Boltzmann's constant, m_k and T_k are respectively the temperature and the mass of heavy species.

5.3. Equivalent electrical circuit model

The equivalent circuit of a dielectric barrier discharge divided into two parts: the dielectric barrier equivalent to a capacitor C_d and the positive column equivalent to a resistance R_p.

The capacitor C_d represents the equivalent capacity of two layers of dielectric. It is the equivalent of two capacitors C_{d1} and C_{d2}, it given by the following formula:

$$C_d = \frac{C_{d1} C_{d2}}{C_{d1} + C_{d2}} \tag{II-33}$$

In the case of coplanar geometry, this capacitor can be given by the following expression:

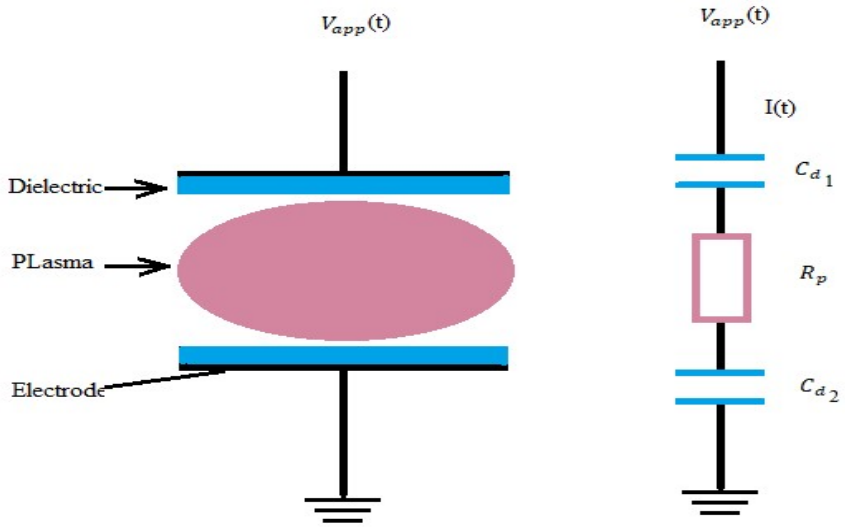

Fig. II-2: The equivalent circuit of DBD

$$C = \frac{\varepsilon_o \varepsilon_r S}{d} \tag{II-34}$$

with *S*: is the dielectric surface and *d*: is the thickness of the dielectric.

The discharge is shown schematically by a current source, $i_{dis}(t)$ from the electrical diagram given in figure II-2, we have:

$$V_{DBD}(t) = V_{dis}(t) + V_{diele}(t) \tag{II-35}$$

$$i_{gap}(t) = C_{gap}\frac{dV_{dis}(t)}{dt} \tag{II-36}$$

The current of the discharge $i_{dis}(t)$ is then obtained:

$$\begin{aligned} i_{dis}(t) &= i_{reactor}(t) - i_{gap}(t) = i_{reactor}(t) - C_{gap}\frac{dV_{dis}(t)}{dt} \\ &= i_{reactor}(t) + C_{gap}\frac{dV_{dis}(t)}{dt} - C_{gap}\frac{dV_{cell}(t)}{dt} \end{aligned} \tag{II-37}$$

The discharge current $i_{dis}(t)$ can be evaluated, if the applied voltage, $V_{app}(t)$ and the cell current, $i_{reactor}(t)$ are measured:

$$i_{dis}(t) = \left(1 + \frac{C_{gap}}{C_{diele}}\right) i_{reactor}(t) - C_{gap}\frac{dV_{app}}{dt} \tag{II-38}$$

6. Geometry of model and simulation and initial conditions used:

6.1. Geometry:

We considered a 1D geometry consisting of two parallel plates covered with a dielectric coating (Alumina Al_2O_3 96%). The confined space of gas between the dielectric surfaces is 1mm as shown in figure II-3.

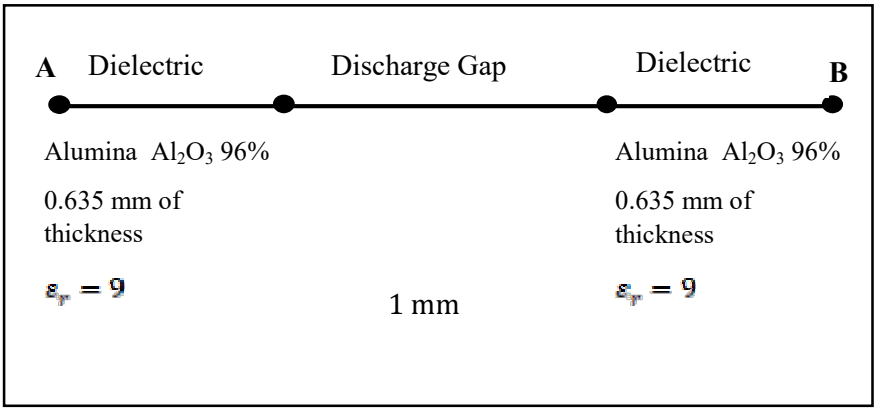

Fig. II-3: Geometry used in our model

6.2. Simulation conditions:

The table II-3 summarizes the discharge parameters used in our model

Table II-3: Discharge parameters

Discharge parameters	Data
Pressure	760 atm
Temperature	295 K
Gap distance	1 mm
Dielectric thickness	0.635 mm
Dielectric material	Al_2O_3 96%
Dielectric relative permittivity ε_r	9
Applied voltage wave form	Sinusoidal
Applied voltage frequency	3kHz
Peak to peak voltage	12 kV

6.3. Initial conditions

Initial distributions of electron and ion densities: $n_e = 2\times10^4 cm^{-3}$, $n_i = 10^4 cm^{-3}$

Initial distribution of metastable density: $n_n = 0$

Initial average electronic energy: $\bar{\varepsilon}=5V$

7. Numerical model

There are several methods for solving partial differential equations. They are analytical, numerical or mixed (semi-analytical). Analytical methods are the first methods used. They consist to solve the differential equations analytically with the separation technique of variables.

They are restricted to simple geometries in a one-dimensional approach, or sometimes in two-dimensional problems (Zienkiewick, 1977).

The finite difference method consists in replacing approximately the differential operator by a difference operator, this by Taylor series expansion. This method gives satisfactory results in many problems, but it is still limited to regular configurations. The finite volume method, the field of study in this method is subdivided into elementary volumes so that each volume surrounds a node of the mesh (that of finite differences). The equation is integrated on each elementary volume. To calculate the integral in this elementary volume, the unknown function is represented using an approximation function (linear, exponential) between two consecutive nodes. Then, the integral form is discretized in the domain of study. This leads to a more precise solution than the finite difference method.

7.1. The finite element method:

The finite element method consists in subdividing the field of study into elementary fields called finite elements (linear, triangular, tetrahedral element, etc.), as shown in figure II-4 and expressing the unknown on each element by the interpolation functions according to the values of the unknown at each of the vertices of this element is at the centers.

For two-dimensional domains, the mesh elements are often triangles, while in three-dimensional problems they are more tetrahedral or prismatic (K. Hameyer, 1999). Figure II-4 presents some typical elements for one-dimensional and two-dimensional problems.

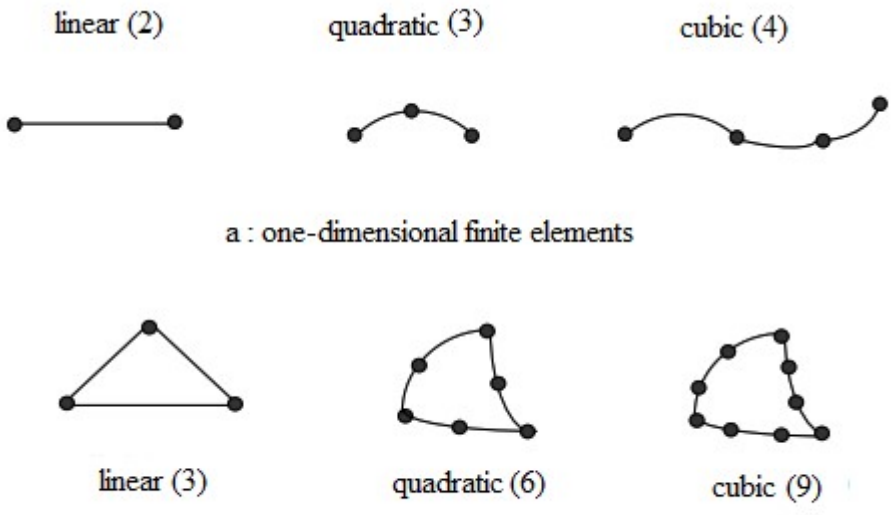

Fig. II-4: Mono and two-dimensional finite elements

Each finite element consists of a set of nodes and edges. The unknown variable is approximated on each finite element using polynomial interpolation. The search for a solution by Finite Elements therefore consists in determining which local field attributes to each subdomain so that the total field obtained by summation of these local fields, is close to the exact solution of the problem. The main stages in the construction of a finite element model are as follows:

- Discretization of the continuous medium into sub-domains;
- Construction of the nodal approximation by subdomain;
- Calculation of the elementary matrices corresponding to the integral form of the problem
- Assembly of elementary matrices;

7.2. Diagram of numerical calculation by COMSOL multi-physics:

First, we introduce the constants used during the calculation. After entering the data we need, we define the geometry, introducing the dimensions. Then we choose the modules to use from the library of COMSOL modules by choosing the type of the desired element as well as the mode of analysis (time dependent, stationary, parametric ....)

The diagram of figure II-5 summarizes the organization of the numerical computation of the coupling.

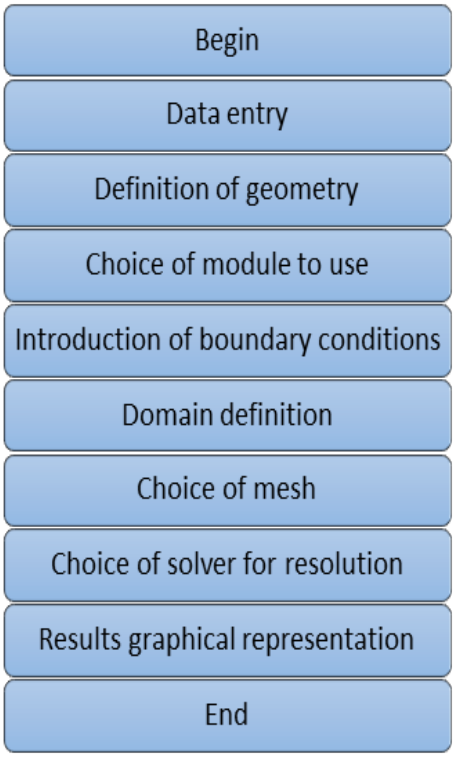

Fig. II-5: flowchart of calculation in COMSOL Multi-physics

8. Conclusion

In this chapter, we have presented the necessary elements that are included in the modeling of a DBD such as existing species during the discharge and the types of collusion between them. After that we have presented the mathematical model of the discharge controlled by dielectric barriers at atmospheric pressure, and the various equations deduced from the model, then we detailed how to calculate the electrical characteristics of the discharge. This model is based on solving the Boltzmann equation.

We have discretized the equations of the model, by a numerical method commonly practiced; it is the finite difference method. We have chosen this method because it is easier to access, since it is based on two concepts, the discretization of the equations on the one hand, and the convergence of the numerical scheme thus obtained on the other hand. The transport parameters are also defined and the initial and boundary conditions.

The next chapters consist to present the chemical reactions and data validation of the three-model proposed in our work, first we start with nitrogen model the oxygen model and finely dry air model using the nitrogen and oxygen mixture gas.

Bibliography

X. Zanhua. S, «Plasma decoloration of dye using dielectric barrier discharges with earthed spraying water electrodes,» *Journal of Electrostatics vol 66,* pp. 476-481, 2008.

Young. S. M, «Degradation of an azo dye Orange II using a gas phase dielectric barrier discharge reactor submerged in water,» *Chemical Engineering Journal, Volume 142,,* pp. 56-64, 2008.

Y. H. Choi, «One-dimensional discharge simulation of nitrogen DBD atmospheric pressure plasma,» *Thin Solid Films, vol. 506,* p. 389–395, 2006.

C. Wadhwa, High Voltage Engineering 2nd edition, New Age International., 2007.

U. Kogelschatz, «High-intensity sources of incoherent UV and VUV excimer radiation for low-temperature materials processing,» *Applied Surface Science 168,* pp. 29-36, 2000.

U. Kogelschatz, «From ozone generators to flat television screens: history and future potential of dielectric-barrier discharges,» *Pure Appl.Chem., Vol. 71, No. 10,* pp. 1819-1828, 1999.

Y. A. Trishin, «Acceleration of rigid bodies by coherent jets,» *Journal of Applied Mechanics and Technical Physics 21,* p. 696–699, 1980.

W. Thornhill, «The Z-Pinch Morphology of Supernova 1987A and Electric Stars.,» *IEEE Transactions on Plasma Science, vol. 35, issue 4,* pp. 832-844, 2007.

G. Thome, «Kurzzeitphysik,» *Springer Berlin,* p. 8, 1967.

T. IKEMATSU, «Advanced oxidation Advanced oxidation,» *Vacuum 73 ,* p. 579–582, 2004.

P. Stern, «The Fluorescent Lamp: A plasma you can use,» *Retrieved ,* pp. 5-19, 2010.

E. Sozer, Gaseous Discharges and Their Applications as High Power Plasma Switches, 2008.

M. Sobolewski et J. &. B. Langan & Felker, «Electrical optimization of plasma - enhanced chemical vapor deposition chamber cleaning plasmas,» *16. J. Vac. Sci. Technol,* pp. 173-182, 1997.

S. Kanazawa, «Stable glow plasma at atmospheric pressure,» *J. Phys. D: Appl. Phys. 21,* p. 838, 1988.

S. Flügge, «The glow discharge at low pressure,» *Encyclopedia of Physics, volume Volume 22:,* pp. 53-61, 1956.

J. Roth, «Glow discharge-like characteristics of a oaugdp revealed by computer modeling,» *IEEE International on Plasma Science,* p. 288, 1998.

B. Ronny, «Dielectric barrier discharges: progress on plasma sources and on the understanding of regimes and single filaments,» *Plasma Sources Science and Technology,* p. 053001, 2017.

L. Reynard, Thèse de doctorat, Modélisation tridimensionnelle de l'amorcage de l'arc électrique dans un disjoncteur basse-tension, Lyon: Ecole Centrale de Lyon, 2006.

Renate Viebahn-Hänsler, «Ozone in Medicine: The Low-Dose Ozone Concept—Guidelines and Treatment Strategies,» *Ozone: Science Engineering, Volume 34, Issue 6, ,* pp. 408-424, 2012.

Y. P. Raizer, Gas Discharge Physics, Allen, John E. (Ed.), 1991.

G. J. Pietsch, «The Development of Dielectric Barrier Discharges in Gas Gaps and on Surfaces,» *Journal of Physics D: Applied Physics. 33(20),* p. 2618, 2000.

S. Pekárek, «Non-Thermal Plasma Ozone Generation,» *Acta Polytechnica Vol. 43 No. 6,* 2003.

W. H. Organisation, «world health organisation,» 14 june 2019. [En ligne]. Available: https://www.who.int/news-room/fact-sheets/detail/drinking-water.

N.N. GUIVAN, «Planar UV excilamp excited by a surface barrier discharge,» *J. Phys. D: Appl. Phys. 38,* p. 3188–3193, 2005.

Z. Y. Meirovich Ariel, «Treatment of Methylene Blue water solution by submerged pulse arc in multielectrode reactor,» *Journal of Water Process Engineering,13,* pp. 53-60, 2016.

Mededovic Thagard Selma, «lasma-based water treatment:development of a general mechanistic model to estimate the treatability of different types of contaminants,» *Journal of Physics D: Applied Physics,,50(1),* p. 014003, 2017.

S.-C. Lin, «Necessary conditions for the homogeneous formation of pulsed avalanche discharges at high gas pressures,» *J. Appl. Phys., 51,* pp. 210-222, 1980.

J. Lichtenberg, Principles of Plasma Discharges and Materials Processing, Second Edition, John Wiley & Sons, Inc., 2005.

LeannePitchford, «ProjectsANR (Microplasré, 2005) Microdéchargeset jets de plasma,» Toulouse, 2005.

I. Langmuir, "Oscillations in Ionized Gases," *Proceedings of the National Academy of Sciences .14 (8),* p. 627–637, 1928.

A. Labergue, PhD thesis. Etude de décharges électriques dans l'air pour le développement d'actionneurs plasmas– Application au contrôle de décollements d'écoulements, université de Poitiers, 2005 .

U. Kogelschatz, «Filamentary and diffuse barrier discharges,» *J. Phys. D: Appl. Phys vol. 20, ,* p. 1421, 1987.

U. Kogelschatz, «Dielectric-barrier Discharges: Their History, Discharge Physics,cs, and Industrial Applications,» *Plasma Chemistry and Plasma Processing, Vol. 23,,* 2003.

U. Kogelschatz, « Silent discharges for the generation of ultraviolet and vacuum,» *Pure & Appl. Chem., Vol. 62, No. 9,* pp. 1667-1674, 1990.

K. C. Kao, Dielectric Phenomena in Solids, London: Elsevier Academic Press, 2004.

K. OKAZAKI, «Direct conversion from methane to methanol for high efficiency energy system with exergy regeneration,» *Energy Conversion and Management 43 ,* p. 1459–1468, 2002.

S. K Koga, «Formation of carbon nanoparticle using Ar+CH4 high pressure nanosecond discharges,» *Journal of Physics: Conference Series 518 ,* p. 012020, 2014.

Jingwei. F, «Gas–liquid hybrid discharge-induced degradation of diuron in aqueous solution,» *Journal of Hazardous Materials Volume 164, ,* pp. 838-846, 2009.

Jingwei. F, «Degradation of diuron in aqueous solution by dielectric barrier discharge,» *Journal of Hazardous Materials Volume 154, Issues 1–3,* pp. 1081-1089, 2008.

O. M. Jean-marie cormiers Ahmed Khacef, «Dépollution des effluents gazeux par plasma; A la pointe de l'instrumentation et de la technologie,» *Centre National de la Recherche Scientifique:(CNRS) France. n.d.,* 2002.

J. Y Jeongy, « Etching materials with anatmospheric-pressure plasma jet,» *Plasma Sources Sci. Technol.,* pp. 282-285, 1998.

Iwabuchi Masashi, «Simultaneous Decomposition of Phenol and Sodium Formate by Discharge Inside Bubble in Water,» *Transactions of the Materials Research Society of Japan,41(2),* pp. 183-187, 2016.

C. M. W. INC, «OZONE PROCESSING,» 2017. [En ligne]. Available: https://www.coloradomedicalwaste.com/ozone-technology/.

https://en.wikipedia.org/wiki/Dielectric, «Dielectric,» 30 January 2021. [En ligne]. Available: https://en.wikipedia.org/wiki/Dielectric.

Holger Krause, «Degradation of the endocrine disrupting chemicals (EDCs) carbamazepine, clofibric acid, and iopromide by corona discharge over water,» *Chemosphere,* pp. 163-168, 2009.

S. Hammami, PHD thesis. Étude de dégradation des colorants de textile par les procédés d'oxydation avancée. Application à la dépollution des rejets industriels, l'Université Paris-Est et Tunis El Manar, 2008.

Gharagozalian Mehrnaz, «Water treatment by the AC gliding arc air plasma,» *Journal of Theoretical and Applied Physics,* pp. 171-180, 2017.

G. Bauville, «Proceeding des résumés du 8eme congrès "Plasma" de la société Française de physique 5-7 Mai,» chez *Traitement de tôles métalliques par décharge à barrière diélectrique monopolaire fonctionnant à pression atmosphérique*, Cadarache- St Paul Lez Durance., 2003.

F. G. Fridman, «Floating electrode dielectric barrier discharge plasma in air promoting apoptotic behavior in melanoma skin cancer cell lines,» *Plasma Chemistry and Plasma Processing, 27(2),* pp. 163-176, 2007.

J. P. Freidberg, «Plasma Physics and Fusion Energy,» *Cambridge University Press,* p. 121, 2008.

Z. Falkenstein, «Applications of dielectric barrier discharges,» chez *in High-Power Particle Beams*, BEAMS ’98. Proceedings of the 12th International , 1998.

F. MASSINES, «The Role of Dielectric Barrier Discharge Atmosphere and Physics on Polypropylene Surface Treatment,» *Plasmas and Polymers, Vol. 6, ,* 2001.

Eun Ha Choi, «Vacuum ultraviolet luminous efficiency and plasma ion density in alternating current plasma display panels,» *Applied Physics Letters 81,* p. 3341, 2002.

E.A. SOSNIN, « Capacitive discharge exciplex lamps,» *J.Phys. D: Appl. Phys. 38 ,* p. 3194–3201, 2005.

Y. J. Du ChangMing, «Degradation and Discoloration of Textile Dyes Using Gliding Arc Plasma Combined with Fenton Catalysis,» pp. 21-39, Plasma Combined with Fenton Catalysis.

M. D, PHD Thesis .Destruction du tributylphosphate par effluvage électrique. Utilisation d'un réacteur à décharges glissantes, Université de Rouen., 1999..

J. D. Craggs, «Electrical breakdown of gases,» *Oxford (Clarendon Press),* pp. vii, 507, 1953.

K.-W. Cheng, «Fluid Modeling of a Nitrogen Atmospheric-Pressure Planar Dielectric Barrier Discharge Driven by a Realistic Distorted Sinusoidal Alternating Current Power Source,» *Japanese Journal of Applied Physics ,* p. 116001, 2012.

F. F. Chen, «Introduction to Plasma Physics and controlled fusion,» *Springer International Publishing,* pp. 2-3, 1984.

Božidar Filipović-Grčić, «Estimation of Load Capacitance and Stray Inductance in Lightning Impulse Voltage Test Circuits,» *Electric Power Systems Research, Volume 119,* pp. 439-446, 2015.

C. S. Bournet, PhD Thesis, Design et réalisation d’un réacteur plasma à pression atmosphérique pour des traitements de surface dans le domaine des biomatériaux, Université de Laval , 2007.

Alban.Sublet, PhD thesis, Caractérisation de décharges à barrière diélectriques atmosphériques et sub-atmosphériques et application à la déposition de couches d’oxyde de silicium, Ecole polytechnique fédérale de Lausanne, 2007.

Ajo Petri, «Pulsed Corona Discharge in Water Treatment: The Effect of Hydrodynamic Conditions on Oxidation Energy Efficiency,» *Industrial & Engineering Chemistry Research,* pp. 7452-7458., 2015.

Abdul SYAKUR Badrus ZAMAN, «International Conference on Information Technology,» chez *Application of dielectric barrier discharge plasma forreducing Chemical Oxygen Demand (COD) on industrial rubber wastewater*, 2017.

A.M. POINTU, "Plasmas froids de décharge : Propriétés électriques" Les techniques de l’ingénieur, 2007.

Y. ZHANG, « Lifetime investigation of excimer UV sources,» *Applied Surface Science 168 ,* pp. 296-299, 2000.

«Plasma (physics),» 15 January 2021. [En ligne]. Available: http://en.wikipedia.org/wiki/Plasma_(physics).

A. TILMATIN, *Cours :Chapitre 2 : Phénomènes d'ionisation dans les gaz,* 2012.

O. Zienkiewick, the finite element method, Mc Graw Hill, 3rd edition, 1977.

K. Hameyer, «The classification of coupled field problems,» *IEEE Transactions On Magnetics, 35(3):1618–1621,,* vol. 35, n° %13, p. 1618–1621, 1999.

Prevosto L, «Modelling of an Atmospheric Pressure Nitrogen Glow Discharge Operating in High-Gas Temperature Regimes,» *Plasma Chem Plasma Process ,* 2016.

Gadkari S, «Fluid model for a partially packed dielectric barrier discharge plasma reactor,» *Physics of Plasmas,* vol. 24, 2017.

Hagelaar GJM, «Solving the Boltzmann equation to obtain electron transport coefficients and rate coefficients for fluid models,» *Plasma Sources Sci. Techno,* vol. 14, p. 722–733, 2005.

Ghassemi M, «Electrical Insulation Conference,» chez *Dielectric Barrier Discharge (DBD) Dynamic Modeling for High Voltage Insulation*, Annapolis, Maryland, USA, 2011.

Boeuf JP, «Two-dimensional model of a capacitively coupled rf discharge and comparisons with experiments in the gaseous electronics conference reference reactor,» *Phys. Rev ,* vol. E, n° %151, p. 1376e1390., 1995.

Wei L .S, «A numerical study of species and electric field distributions in pulsed DBD in oxygen for ozone generation,» *Vacuum,* vol. 125, pp. 123- 132, 2016.

Chapter III:

Dielectric barrier discharge modeling in pure nitrogen

1. Introduction:

Dielectric barrier discharges are used as sources of neutral (atoms, radicals, excited molecules) and ionized (positive and negative ions) species generated at atmospheric pressure. The chemical and energetic properties of these cold plasmas are used in processes of treatment and / or modification of the surface state of materials and for the deposition of thin films as well as etching. To improve these processes, it is necessary to have a good understanding of the electrical, energetic and chemical properties as a function of the various operating parameters, with the help of models.

In this chapter, a simulation of the behavior of the discharge is carried out according to the state of the newly created species by varying the different parameters used for the creation of this type of plasma. The one-dimensional model used for the simulation of DBD in nitrogen considers the most important chemical reactions from reliable and revised previous studies. The results of the calculations obtained are compared with the available experimental data

2. Basic data of charged particles in nitrogen:

2.1 Macroscopic database:

- **Ion mobility**

The physical quantity ion mobility K is defined as the proportionality factor between an ion's drift velocity v_d in a gas and an electric field of strength **E**.

$$\mathbf{v_d} = K.\,\mathbf{E} \qquad \text{(III-1)}$$

Ion mobility's are commonly reported as reduced mobility's, correcting to standard gas density n_0, which can be expressed in standard temperature $T_0 = 273\,K$ and standard pressure $p_0 = 1013\,hPa$. This does not correct for other effects than the change in gas density and the reduced ion mobility is therefore still temperature dependent (Wikipedia, 2020).

$$K_0 = K\frac{n}{n_0} = K\frac{T_0}{T}\frac{p}{p_0} \qquad \text{(III-2)}$$

Reduced mobility K_0 characterizes the displacement of the ion cloud under the action of the reduced electric field $E\,/\,N$, this is the phenomenon of ion drift.

In our model the mobility coefficients of ions are taken from (Moseley ZT, 1969) and (Ellis HW, 1976) using the reduced mobility expression K_0 defined by:

$$K_0 = K \times \left(237 / T_g\right) \qquad \text{(III-3)}$$

Where T_g is the gas temperature at which the measurement of mobility K was made.

2.2. Cross section electron-Nitrogen:

Electrons with an energy range from10^{-3}eV to $10{,}000\ eV$ interact with N_2, elastically and inelastically. An inelastic collision occurs when the molecules are left in an excited state with a lifetime greater than the relaxation time of the molecular gas. Inelastic reactions can leave the molecule in a rotational, vibrational, or electronically excited state. Electrons can also dissociate the molecule if the excited state is weakly bound or they can produce ionization. Inelastic interactions have threshold electron energy, which is also the energy lost per inelastic collision. The probability for each of these types of collisional interactions to occur is quantified by the cross section, which is measured in unit area.

For electrons in this energy range, it is common to use an effective momentum transfer cross section, which includes all elastic and inelastic collisions that transfer momentum. This is a convenient parameter to use in the Boltzmann equation. For each cross section, the type of cross section, original reference for the cross-section data, and the last time the cross-section data were changed, or updated, in the database are provided. The changes to the cross sections are made so that, for a complete set of cross sections, the accuracy of swarm and transport parameters calculated with a Boltzmann solver should be within 10% (Pancheshnyi, 2012). Accuracy is based-off of experimental measurements or a sensitivity test when no experimental data are available. The cross sections shown in the figure below are plotted for the energy range published on the LXcat website in the Phelps database. BOLSIG+ extrapolates cross sections by adding data points beyond the last published energy by increasing ε by a factor 1.5 for ε up to 10 keV and assuming that the cross section decreases as ln(ε)/ε (Hagelaar, 2005).

Figure III-1 and Figure III-2 provides information on the energies at which the corresponding cross section is significant. The legend is tabulated in table III-1. The elastic scattering cross section is not plotted in figure III-1 for N_2, or figure III-2 for N, but is included in the given effective momentum transfer cross section (labeled as 1). The momentum transfer cross section extends over all energies since it is dominated by elastic scattering. Momentum transfer has a peak at around 2 eV, which is due to the large rotational and vibrational resonances around that energy (labeled as 2–11). The low-energy tail of the rotational cross section (labeled as 2) extends to the lowest energies of all of the inelastic cross sections. Higher-energy electronic excitation cross sections (labeled as 12–23) usually have a maximum at around 10–11 eV but are

commonly an order of magnitude or lower than the vibrational cross section. An exception to this is singlet-state excitation (labeled as 24) which has a high-energy tail that corresponds to a relatively large cross section. The ionization cross section (labeled as 25) is also large at high energies.

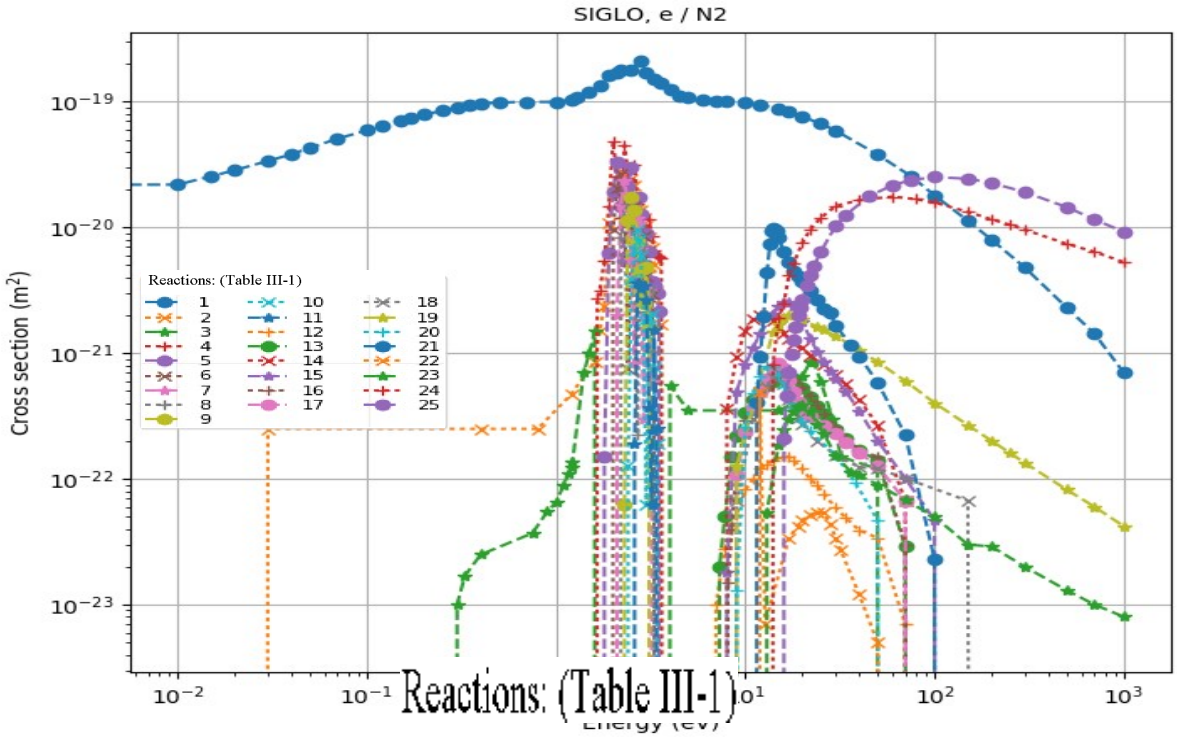

Fig. III-1: Cross sections for electrons interacting with N2 [Phelps, 2014a]

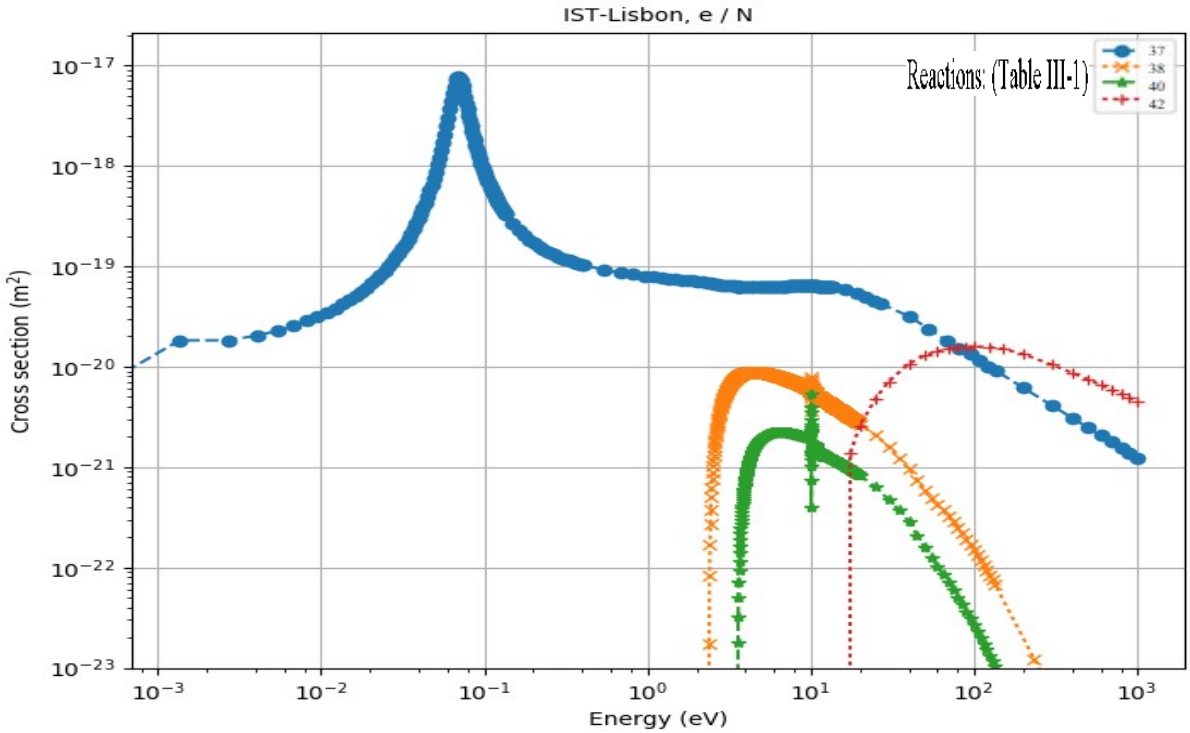

Fig. III-2: Cross sections for electrons interacting with N [Phelps, 2014a]

2.3. Electron-neutral cross sections validation by Transport parameters:

- **Monte-Carlo Method:**

The Monte-Carlo algorithm simulates the transport of a cloud of N_i ions of charge q and mass m ion in a molecular gas of density N under the action of a uniform electric field E. From the simulations performed, we determine the basic data of the ions in the M gas, the ion/gas system, based on the reduced electric field E/N.

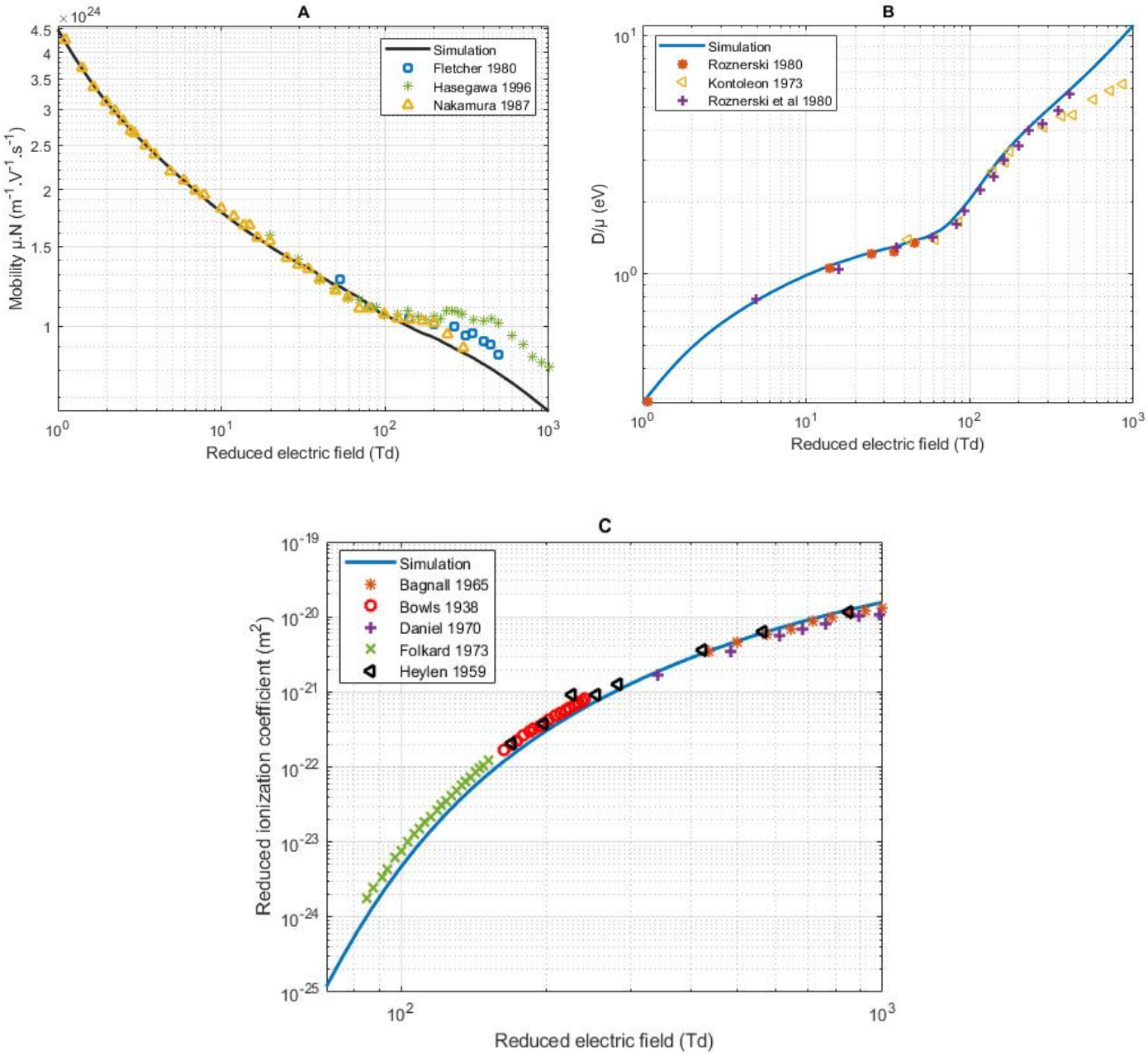

Fig. III-3: Comparison between the calculated and the measured transport coefficients of the electrons in Nitrogen (A: Mobility, B: Diffusion, C: ionization coefficient)

Due to the numerous data proposed in the literature on electron-nitrogen cross sections, our choice was made by comparing certain transport parameters (mobility or drift velocity and the ionization coefficient) calculated from the cross sections with experimental measurements available in the literature. These mobility coefficients, drift diffusion and the reduced ionization coefficient calculated by the Monte Carlo method are shown in Fig. III-3 (a), Fig. III-3 (b) and Fig. III-3 (c) respectively.

Figure III-3 (a) shows the variation of electron mobility in the parent gas with the reduced field, it is very important for weak reduced fields. This figure also shows the evolution of the electron drift velocity (Fig. III-3 (b)). For reduced ionization coefficient (α / p) shown in Figure III-3 (c), we note the excellent agreement between measurements and calculations, in particular for a reduced field between 30 V.cm and 600 V.cm.

3. Secondary chemical reactions:

The number of processes and reactions involved in DBD plasma is considerably large and their in-depth study is out of the scope of this section. It is appropriate; however, to describe those, which are more significant to this research, like, those related to ozone formation.

In our study, we took into account 13 species: ($electron, N,\ N^+, N_2, N_2^+,\ N_3^+, N_4^+, N_2(A^3\sum_u^+)$, $N_2(B^3\prod g),\ N_2(C^3\prod u), N_2(a'^1\sum_u^-), N(P),\ N(D)$) including 71 reactions: dissociation and ionization; recombination processes, neutrals-neutrals reactions; three-body reactions, excitation and de-excitation. All the processes mentioned are gathered in table III-1, each reaction is characterized by its rate coefficient. The reactions for the production and destruction of the heavy species are shown in table III-1 with their corresponding rate coefficients. The reaction rate constant k^f is determined by the Arrhenius equation:

$$k^f = Ae^{-E_a/RT} \qquad \text{(III-4)}$$

Where A is the pre-exponential factor, T is the temperature of the gas, E_a is the activation energy of the reaction and R is the gas constant. The Reactions (43), (44), (56), (57), (59), (74) and (73) illustrated in table III-1, represent associative ionization. This process has an influence on the development of discharges by metastable species (Kossyi IA, 1992). The main mechanisms of loss of the metastable state are presented by reactions (43) and (44). An important process that cannot be neglected at atmospheric pressure is the extinction of metastable states ($N_2(A^3\sum_u^+)$,$N_2(B^3\prod g)$, $N_2(C^3\prod u)$, $N_2(a'^1\sum_u^-)$, $N(P)$,$N(D)$); this process is taken into account by the reactions of (48) to (54) and (70), (71). It is necessary to include 3 reactions for their involvement

in the charge transfer process (Lazarou C, 2015), which are illustrated in (45) and (55) to (58). The reactions (64)-(67) describe the decay of ($N_2(A^3\sum_u^+)$, $N_2(B^3\prod g)$, $N_2(C^3\prod u)$, $N_2(a'^1\sum_u^-)$.

Table III-1: reaction set for Nitrogen

N.	Reaction	E_{th} (eV)	Rate coefficient [m^3/s.mol or m^6/s.mol(*) or 1/s(**)]	Ref
1	$e + N_2 \rightarrow e + N_2$	0.00	Cross section	(phelps, 2019)
2	$e + N_2 \rightarrow e + N_2$	0.02	Cross section	(phelps, 2019)
3	$e + N_2 \rightarrow e + N_2$	0.29	Cross section	(phelps, 2019)
4	$e + N_2 \rightarrow e + N_2$	0.29	Cross section	(phelps, 2019)
5	$e + N_2 \rightarrow e + N_2$	0.59	Cross section	(phelps, 2019)
6	$e + N_2 \rightarrow e + N_2$	0.88	Cross section	(phelps, 2019)
7	$e + N_2 \rightarrow e + N_2$	1.17	Cross section	(phelps, 2019)
8	$e + N_2 \rightarrow e + N_2$	1.47	Cross section	(phelps, 2019)
9	$e + N_2 \rightarrow e + N_2$	1.76	Cross section	(phelps, 2019)
10	$e + N_2 \rightarrow e + N_2$	2.06	Cross section	(phelps, 2019)
11	$e + N_2 \rightarrow e + N_2$	2.35	Cross section	(phelps, 2019)
12	$e + N_2 \rightarrow e + N_2(A^3\sum^+_u)$	6.17	Cross section	(phelps, 2019)
13	$e + N_2 \rightarrow e + N_2(A^3\sum^+_u)$	7.00	Cross section	(phelps, 2019)
14	$e + N_2 \rightarrow e + N_2(B^3\prod g)$	7.35	Cross section	(phelps, 2019)
15	$e + N_2 \rightarrow e + N_2$	7.36	Cross section	(phelps, 2019)
16	$e + N_2 \rightarrow e + N_2(A^3\sum^+_u)$	7.80	Cross section	(phelps, 2019)
17	$e + N_2 \rightarrow e + N_2$	8.16	Cross section	(phelps, 2019)
18	$e + N_2 \rightarrow e + N_2(a'^3\sum^-_u)$	8.40	Cross section	(phelps, 2019)
19	$e + N_2 \rightarrow e + N_2$	8.55	Cross section	(phelps, 2019)
20	$e + N_2 \rightarrow e + N_2$	8.89	Cross section	(phelps, 2019)
21	$e + N_2 \rightarrow e + N_2(C^3\prod u)$	11.03	Cross section	(phelps, 2019)
22	$e + N_2 \rightarrow e + N_2$	11.87	Cross section	(phelps, 2019)
23	$e + N_2 \rightarrow e + N + N(D)$	12.14	Cross section	(phelps, 2019)
24	$e + N_2 \rightarrow e + N_2$	12.25	Cross section	(phelps, 2019)
25	$e + N_2 \rightarrow e + N + N(P)$	13.33	Cross section	(phelps, 2019)
26	$e + N_2^+ \rightarrow N + N(P)$	0.00	$0.11\times1.75\times10^{-13}\times(0.026/T_e)^{0.3}$	(Tsai H, 2010)
27	$e + N_2^+ \rightarrow N + N(D)$	0.00	$0.37\times1.75\times10^{-13}\times(0.026/T_e)^{0.3}$	(Tsai H, 2010)
28	$e + N_2^+ \rightarrow N(D) + N(D)$	0.00	$0.52\times1.75\times10^{-13}\times(0.026/T_e)^{0.3}$	(Tsai H, 2010)
29	$e + N_4^+ \rightarrow N_2(C^3\prod u) + N_2$	0.00	$2\times10^{-12}\times(0.026/T_e)^{0.5}$	(Prevosto L, 2016)
30	$e + N_3^+ \rightarrow N_2 + N$	0.00	$2\times10^{-13}\times(0.026/T_e)^{0.5}$	(Choi YH, 2006;)
31	$e + N_2 \rightarrow e + e + N_2^+$	15.06	Cross section	(phelps, 2019)
32	$e + N_2 \rightarrow e + e + N + N^+$	24.34	Cross section	(phelps, 2019)

33	$e + N_2(A^3\sum^+_u) \rightarrow e + e + N_2^+$	9.43	Cross section	(Bacri J, 1982)
34	$e + N_2(B^3\prod g) \rightarrow e + e + N_2^+$	8.25	Cross section	(Bacri J, 1982)
35	$e + N_2(C^3\prod u) \rightarrow e + e + N_2^+$	4.57	Cross section	(Bacri J, 1982)
36	$e + N_2(a',^3\sum^-_u) \rightarrow e + e + N_2^+$	7.20	Cross section	(Bacri J, 1982)
37	$e + N \rightarrow e + N$	0.00	Cross section	(phelps, 2019)
38	$e + N \rightarrow e + N(D)$	2.38	Cross section	(phelps, 2019)
39	$e + N(D) \rightarrow e + N$	-2.38	Cross section	(phelps, 2019)
40	$e + N \rightarrow e + N(P)$	3.57	Cross section	(phelps, 2019)
41	$e + N(P) \rightarrow e + N$	-3.57	Cross section	(phelps, 2019)
42	$e + N \rightarrow e + e + N^+$	14.54	Cross section	(phelps, 2019)
43	$N_2\ (a^{'1}\sum_u^-) + N_2\ (A^3\sum_u^+) \rightarrow N_4^+ + e$	0.00	0.25×10^{-17}	
44	$N_2\ (a^{'1}\sum_u^-) + N_2(a^{'1}\sum_u^-) \rightarrow N_4^+ + e$	0.00	10^{-16}	
45	$N + N + N_2 \rightarrow N_2 + N_2$	0.00	$8.3 \times 10^{-46} \times exp(493/T)^*$	(Cheng KW, 2012)
46	$N_2(A^3\sum_u^+) + N_2(A^3\sum_u^+) \rightarrow N_2(C^3\prod u) + N_2$	0.00		
47	$N_2(A^3\sum_u^+) + N_2(A\hat{}3\sum_u^+) \rightarrow N_2(B^3\prod g) + N_2$	0.00		
48	$N_2(A^3\sum_u^+) + N_2 \rightarrow N_2 + N_2$	0.00		(Cheng KW, 2012)
49	$N_2(A^3\sum_u^+) + N \rightarrow N_2 + N(P)$	0.00		(Choi YH, 2006;)
50	$N_2(A^3\sum_u^+) + N \rightarrow N_2 + N$	0.00		(Tsai H, 2010)
51	$N_2\ (B^3\prod g) + N_2 \rightarrow N_2(A^3\sum_u^+) + N_2$	0.00		(Tsai H, 2010)
52	$N_2\ (a^{'1}\sum u\text{-}) + N_2 \rightarrow N_2(B^3\prod g) + N_2$	0.00		(Choi YH, 2006;)
53	$N_2\ (C^3\prod u) + N_2 \rightarrow N_2(a^{'1}\sum_u^-) + N_2$	0.00		(Choi YH, 2006;)
54	$N(P) + N_2 \rightarrow N(D) + N_2$	0.00		(Lazarou C, 2015)
55	$N_2^+ + N_2 + N_2 \rightarrow N_4^+ + N_2$	0.00	$5.2 \times 10^{-41} \times (300/T)^{2.2*}$	(Massines F, 2003)
56	$N_2^+ + N + N_2 \rightarrow N_3^+ + N_2$	0.00	$9 \times 10^{-42} \times exp(400/T)^*$	(Massines F, 2003)
57	$N^+ + N_2 + N_2 \rightarrow N_3^+ + N_2$	0.00	$17 \times 10^{-42} \times (300/T)^{2.1*}$	(Massines F, 2003)
58	$N^+ + N + N_2 \rightarrow N_2^+ + N_2$	0.00	10^{-41*}	(Massines F, 2003)
59	$N_2^+ + N_2(A^3\sum u+) \rightarrow N_3^+ + N$	0.00	3×10^{-16}	(Panousis E, 2007)
60	$N_2^+ + N \rightarrow N^+ + N_2$	0.00		(Massines F, 2003)
61	$N_3^+ + N \rightarrow N_2^+ + N_2$	0.00		(Massines F, 2003)
62	$N_4^+ + N_2 \rightarrow N_2^+ + N_2 + N_2$	0.00		(Massines F, 2003)
63	$N_4^+ + N \rightarrow N^+ + N_2 + N_2$	0.00		(Massines F, 2003)
64	$N_2\ (B^3\prod g) \rightarrow N_2(A^3\sum_u^+)$	0.00	$1.5 \times 10^{5**}$	(Cheng KW, 2012)
65	$N_2\ (C^3\prod u) \rightarrow N_2(B^3\prod g)$	0.00	$2.7 \times 10^{7**}$	(Cheng KW, 2012)
66	$N_2\ (A^3\sum_u^+) \rightarrow N_2$	0.00	0.5^{**}	(Cheng KW, 2012)
67	$N_2\ (a^{'1}\sum_u^-) \rightarrow N_2$	0.00	100^{**}	(Cheng KW, 2012)
68	$N(D) + N_2 \rightarrow N + N_2$	0.00		(Tsai H, 2010)
69	$N(P) + N_2 \rightarrow N + N_2$	0.00		(Tsai H, 2010)
70	$N(D) + N(P) \rightarrow N_2^+ + e$	0.00	$3.2\times10^{-21}\times T^{0.98}/(1\text{-}\exp(-3129/T))$	(Choi YH, 2006;)
71	$N(P) + N(P) \rightarrow N_2^+ + e$	0.00	$1.92\times10^{-21}\times T^{0.98}/(1\text{-}\exp(-3129/T))$	(Choi YH, 2006;)

4. Surface reactions

Interactions with electrodes and plasma / surface interaction processes can also play an essential role in the formation and development of discharge. The charged particles incident on the walls can be reflected by the surface. Upon impact with the surface, the ions can be electrically neutralized and thus lose most of their energy.

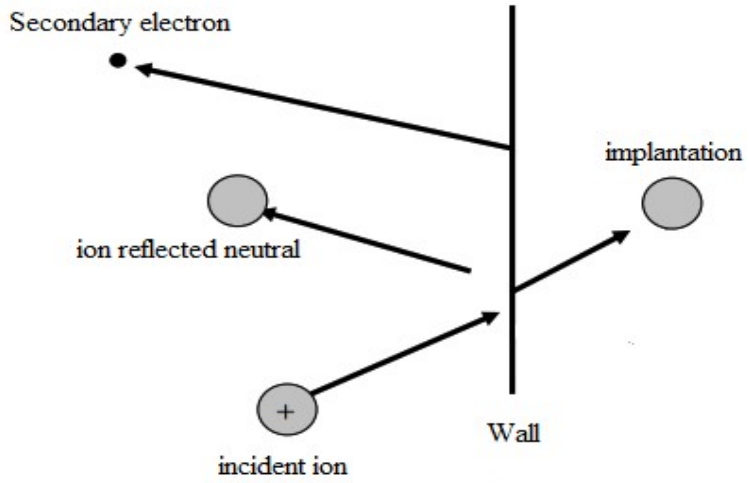

Fig. III-4: possible processes with the wall

If the ions are sufficiently energetic, they can then be implanted in the wall. In this case, structural rearrangements can occur at the wall level, secondary electrons can be emitted from the cathode under the impact of the incident beam (case of a metal wall). In addition to electrons, particles from the surface can be torn off by incident particles if they are sufficiently energetic. The wall reactions are shown in following table.

Table III-2: Surface reaction

N°	Reaction
1	$N_2^+ \rightarrow N_2$
2	$N_3^+ \rightarrow N_2 + N$
3	$N_4^+ \rightarrow N_2 + N_2$
4	$N^+ \rightarrow N$
5	$N_2 (A^3 \sum_u^+) \rightarrow N_2$
6	$N_2 (B_3 \prod g) \rightarrow N_2$
7	$N_2 (C^3 \prod u) \rightarrow N_2$
8	$N_2 (a'^1 \sum_u^-) \rightarrow N_2$
9	$N(P) \rightarrow N$
10	$N(D) \rightarrow N$
11	$N \rightarrow 1/2\ N_2$

5. Simulation Results:

We discuss in this section the results obtained from the model of a dielectric barrier discharge in the case of nitrogen for the discharge parameters. Figure III-5 shows a comparison of the total current of the dielectric barrier discharge in Nitrogen obtained from our model and that measured (BOUZIDI, 2013). From this figure, we observe a good agreement between the temporal evolution of the two currents. When we apply a voltage between the electrodes for a time, in the nanosecond order the gas becomes a conductor. This time is necessary for ionization and secondary emission and for the creation of sufficient charges to ensure breakdown.

5.1. Current and voltage characteristics:

Figure III-5 shows a comparison of the total current of the dielectric barrier discharge in Nitrogen obtained from our model and that measured (BOUZIDI, 2013). From this figure, we observe a good agreement between the temporal evolution of the two currents. When we apply a voltage between the electrodes for a time, in the nanosecond order the gas becomes a conductor. This time is necessary for ionization and secondary emission and for the creation of sufficient charges to ensure breakdown.

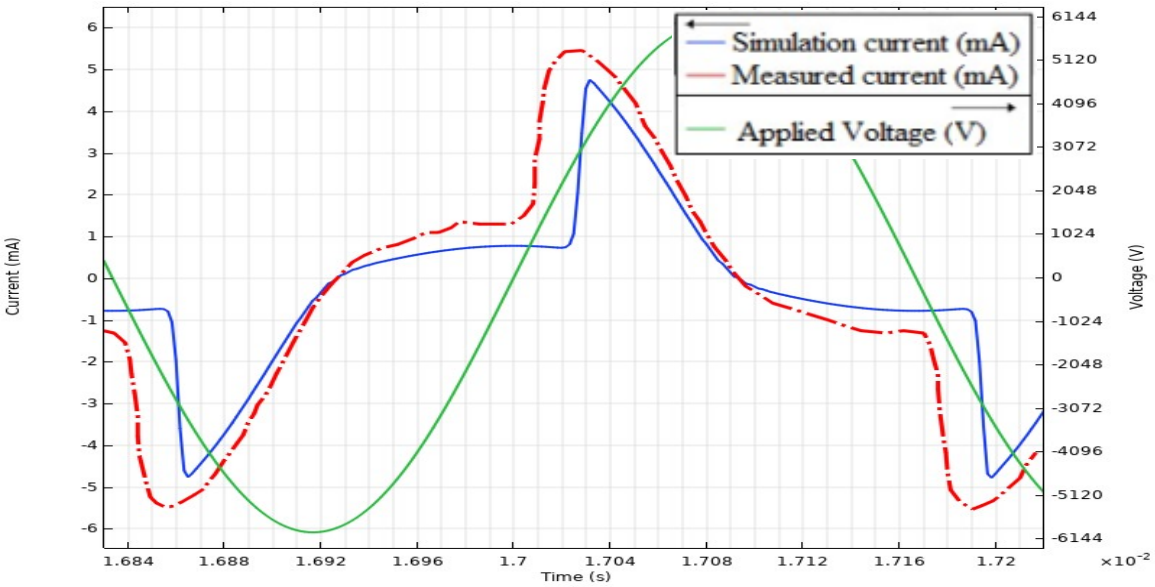

Fig. III-5: Comparison between the calculated and measured discharge current

5.2. Plasma chemistry results:

The current peak moment during breakdown t_p=0.017s which we choose to take the instantaneous distributions of the different species in the plasma, leads to obtain figure III-6 for the charged species and figure III-7 for the neutral and excited species.

Figure III-6 clearly shows that the ion densities are almost stable in the inter-electrode space while the electron density varies between (10^6 and 10^{12}) $1 / m^3$. It is a characteristic of the Townsend discharge. The ionization and excitation collisions produced by the electron-molecule impact of nitrogen N_2 under a strong electric field, are the main causes of the increase in the densities of the ions and excited particles near the anode (see figure III-6 and figure III-7).

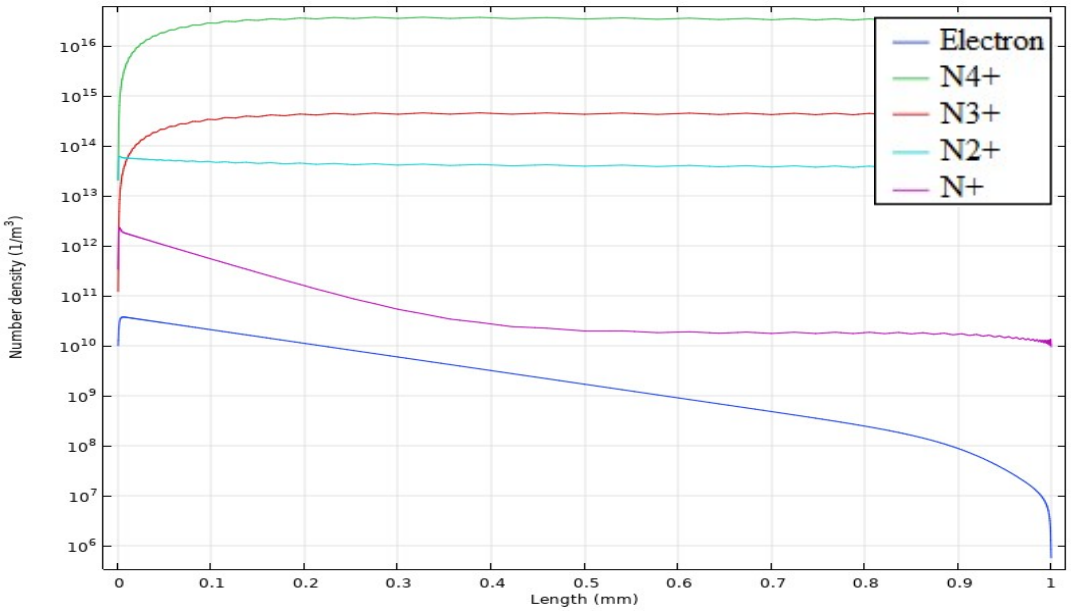

Fig. III-6: Spatial distributions of electronic and ionic densities at 0.017s

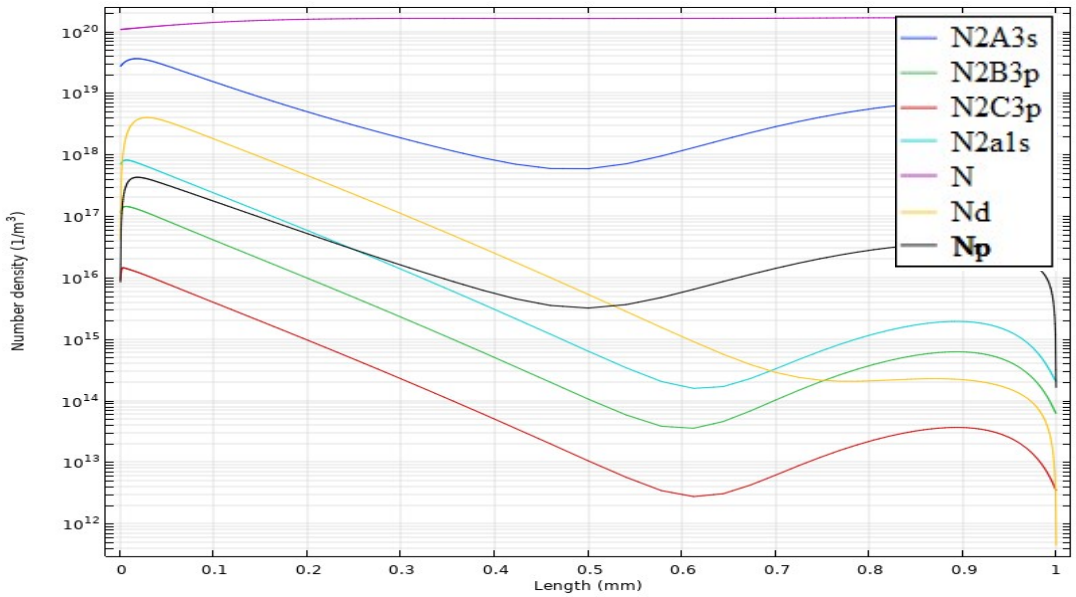

Fig. III-7:Spatial distributions of the densities of neutral and excited species at t=0.017s

Figure III-8 and figure III-9 show the temporal variations of the number density of charged and neutral species respectively at the dielectric surface that cover the electrode A (figure III-3). Figure III-8 show that in positive alternate of voltage wave, the electrons number density increases by the increasing of applied voltage and its greater than other ions number densities. That's because of ionization process when electrons gain the required energy for it, for this

reason we also observe the growth of ion number density. Moreover, only at the moment of breakdown (t=0.017s), electrons and ions number densities are the same. In the next negative alternate, we can see that the electron number density getting low when they are heading to the other boundaries of point B (Fig. III-3). The same manners manifest with the ions, but with a lower length for their heaviness. N_4^+ dominate because of the associative ionization process, as mentioned in reaction (43) and (44) from table III-1. The dominate metastables are shown in figure III-9 is between $N_2(A^3\sum_u^+)$ and $N_2(a'^1\sum_u^-)$. In addition, this process can produce N_2^+ as mentioned in reaction (70) and (71) by $N(P)$ and $N(D)$ which they dominate in discharge gap.

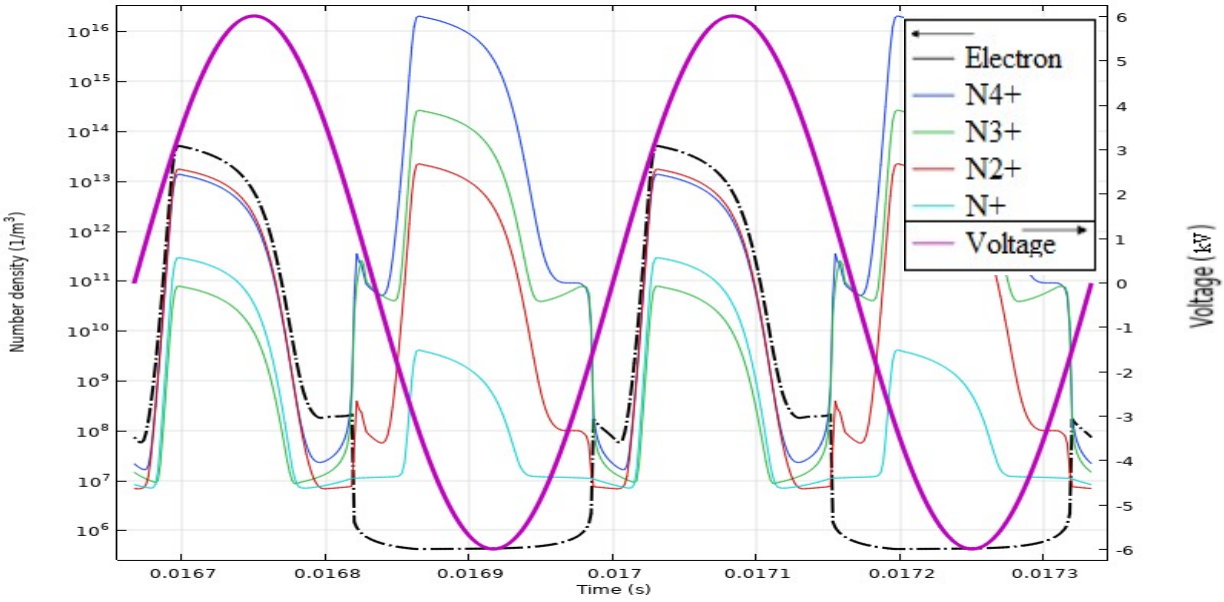

Fig. III-8: Temporal variation of charged species number density

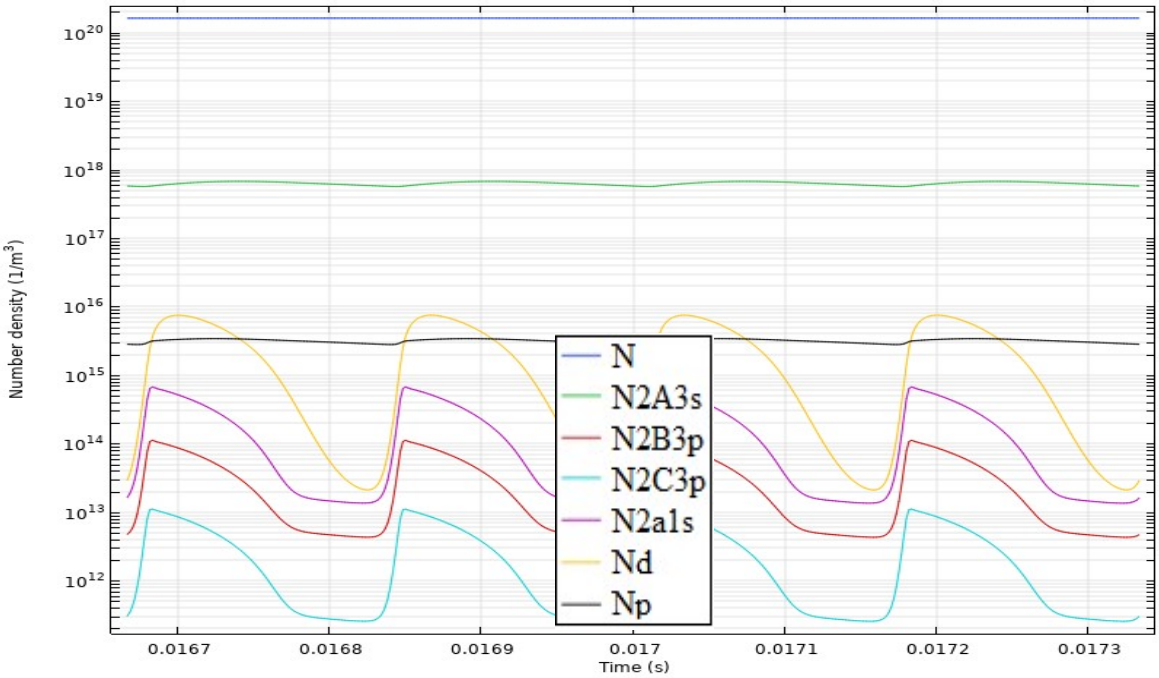

Fig. III-9: Temporal variation of exited and neutrals species number *density*

6. Parametric study

6.1. Dielectric coating effect

Several dielectric materials used in dielectric barrier discharges (DBD) as ceramics (Alumin 96% used in this model), glass, silicon and polymer. These materials have the relative permittivity under 10 ($\varepsilon_r < 10$) which give an ability to take the thickness of each dielectric coating in order of mm. Figure III-10 shows the discharge current variation (Figure III-10 (a)), electron density (Figure III-10 (b)) and $N_2(A^3\sum_u^+)$ density (Figure III-10 (c)) for each dielectric material (Alumina $\varepsilon_r = 9$, Glass $\varepsilon_r = 8.2$, Stumatite $\varepsilon_r = 7.3$). As we observe in figure III-10 (a, b, c), the discharge current is proportional to the relative permittivity while the electron density and the density $N_2(A^3\sum_u^+)$ are almost the same for the three types of dielectric. The change in dielectric materials (relative permittivity ε_r) makes it possible to estimate the density of the plasma (electrons and heavy species) through space and the discharge current.

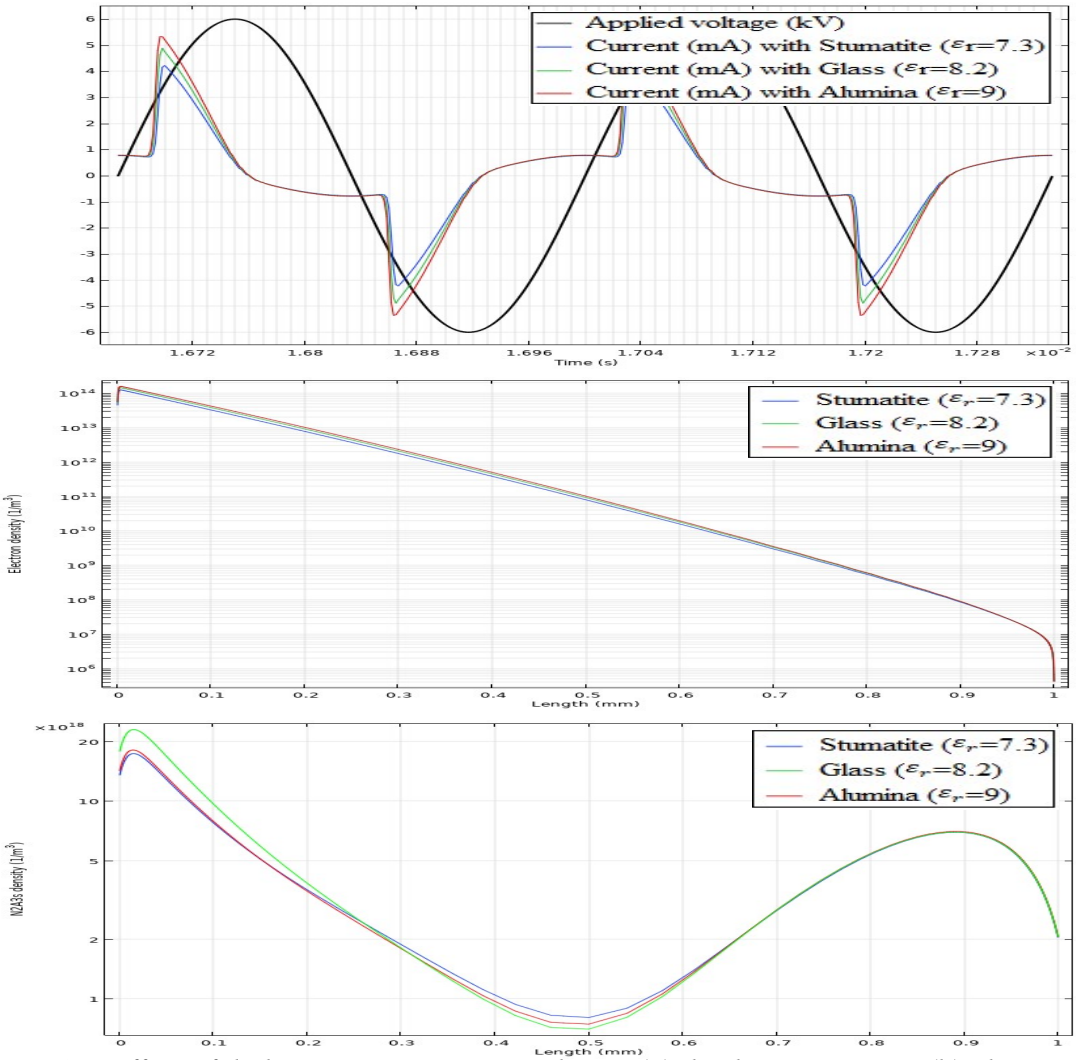

Fig. III-10: Effect of dielectric coating materials on: (a) discharge current, (b) electron density, (c) $N_2(A^3\Sigma_u^+)$ *density.*

6.2. Applied voltage effect

To study the effect of the applied voltage on the characteristics of the DBD discharge in nitrogen, we used alumina as dielectric coating material and considered three voltage values namely: 4.5 kV, 6 kV and 8 kV. The influence of the applied voltage on the discharge current, on the electron density and on $N_2(A^3\sum_u^+)$ is shown in figure III-11 (a, b and c) respectively.

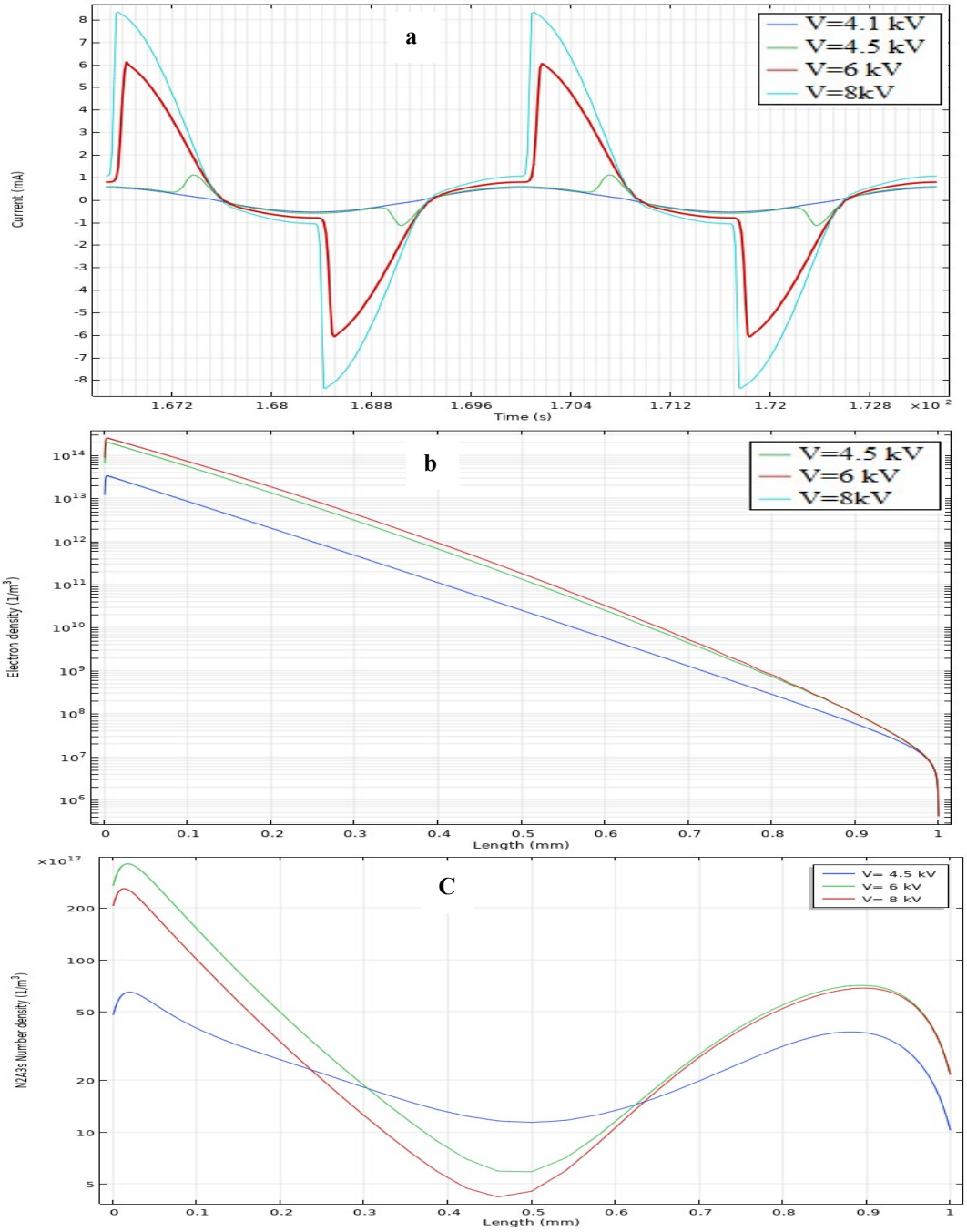

Fig. III-11: Effect of applied voltage on: (a) discharge current, (b) electron density, (c) $N_2(A^3\Sigma_u^+)$ *density.*

According to Dakin and al. (Dakin TW, 1974), breakdown voltage in a gap of 2 mm of thickness filled with Nitrogen gas at atmospheric pressure is 8.2 kV. The gap gas of our model has 1 mm of thickness, so as it shown in figure III-11 (a), that under a voltage of 4.5 kV, there is no breakdown just a streamer discharge (sinusoidal waveform of current). Discharge current increase with voltage, and the displacement current get shorter period. From figure III-11 (b and c), it appears that the density of the electron and the density of $N_2(A^3\sum_u^+)$ are almost the same for V = 6 kV and V = 8 kV on the anode side, the density of metastable has minimum values between electrodes (0.5 mm), whereas with V = 4.5 kV in this position, there are fewer metastable species (15 * 10^{18} / m^3 approximately)

6.3. Frequency effect

This section shows the influence of applied voltage frequency on discharge current (figure III-12 (a)), electron density (figure III-12 (b)) and $N_2(A^3\sum_u^+)$ density (figure III-12 (c)). As it's shown in this figure, the waveform doesn't change, but the peak of current increase with frequency. Also, we can see that the electron density undergoes a slight change in space, while the density $N_2(A^3\sum_u^+)$ at 3 kHz is greater than the density at 5 kHz and 7 kHz near the anode. Increasing the frequency makes the ionization of the particles weaker, so there are less $N_2(A^3\sum_u^+)$ particles near the anode at 7 kHz.

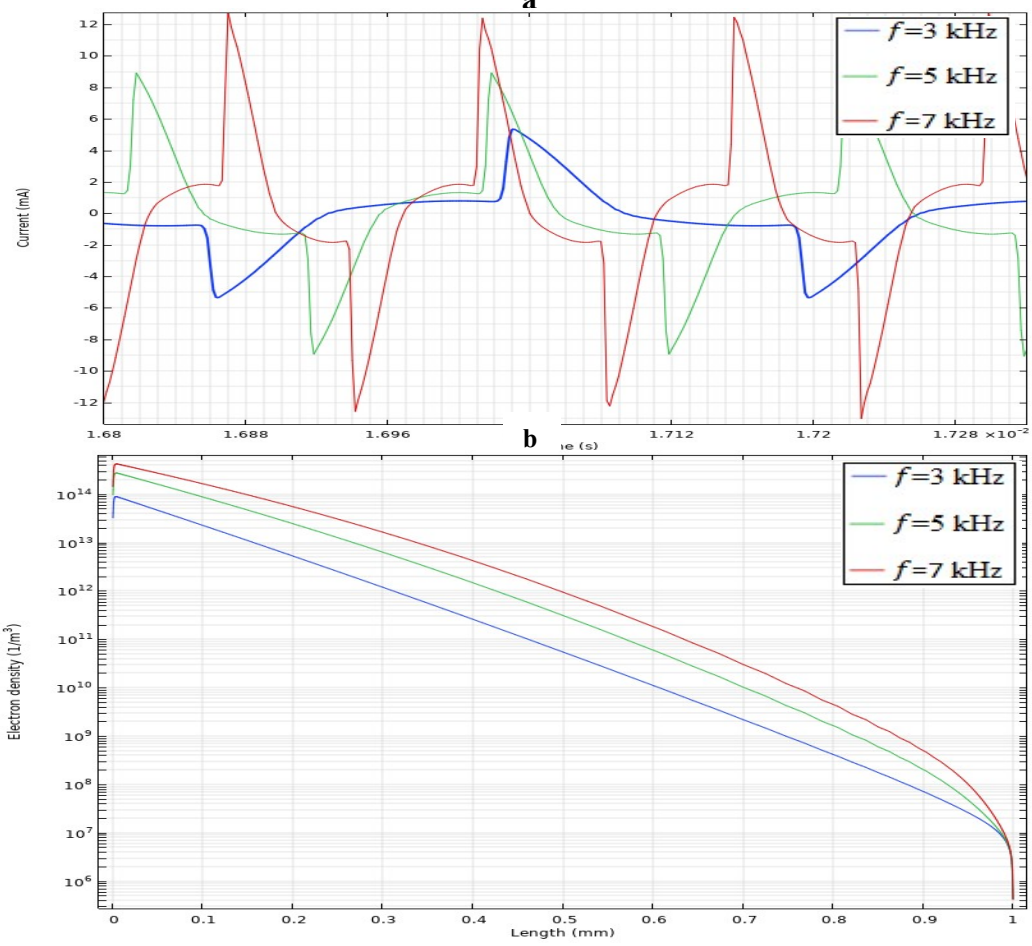

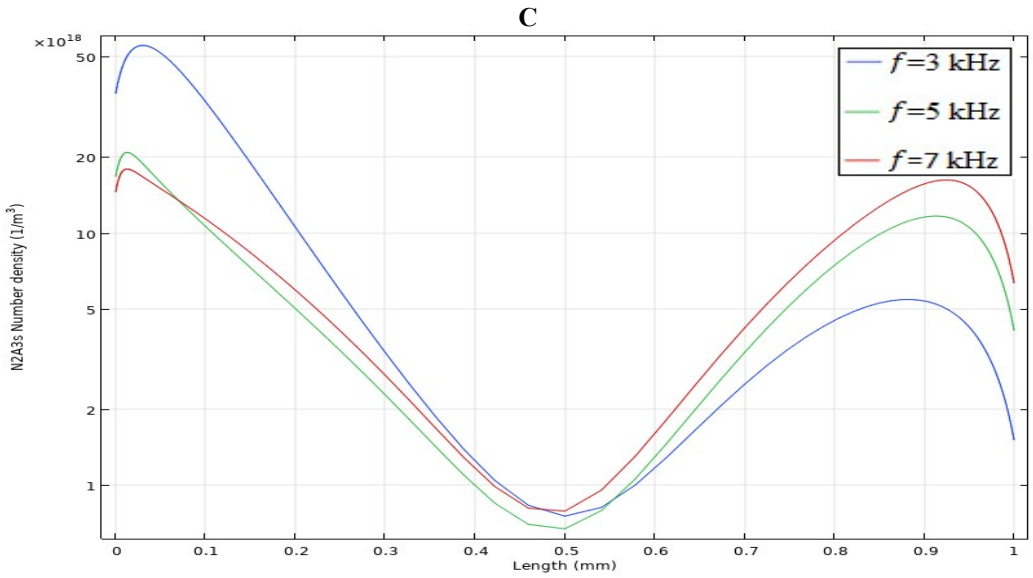

Fig. III-12 :Effect of frequency on: (a) discharge current, (b) electron density, (c) $N_2(A^3\Sigma_u^+)$ *density.*

7. Conclusion

This chapter aimed to study by simulation the dielectric barrier discharge (DBD) in pure nitrogen at atmospheric pressure in 1D parallel-plate geometry, driven by a sinusoidal voltage power source using a self-consistent fluid model. The simulated discharge currents obtained are in very good agreement with the experimental measurements. All the nitrogen reactions have led to an interpretation of the behavior of 13 species present in the plasma with regard to the evolution in space and time. The parametric study carried out on some parameters of the DBD has proved that the discharge current is proportional to the relative permittivity while the electron density and the density $N_2(A^3\sum_u^+)$ are about the same for the types of dielectrics considered, thus, the discharge current increases with the voltage and the displacement current becomes shorter. Also, the waveform of the discharge current does not change but the peak current increases with the frequency value. This section approves that by manipulating each of these parameters; it can optimize the discharge current or density of the plasma.

Bibliography

L. C. P. Pancheshnyi, "The LXCat project: Electron scattering cross sections and swarm parameters for low temperature plasma modeling," *Chem. Phys.,(1),* p. 148–153, 2012.

P. Hagelaar, "Solving the Boltzmann equation to obtain electron transport coefficients and rate coefficients for fluid models,," *Plasma Sources Sci. Technol 14(4),* p. 722–733, 2005.

t. f. e. Wikipedia, "Ion-mobility spectrometry," 06 december 2020. [Online]. Available: https://en.wikipedia.org/wiki/Ion-mobility_spectrometry.

Moseley ZT, "Mobilities, Diffusion Coefficients, and Reaction Rates of Mass-Indentified Nitrogen Ions in Nitrogen," *physical review Volume 178 ,* p. 240, 1969.

Ellis HW, " Transport properties of gaseous ions over a wide energy range," *Atomic Data And Nuclear Data Tables 17,* pp. 177-210, 1976.

Kossyi IA, "Kinetic scheme of the non-equilibrium discharge in nitrogen-oxygen mixtures," *Plasma Sources Sci. Technol 1,* pp. 207-220, 1992.

KLazarou C, "Numerical modeling of the effect of the level of nitrogen impurities in a helium parallele plate dielectric barrier discharge," *Plasma Sources Sci. Technol 24 ,* p. 13, 2015.

H. C. Tsai H, "Numerical Simulation of Downstream Kinetics of an Atmospheric-Pressure Nitrogen Plasma Jet.," *IEEE Transactions on Plasma Science ,* 2010.

phelps, "SIGLO Database," 14 february 2019. [Online]. Available: LXCat.net.

Bacri J, "Electron diatomic molecule weighted total cross section calculation," *Physica ,* pp. 101-l 18, 1982.

Prevosto L, "Modelling of an Atmospheric Pressure Nitrogen Glow Discharge Operating in High-Gas Temperature Regimes," . *Plasma Chem Plasma Process ,* 2016.

Choi YH, "One-dimensional discharge simulation of nitrogen DBD atmospheric pressure plasma," *Thin Solid Films ,* p. 506 – 507 , 2006; .

Cheng KW, "Fluid Modeling of a Nitrogen Atmospheric-Pressure Planar Dielectric Barrier Discharge Driven by a Realistic Distorted Sinusoidal Alternating Current Power Source.," *Japanese Journal of Applied Physics ,* 2012.

Massines F, "Physics and chemistry in a glow dielectric barrier discharge at atmospheric pressure: diagnostics and modelling.," *Surface and Coatings Technology,* p. 174 – 175, 2003.

Panousis E, "Numerical modelling of an atmospheric pressure dielectric barrier discharge in nitrogen: electrical and kinetic description.," *J. Phys. D: Appl. Phys ,* p. 4168–4180, 2007.

M. C. BOUZIDI, PhD Thesis. Étude d'une Décharge à Barrière Diélectrique (DBD) homogène dans l'azote à pression atmosphérique :Effet mémoire et Optimisation du transfert de Puissance, TOULOSE University UT3 , 2013.

L. G. O. G. V. J. W. G. Dakin TW, "Breakdown in gases in uniform fields, Paschen's curves for nitrogen, air and sulphur hexafluoride," *H. Electra 32 ,* p. 61–82, 1974.

Chapter IV:

Dielectric barrier discharge modeling in pure oxygen

1. Introduction:

DBD certified as a valuable alternative technology for removing gaseous pollutants, as air purification and water treatment by Ozone (How Ming Lee, 2004). When ozone exposed to organic compounds or bacteria, begin to destroy the contaminant by oxidation. Thus, ozone will neutralize virtually all organic odours, and those containing carbons. This will include all bacteria, smoke, decay and cooking odours (Pekárek., 2003). Ozone must be generated at the place of use for the instability of their molecules, which quickly split to Oxygen molecules depending on temperature and presence of oxidable organic compounds (B Mennad, 2010). The generation of ozone by DBDs depends on (Moo Been Chang):

- The magnitude of the voltage and frequency of power supply;
- Configuration of the reactor;
- Gas stream composition, pressure, and temperature.

The global reaction that consists to generate ozone by oxygen discharge at atmospheric pressure and is: $O_2 + O + O_2 \rightarrow O_3 + O_2$ and their rate constant at 298 K of temperature is: $K_{298}=6.2\times10^{-34}\ cm^6/mol.s$

This chapter show a 1D modelling of ozone generation by a DBD reactor filling up with Oxygen. As we organized the model of DBD in Nitrogen in previous chapter, also this model, contain the plasma chemistry of DBD in oxygen gas, to get in the results the optimums characteristics that help to producing Ozone, and either the influence of some discharge parameters on Ozone molecules densities.

2. Basic data of charged particles in oxygen:

2.1. Ion mobility:

In our model the mobility coefficients of ions are taken from (Zhilong Zou, 2016) and (G. Sinnott, 1968) using the reduced mobility expression K_0 as the following table (Table IV-1):

Table IV-1: Oxygen ions mobility

Ions		Measured mobility $\mu * 10^{-4}$ ($m^2/V.s$)	Reference
Negative ions	O^-	3.2	(Zhilong Zou, 2016)
	O_2^-	2.17	
	O_3^-	2.56	
	O_4^-	2.27	
Positive ions	O^+	3.68	

	O_2^+	2.23	(G. Sinnott, 1968)
	O_3^+	2.56	
	O_4^+	2.08	

2.2. Cross section of electron-Oxygen:

The cross sections for O_2, O and O_3 using the Phelps compilation from the LXcat website are plotted in figure IV-1 and figure IV-2 and figure IV-3 respectively.

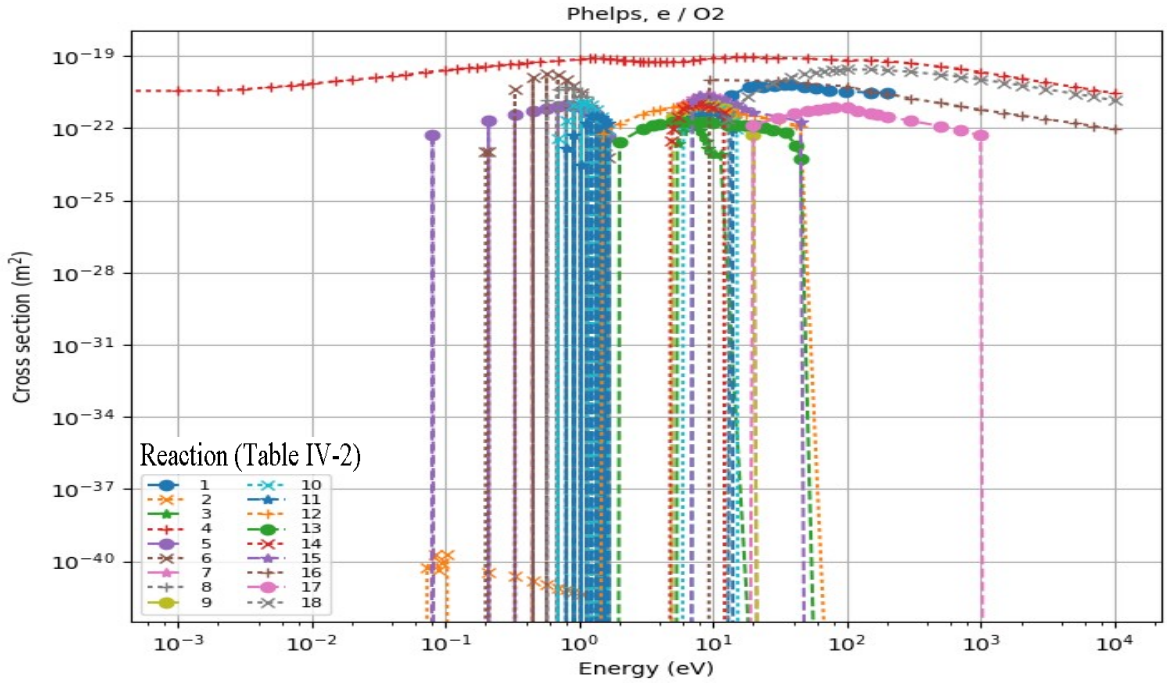

Fig. IV-1: Oxygen molecules cross section

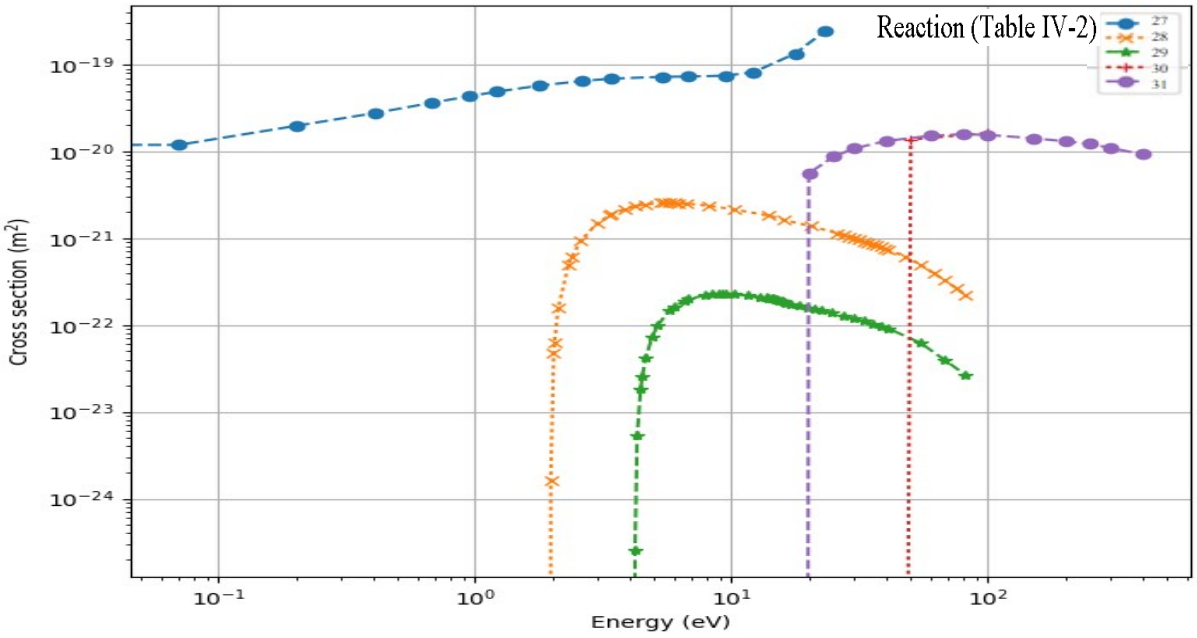

Fig. IV-2: Oxygen atom cross section

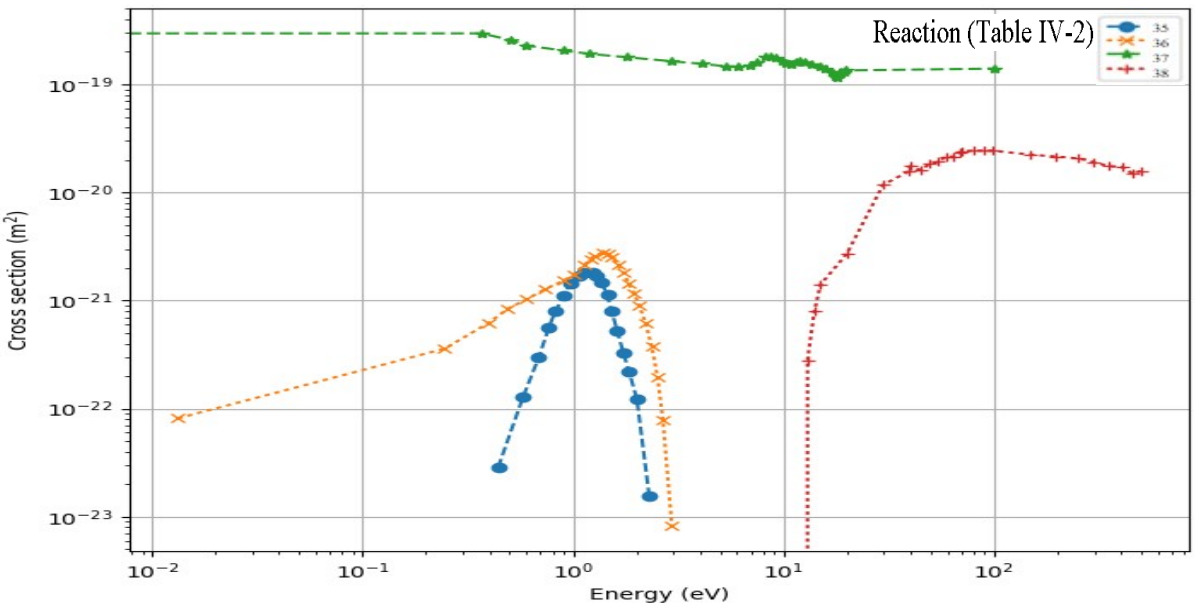

Fig. IV-3: Ozone cross section

Similar to N_2, the momentum transfers cross section for O_2 is defined for all electron energies. In contrast, there is a depression from 1 to 6 eV since the cross-section magnitude for all inelastic scattering cross sections is low at these energies. There are sharp rotational and vibrational resonances at low energies and wider, 9 eV vibrational resonances. The 8.4 eV excitation cross section has a high-energy tail that corresponds to a relatively large cross section, as does ionization.

3. Primary chemical reactions:

This part consists to set a 155 chemical reactions between 18 species exist in discharge oxygen gap, which are electron, O^+ , O^-, O_2 , O_2^+, O_2^-, O_3, O_3^+,O_3^-,O_4^+, O_4^- , $O_2(a^1\Delta)$, $O_2(a^1\sum)$), $O_2(b^1\sum)$, $O_2(4.5V)$, $O(^1D)$, $O(^1S)$. This number of reactions divided into three types: electron and heavy species interactions, heavy species reaction as it listed in table IV-2, and heavy species interaction at the dielectric surface, which listed in table IV-3.

Table IV-2 : reaction set for Oxygen

No.	Reaction	Rate coefficient [m^3/s.mol or m^6/s.mol(*) or 1/s(**)]	Ref
1	$e + O_2 \rightarrow e + O_2$	Cross section	(phelps, 2019)
2	$e + O_2 \rightarrow O + O^-$	Cross section	(phelps, 2019)
3	$e + O_2 \rightarrow e + O_2$	Cross section	(phelps, 2019)
4	$e + O_2 \rightarrow e + O_2$	Cross section	(phelps, 2019)
5	$e + O_2 \rightarrow e + O_2$	Cross section	(phelps, 2019)
6	$e + O_2 \rightarrow e + O_2$	Cross section	(phelps, 2019)
7	$e + O_2 \rightarrow e + O_2$	Cross section	(phelps, 2019)
8	$e + O_2 \rightarrow e + O_2$	Cross section	(phelps, 2019)

9	$e + O_2 \rightarrow e + O_2$	Cross section	(phelps, 2019)
10	$e + O_2 \rightarrow e + O_2(a^1\Delta)$	Cross section	(phelps, 2019)
11	$e + O_2(a^1\Delta) \rightarrow e + O_2$	Cross section	(phelps, 2019)
12	$e + O_2 \rightarrow e + O_2(b^1\sum)$	Cross section	(phelps, 2019)
13	$e + O_2(b^1\sum) \rightarrow e + O_2$	Cross section	(phelps, 2019)
14	$e + O_2 \rightarrow e + O_2(4{,}5eV)$	Cross section	(phelps, 2019)
15	$e + O_2(4{,}5eV) \rightarrow e + O_2$	Cross section	(phelps, 2019)
16	$e + O_2 \rightarrow e + O + O$	Cross section	(phelps, 2019)
17	$e + O_2 \rightarrow e + O + O(^1D)$	Cross section	(phelps, 2019)
18	$e + O_2 \rightarrow e + O + O(^1D)$	Cross section	(phelps, 2019)
19	$e + O_2 \rightarrow e + e + O_2^+$	Cross section	(phelps, 2019)
20	$e + O_2 \rightarrow e + e + O + O^+$	Cross section	(phelps, 2019)
21	$e + O_2(a^1\Delta) \rightarrow e + O + O$	Cross section	(phelps, 2019)
22	$e + O_2(a^1\Delta) \rightarrow 2e + O_2^+$	Cross section	(phelps, 2019)
23	$e + O_2(b^1\sum) \rightarrow e + O + O$	Cross section	(phelps, 2019)
24	$e + O_2(b^1\sum) \rightarrow 2e + O_2^+$	Cross section	(phelps, 2019)
25	$e + O_2(4{,}5eV) \rightarrow e + O + O$	Cross section	(phelps, 2019)
26	$e + O_2(4{,}5eV) \rightarrow 2e + O_2^+$	Cross section	(phelps, 2019)
27	$e + O \rightarrow e + O(^1D)$	Cross section	(Morgan, 2019)
28	$e + O(^1D) \rightarrow e + O$	Cross section	(Morgan, 2019)
29	$e + O \rightarrow e + O(^1S)$	Cross section	(Morgan, 2019)
30	$e + O(^1S) \rightarrow e + O$	Cross section	(Morgan, 2019)
31	$e + O \rightarrow 2e + O^+$	Cross section	(Morgan, 2019)
32	$e + O(^1D) \rightarrow e + O(^1S)$	Cross section	(Morgan, 2019)
33	$e + O(^1D) \rightarrow 2e + O^+$	Cross section	(Morgan, 2019)
34	$e + O(^1S) \rightarrow 2e + O^+$	Cross section	(Morgan, 2019)
35	$e + O_3 \rightarrow e + O_3$	Cross section	(Morgan, 2019)
36	$e + O_3 \rightarrow O_2^- + O$	Cross section	(Morgan, 2019)
37	$e + O_3 \rightarrow O^- + O_2$	Cross section	(Morgan, 2019)
38	$e + O_3 \rightarrow 2e + O_3^+$	Cross section	(Morgan, 2019)
39	$e + O^+ \rightarrow O$	$2.9e-19 * T_e^{-0.66}$	(A I Florescu-Mitchell, 2006)
40	$e + O_2^+ \rightarrow O + O$	$0.32 * 1.5e-14 * T_e^{-0.7}$	(A I Florescu-Mitchell, 2006)
41	$e + O_2^+ \rightarrow O + O(^1D)$	$0.43 * 1.5e-14 * T_e^{-0.7}$	(A I Florescu-Mitchell, 2006)
42	$e + O_2^+ \rightarrow O(^1D) + O(^1D)$	$0.2 * 1.5e-14 * T_e^{-0.7}$	(A I Florescu-Mitchell, 2006)
43	$e + O_2^+ \rightarrow O(^1D) + O(^1S)$	$0.04 * 1.5e-14 * T_e^{-0.7}$	(A I Florescu-Mitchell, 2006)
44	$e + O_3^+ \rightarrow O + O + O$	$0.94 * 7.37e-13 * (0.026/T_e)^{0.55}$	(V Zhaunerchyk, 2007)
45	$e + O_3^+ \rightarrow O_2 + O$	$0.06 * 7.37e-13 * (0.026/T_e)^{0.55}$	(V Zhaunerchyk, 2007)
46	$e + O_4^+ \rightarrow O_2 + O_2$	$4.2e-12 * (0.026/T_e)^{0.5}$	(V Zhaunerchyk, 2007)
47	$e + O_2 + O_2 \rightarrow O_2^- + O_2$	$2.46e-42^*$	(Kossyi IA, 1992)
48	$e + O + O_2 \rightarrow O^- + O_2$	$1.00e-43^*$	(J T Gudmundsson, 2001)
49	$e + O + O_2 \rightarrow O + O_2^-$	$1.00e-43^*$	(J T Gudmundsson, 2001)

50	$e + O_3 + O_2 \rightarrow O_3^- + O_2$	$1.00e-43^{*}$	(J T Gudmundsson, 2001)
51	$O^- + O \rightarrow O_2 + e$	$1.90e-16^{**}$	(S G Belostotsky, 2005)
52	$O^- + O2 \rightarrow O_3 + e$	$5.00e-21^{**}$	(Kossyi IA, 1992)
53	$O^- + O_3 \rightarrow O_3^- + O$	$5.30e-16^{**}$	(Kossyi IA, 1992)
54	$O_2^- + O \rightarrow O_3 + e$	$1.50e-16^{**}$	(Kossyi IA, 1992)
55	$O_2^- + O \rightarrow O^- + O_2$	$3.30e-16^{**}$	(Kossyi IA, 1992)
56	$O_2^- + O_2 \rightarrow O_2 + O_2 + e$	$2.7e-16*(T/300)^{0.5} * exp(-5590/T)$	(S G Belostotsky, 2005)
57	$O_2^- + O_3 \rightarrow O_3^- + O_2$	$4.00e-16^{**}$	(Kossyi IA, 1992)
58	$O_3^- + O \rightarrow O_2 + O_2 + e$	$3.00e-16^{**}$	(Kossyi IA, 1992)
59	$O_3^- + O \rightarrow O_2^- + O_2$	$3.2e-16*(300/T)^{0.5}$	(J T Gudmundsson, 2001)
60	$O_3^- + O_3 \rightarrow O_2 + O_2 + O_2 + e$	$1.00e-16^{*}$	(Kossyi IA, 1992)
61	$O_4^- + O_2 \rightarrow O_2^- + O_2 + O_2$	$1e-16*exp(-1044/T)$	(Kossyi IA, 1992)
62	$O_4^- + O \rightarrow O_3^- + O_2$	$4.00e-16^{*}$	(Kossyi IA, 1992)
63	$O_4^- + O \rightarrow O^- + O_2 + O_2$	$3.00e-16^{*}$	(Kossyi IA, 1992)
64	$O_2^- + O_2 + O_2 \rightarrow O_4^- + O_2$	$3.5e-42*(300/T)^{*}$	(Kossyi IA, 1992)
65	$O^- + O2 + O_2 \rightarrow O_3^- + O_2$	$1.1e-42*(300/T)^{*}$	(Kossyi IA, 1992)
66	$O^+ + O_2 \rightarrow O_2^+ + O$	$2e-17*(300/T)^{0.5}$	(Kossyi IA, 1992)
67	$O^+ + O_3 \rightarrow O_2^+ + O_2$	$1.00e-16^{**}$	(Kossyi IA, 1992)
68	$O_4^+ + O \rightarrow O_2^+ + O_3$	$3.00e-16^{**}$	(Kossyi IA, 1992)
69	$O_4^+ + O_2 \rightarrow O_2^+ + O_2 + O_2$	$3.3e-12*((300/T)^4) * exp(-5030/T)$	(Kossyi IA, 1992)
70	$O_2^+ + O_2 + O_2 \rightarrow O_4^+ + O_2$	$(2.4e-42)*((300/T)^{3.2})^{*}$	(Kossyi IA, 1992)
71	$O^+ + O + O_2 \rightarrow O_2^+ + O_2$	$1.00e-41^{**}$	(Kossyi IA, 1992)
72	$O_4^+ + O_2(a^1\Delta) \rightarrow O_2^+ + O_2 + O_2$	$1.00e-16^{**}$	(Kossyi IA, 1992)
73	$O_4^+ + O_2(b^1\sum) \rightarrow O_2^+ + O_2 + O_2$	$1.00e-16^{**}$	(Kossyi IA, 1992)
74	$O_4^- + O_2(a^1\Delta) \rightarrow O_2^- + O_2 + O_2$	$1.00e-16^{**}$	(Kossyi IA, 1992)
75	$O_4^- + O_2(b^1\sum) \rightarrow O_2^- + O_2 + O_2$	$1.00e-16^{**}$	(Kossyi IA, 1992)
76	$O_2^- + O_2(a^1\Delta) \rightarrow O_2 + O_2 + e$	$7.00e-16^{**}$	(Anthony Midey, 2008)
77	$O^- + O_2(a^1\Delta) \rightarrow O_3 + e$	$6.10e-17^{**}$	(Anthony Midey, 2008)
78	$O^- + O_2(a^1\Delta) \rightarrow O2 - +O$	$7.3e-16*exp(-890/T)$	(Anthony Midey, 2008)
79	$O_2^- + O_2(b^1\sum) \rightarrow O_2 + O_2 + e$	$3.60e-16^{**}$	(Kossyi IA, 1992)
80	$O^- + O_2(b^1\sum) \rightarrow O_2 + O + e$	$6.90e-16^{**}$	(Kossyi IA, 1992)
81	$O + O_3 \rightarrow O_2 + O_2$	$1.43e-20*(T/300)^{4.13}$	(Kossyi IA, 1992)
82	$O + O + O_2 \rightarrow O_2 + O_2$	$1.56e-45*(T/300)^{-3^{*}}$	(Leu, 1982)
83	$O + O_2 + O_2 \rightarrow O_3 + O_2$	$6e-46*(T/300)^{-1.7^{*}}$	(Leu, 1982)
84	$O_2(a^1\Delta) + O_3 \rightarrow O_2 + O_2 + O$	$3.5e-21*(T/300)^{5.8}$	(Kossyi IA, 1992)
85	$O_2(a^1\Delta) + O_2 \rightarrow O_2 + O_2$	$2.2e-24*(T/300)^{0.8}$	(Dieter Braun, 1992)
86	$O_2(a^1\Delta) + O \rightarrow O_2 + O$	$7.00e-22^{**}$	(Valeriy N. Azyazov, 2009)
87	$O_2(b^1\sum) + O_3 \rightarrow O_2 + O_2 + O$	$1.50e-17^{**}$	(Valeriy N. Azyazov, 2009)
88	$O_2(b^1\sum) + O_3 \rightarrow O_2(a^1\Delta) + O_3$	$3.30e-18^{**}$	(Valeriy N. Azyazov, 2009)
89	$O_2(b^1\sum) + O_3 \rightarrow O_2 + O_3$	$3.30e-18^{**}$	(Valeriy N. Azyazov, 2009)
90	$O_2(b^1\sum) + O_2 \rightarrow O_2(a^1\Delta) + O_2$	$4.3e-28*T^{2.4}*exp(-241/T)$	(Kossyi IA, 1992)

91	$O_2(b^1\sum) + O \rightarrow O_2(a^1\Delta) + O$	$8.10e-20^{**}$	(Kossyi IA, 1992)
92	$O_2(b^1\sum) + O \rightarrow O_2 + O(^1D)$	$3.39e-17 * (T/300)^{0.1} * exp(-4201/T)$	(Kossyi IA, 1992)
93	$O245 + O_2 \rightarrow O_2(b^1\sum) + O_2(b^1\sum)$	$2.90e-19^{**}$	(Kossyi IA, 1992)
94	$O245 + O \rightarrow O_2(b^1\sum) + O(^1D)$	$9.00e-18^{**}$	(Kossyi IA, 1992)
95	$O(^1D) + O_2 \rightarrow O_2(a^1\Delta) + O$	$0.25 * 6.4e-18 * exp(67/T)$	(Kossyi IA, 1992)
96	$O(^1D) + O_2 \rightarrow O_2(b^1\sum) + O$	$2.56e-17 * exp(67/T)$	(Kossyi IA, 1992)
97	$O(^1D) + O_2 \rightarrow O_2 + O$	$0.75 * 6.4e-18 * exp(67/T)$	(Kossyi IA, 1992)
98	$O(^1D) + O_3 \rightarrow O_2 + O + O$	$1.20e-16^{**}$	(Kossyi IA, 1992)
99	$O(^1D) + O_3 \rightarrow O_2 + O_2$	$1.20e-16^{**}$	(Kossyi IA, 1992)
100	$O1s + O_2 \rightarrow O + O_2(4{,}5eV)$	$0.69 * 4.3e-18 * exp(-850/T)$	(Kossyi IA, 1992)
101	$O1s + O_2 \rightarrow O(^1D) + O_2$	$0.31 * 4.3e-18 * exp(-850/T)$	(Kossyi IA, 1992)
102	$O(^1S) + O_3 \rightarrow O(^1D) + O + O_2$	$0.5 * 5.8e-16^{**}$	(Kossyi IA, 1992)
103	$O(^1S) + O_3 \rightarrow O_2 + O_2$	$0.5 * 5.8e-16^{**}$	(Kossyi IA, 1992)
104	$O(^1S) + O_2(a^1\Delta) \rightarrow O_2(b^1\sum) + O(^1D)$	$3.60e-17^{**}$	(Kossyi IA, 1992)
105	$O(^1S) + O_2(a^1\Delta) \rightarrow O_2(4{,}5eV) + O$	$1.30e-16^{**}$	(Kossyi IA, 1992)
106	$O(^1S) + O_2(a^1\Delta) \rightarrow O + O + O$	$3.40e-17^{**}$	(Kossyi IA, 1992)
107	$O(^1S) + O \rightarrow O(^1D) + O$	$5e-17 * exp(-300/T)$	(Kossyi IA, 1992)
108	$O^- + O^+ \rightarrow O + O$	$2.7e-13 * (T/300)^{0.5}$	(J T Gudmundsson, 2001)
109	$O^- + O_2^+ \rightarrow O + O + O$	$7.51e-14 * (T/300)^{0.5}$	(Kossyi IA, 1992)
110	$O^- + O_4^+ \rightarrow O + O_2 + O_2$	$7.51e-14 * (T/300)^{0.5}$	(Kossyi IA, 1992)
111	$O_2^- + O^+ \rightarrow O_2 + O$	$2.0e-13 * (T/300)^{0.5}$	(J T Gudmundsson, 2001)
112	$O_2^- + O_2^+ \rightarrow O_2 + O + O$	$7.51e-14 * (T/300)^{0.5}$	(Kossyi IA, 1992)
113	$O_2^- + O_4^+ \rightarrow O_2 + O_2 + O_2$	$7.51e-14 * (T/300)^{0.5}$	(Kossyi IA, 1992)
114	$O_3^- + O^+ \rightarrow O_3 + O$	$7.51e-14 * (T/300)^{0.5}$	(Kossyi IA, 1992)
115	$O_3^- + O_2^+ \rightarrow O_2 + O + O$	$1.01e-13 * (T/300)^{0.5}$	(J T Gudmundsson, 2001)
116	$O_3^- + O_4^+ \rightarrow O_3 + O_2 + O_2$	$7.51e-14 * (T/300)^{0.5}$	(Kossyi IA, 1992)
117	$O_4^- + O^+ \rightarrow O_2 + O_2 + O$	$7.51e-14 * (T/300)^{0.5}$	(Kossyi IA, 1992)
118	$O_4^- + O_2^+ \rightarrow O_2 + O_2 + O_2$	$7.51e-14 * (T/300)^{0.5}$	(Kossyi IA, 1992)
119	$O_4^- + O_4^+ \rightarrow O_2 + O_2 + O_2 + O_2$	$7.51e-14 * (T/300)^{0.5}$	(Kossyi IA, 1992)
120	$O_4^- + O_4^+ \rightarrow O_2 + O_2 + O_2 + O_2$	$7.51e-14 * (T/300)^{0.5}$	(Kossyi IA, 1992)
121	$O_2^- + O_2^+ + O_2 \rightarrow O_2 + O_2 + O_2$	$2e-37 * (300/T)^{2.5^*}$	(Kossyi IA, 1992)
122	$O_2^- + O^+ + O_2 \rightarrow O_2 + O + O_2$	$2e-37 * (300/T)^{2.5^*}$	(Kossyi IA, 1992)
123	$O^- + O_2^+ + O_2 \rightarrow O + O_2 + O_2$	$2e-37 * (300/T)^{2.5^*}$	(Kossyi IA, 1992)
124	$O^- + O^+ + O_2 \rightarrow O + O + O_2$	$2e-37 * (300/T)^{2.5^*}$	(Kossyi IA, 1992)
125	$O_2^- + O^+ + O_2 \rightarrow O_3 + O_2$	$2e-37 * (300/T)^{2.5^*}$	(Kossyi IA, 1992)
126	$O^- + O_2^+ + O_2 \rightarrow O_3 + O_2$	$2e-37 * (300/T)^{2.5^*}$	(Kossyi IA, 1992)
127	$O^- + O^+ + O_2 \rightarrow O_2 + O_2$	$2e-37 * (300/T)^{2.5^*}$	(Kossyi IA, 1992)
128	$O_2(b^1\sum) \rightarrow O_2(a^1\sum)$	$1.50e-03^{**}$	(Joseph K. Lefkowitz, 2014)
129	$O_2(b^1\sum) \rightarrow O_2$	$8.50e-02^{**}$	(Joseph K. Lefkowitz, 2014)
130	$O2a1s \rightarrow O_2$	$2.60e-04^{**}$	(Joseph K. Lefkowitz, 2014)
131	$O_2 \rightarrow O_2$	11^{**}	(Joseph K. Lefkowitz, 2014)

Table IV-3: surface reactions

Reaction	Formula
1	$O^+ \rightarrow O$
2	$O_2^+ \rightarrow O_2$
3	$O_3^+ \rightarrow O_3$
4	$O_4^+ \rightarrow O_2 + O_2$
5	$O^- \rightarrow O$
6	$O_2^- \rightarrow O_2$
7	$O_3^- \rightarrow O_3$
8	$O_4^- \rightarrow O_2 + O_2$
9	$O(^1D) \rightarrow O$
10	$O(^1S) \rightarrow O$
11	$O_2(a^1\Delta) \rightarrow O_2$
12	$O_2(b^1\sum) \rightarrow O_2$
13	$O \rightarrow 0.5O_2$
14	$O_3 \rightarrow O_2 + O$

4. Simulation results

As seen, discharge current (fig. IV-4) takes an alternative waveform, and during a half period of voltage (positive or negative), current appear with two discharge, one is a peak when applied voltage rise up to the maximum value. Two is a hump start when applied voltage getting down from the peak to zero-volt value. That induced for charge accumulation on the dielectric surface.

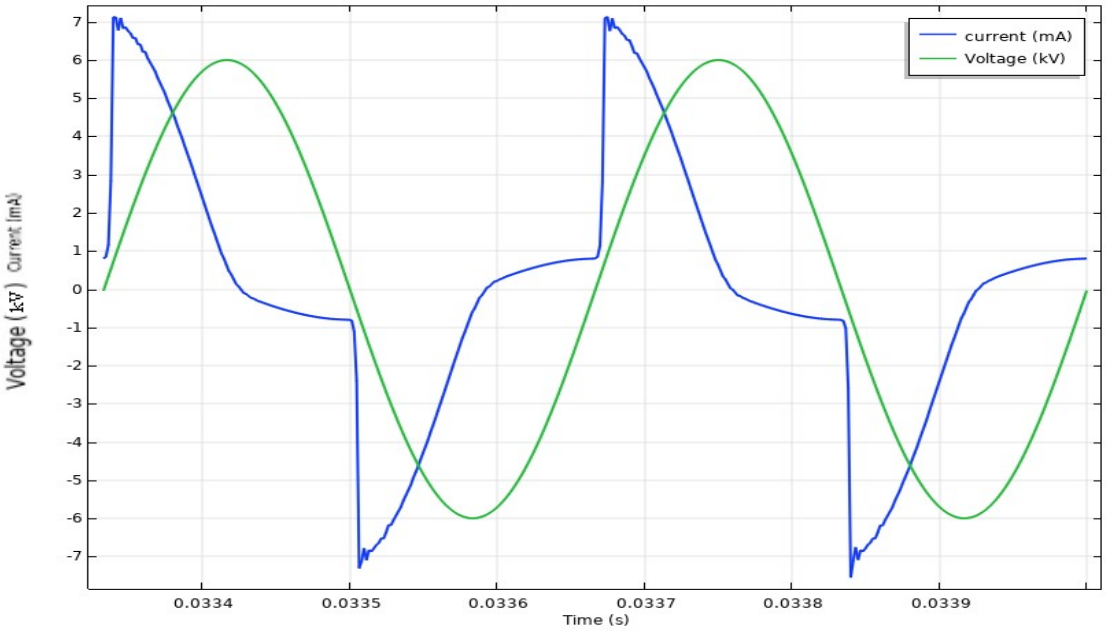

Fig. IV-4: Discharge current and voltage waveform

Figure IV-5 and figure IV-6 show the temporal distribution of charged and neutral species respectively on the dielectric surface of high voltage electrode. As seen clearly, the discharge follows a "Towsend discharge" behavior, which means that under the application of a high electric field (in positive or negative polarity) on gas gap, create a conductor channels across the

gap, therefore an appearance of space charge. The charge accumulation on the dielectric surface (Figure IV-5) make a potential difference reduction, which that interrupts arc creation.

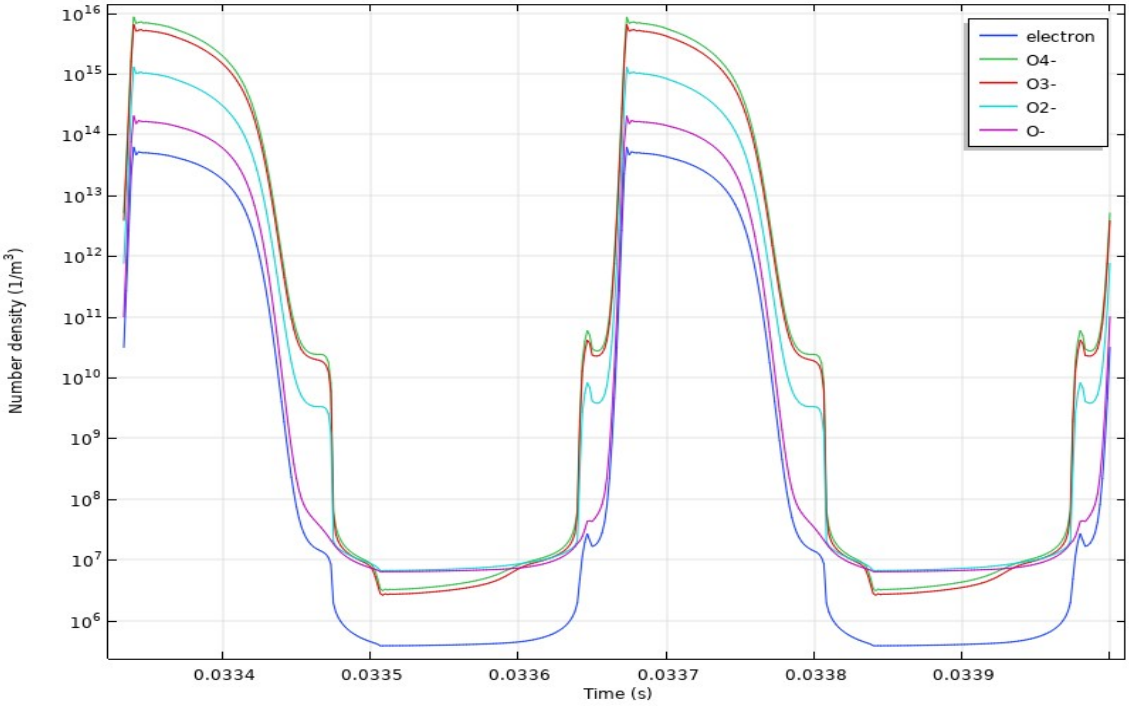

Fig. IV-5:Temporal variation of charged species

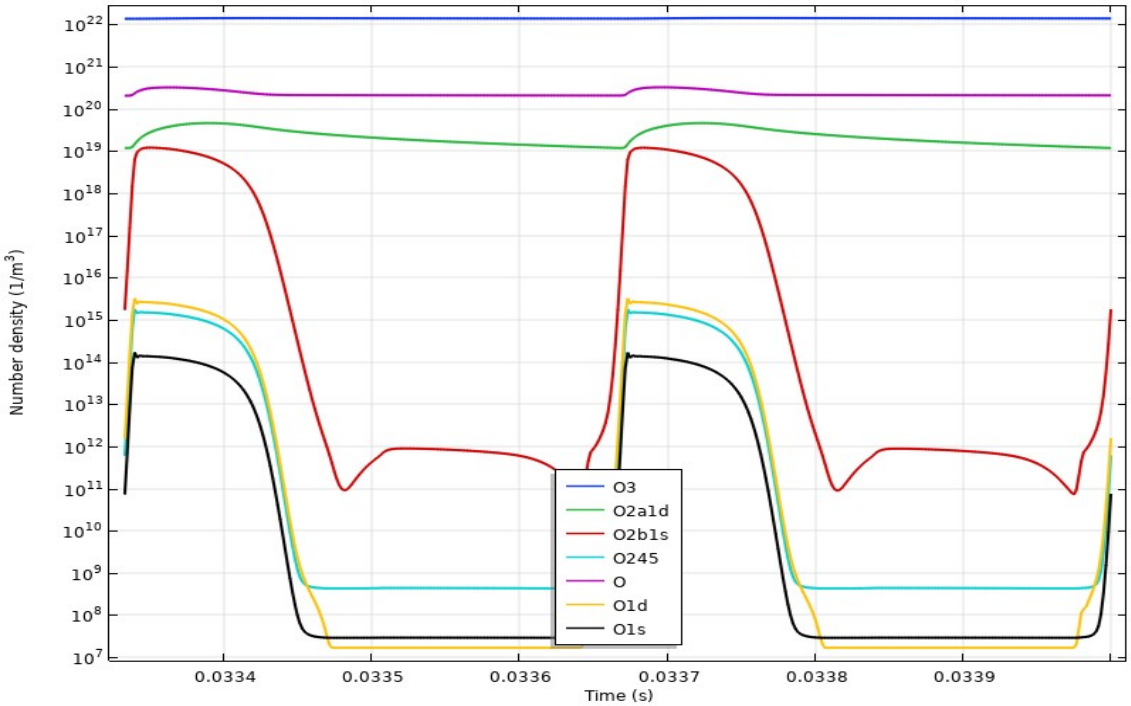

Fig. IV-6: Temporal variation of neutral species

Figure IV-7 and figure IV-8 show the temporal variation of positive and negative ions respectively on the dielectric surface of high voltage electrode. As seen clearly, the discharge follows a “Towsend discharge” behaviour, which means that under the application of a high

electric field (in positive or negative polarity) on gas gap, create a conductor channels across the gap, therefore an appearance of space charge. The charge accumulation on the dielectric surface (Figure IV-7) make a potential difference reduction, which that interrupts arc creation.

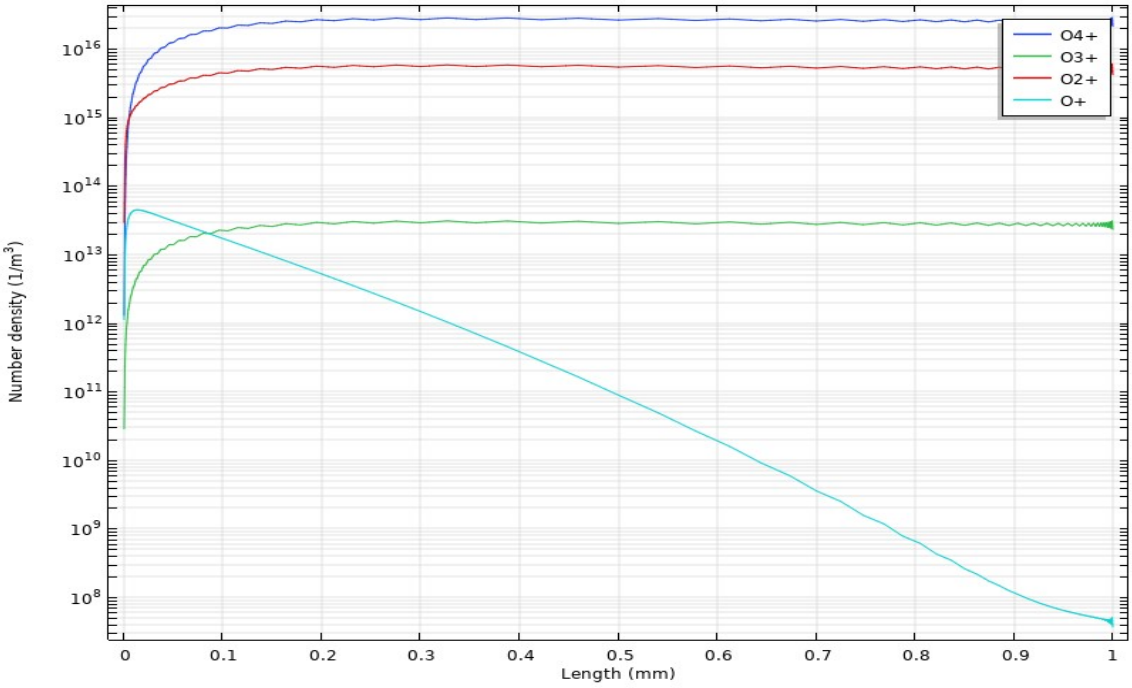

Fig. IV-7: Positive specie number density

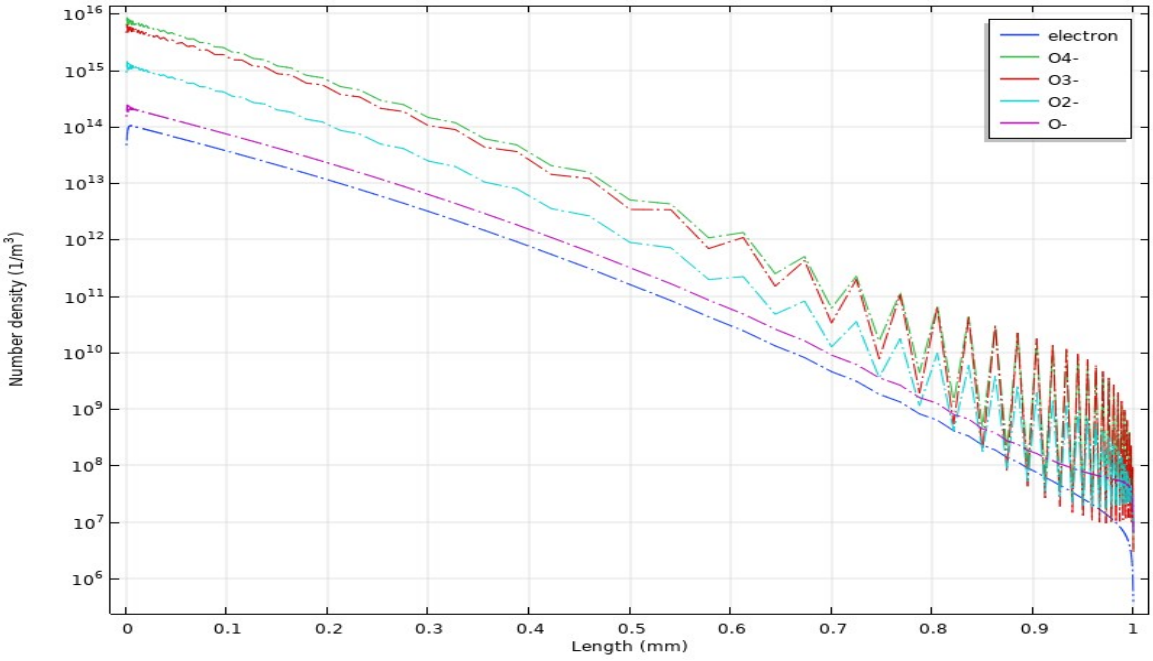

Fig. IV-8: Negative specie number density

Figure IV-9 reports the temporal evolution of the ionic power deposited in the DBD. We note here that the product of electric field and ion current density gives this deposited power. The magnitude of these parameters is maximal near the cathode region. The power reaches a peak of about 2.7×10^7.

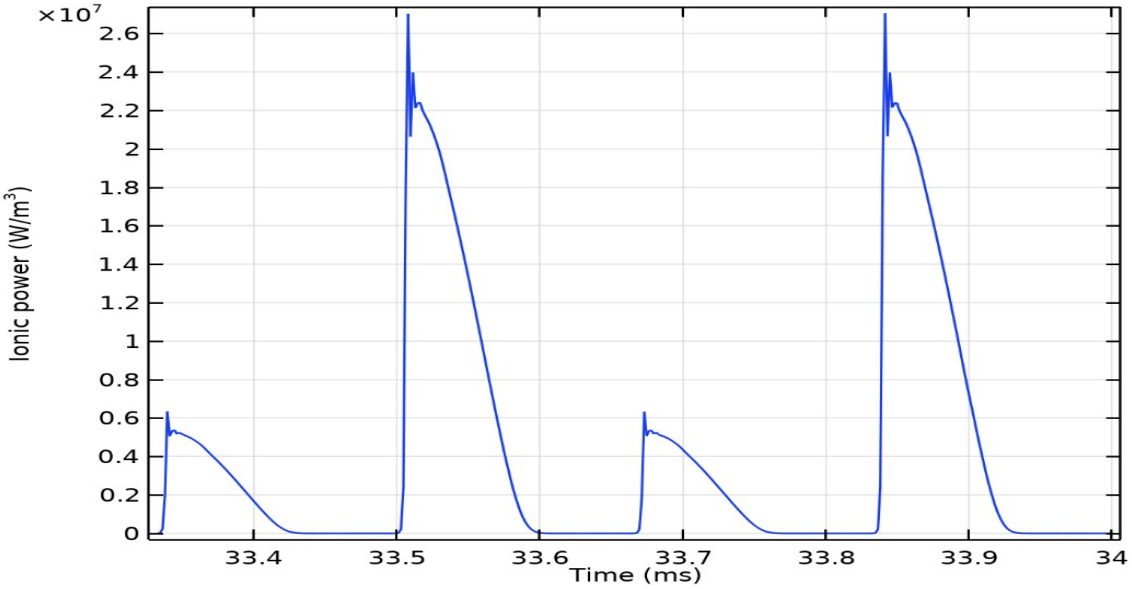

Fig. IV-9:Time evolution of the ionic power deposited in oxygen DBD

5.1. Ozone creation parametric

As mentioned in introduction ozone used for sterilization and purification of water and air. A limited ozone concentration value must not exceed. Thus, ozone should generate under specified characteristics. This section shows the ozone generation by a variation of applied voltage.

- **Applied voltage effect:**

It is well known that when the applied voltage is increased, a higher fraction of the power deposition enters the process of producing excitation and ionization. We have studied three values of the applied voltage (4.5, 6 and 8.5 kilovolts). The temporal variation of the current for these three values of the applied voltage is shown in Figure IV-10. It clearly shows the increase in peak current, when there is more power deposited in the discharge.

The effect of the applied voltage on the temporal evolution of ozone is reported in figure IV-11. The results confirm that the efficiency of ozone production is more dependent on pulse power, and it is clear that the concentration of ozone increases as the applied voltage increases. It should be noted that the rates of electron-impact reactions depend on the density and kinetic energy of the electrons in the discharge.

However, the increase in electron density at high voltage induces a large dissociation of O_2 by electron impact and then the concentration of atomic oxygen will increase (Fig. IV-12) to contribute significantly to the loss ozone generation.

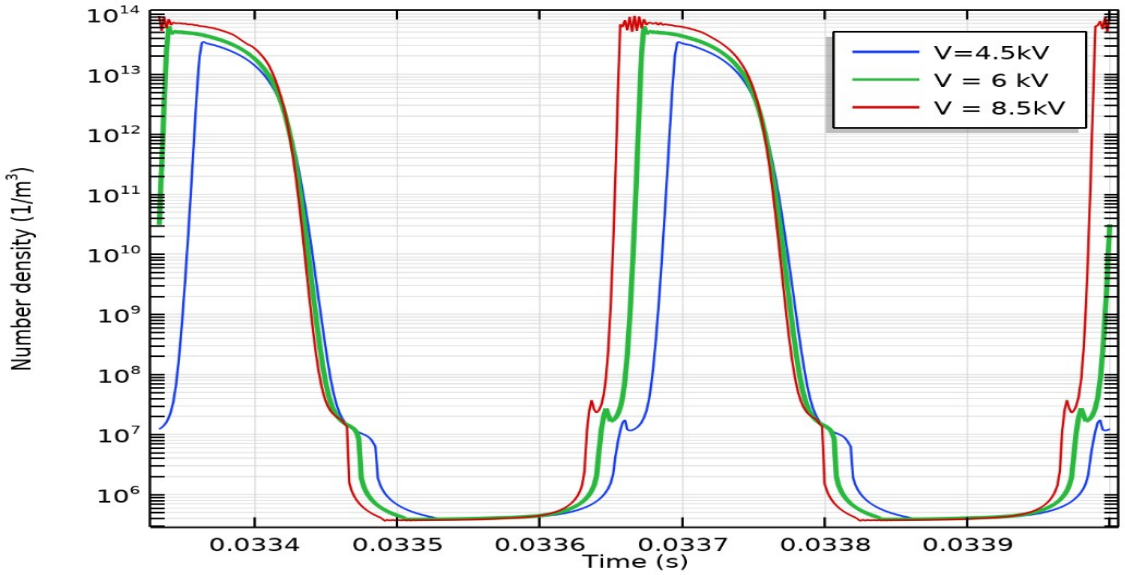

Fig. IV-10: Temporal variation of electron density with variation of voltage

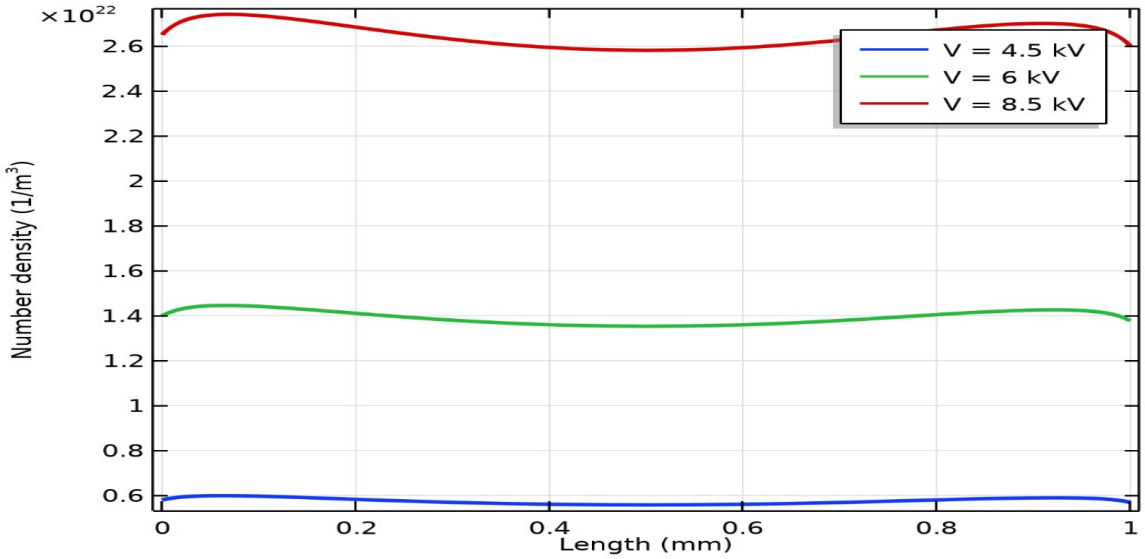

Fig. IV-11: Temporal variation of ozone density with variation of voltage

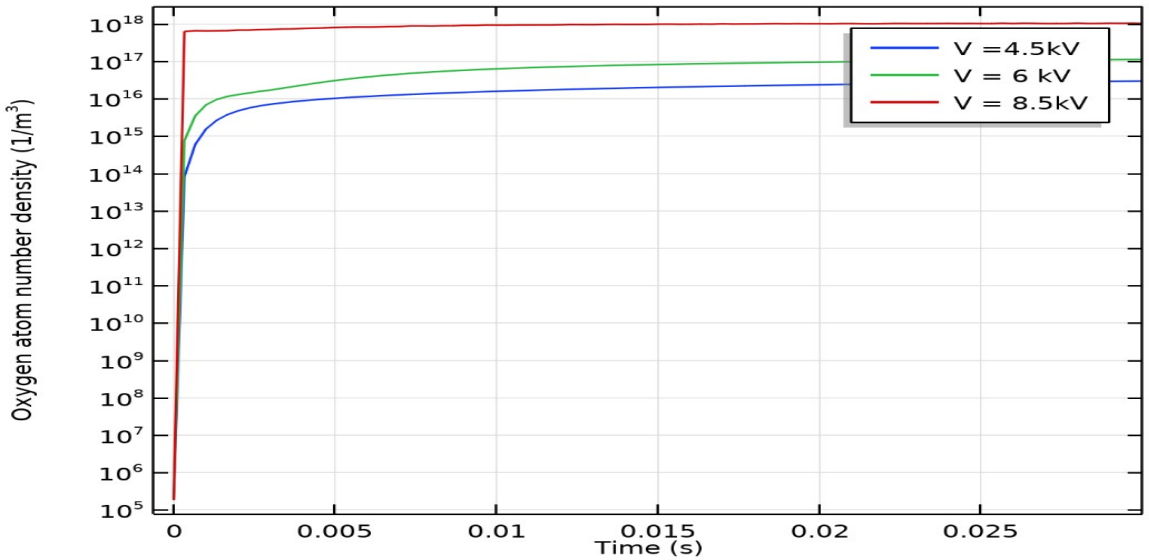

Fig. IV-12: Temporal variation of oxygen atoms density with variation of voltage

6. Conclusion

Many of previous works show valuable results about ozone formation or destruction by a DBD, in pure oxygen gap or nitrogen oxygen mixture (dry air), in different discharge conditions as voltage waveform, gas pressure and temperature… Our work in this section consist to make a place of a model of DBD in pure oxygen at atmospheric pressure and ambient temperature, to investigate about ozone generation by the variation of applied voltage on the gap which effect proportionally on ozone formation. This parameter effect by way or another on discharge and plasma density, thus the purpose from this study is to ameliorate discharge for ozone generation in the optimum voltage conditions.

Bibliography

How Ming Lee, "Kinetic Modeling of Ozone Generation via Dielectric Barrier Discharges.," *Ozone: Science and Engineering, 26,* p. 551–562, 2004.

S. Pekárek., "Non-Thermal Plasma Ozone Generation.," *Acta Polytechnica Vol. 43,* 2003.

B Mennad, "Theoretical investigation of ozone production in negative corona discharge," *Current Applied Physics 10 ,* pp. 1391-1401, 2010.

Moo Been Chang, " Experimental Study on Ozone Synthesis via Dielectric Barrier Discharges," *OZONE SCIENCES. ENGINEERING Vol. 19,* pp. 241-254.

. Moseley ZT, "Mobilities, Diffusion Coefficients, and Reaction Rates of Mass-Indentified Nitrogen Ions in Nitrogen," *physical review Volume 178 ,* p. 240, 1969.

Ellis HW, " Transport properties of gaseous ions over a wide energy range," *Atomic Data And Nuclear Data Tables 17,* pp. 177-210, 1976.

Zhilong Zou, " Meusurment method of Ionic mobilities in direct corona discharge in air," *IEEE transactions on dielectric and insulation Vol.23, No.3,* 2016.

G. Sinnott, "Positive-Ion Mobilities in Dry Air," *Physical Review Vol 170, No 1,* 1968.

A I Florescu-Mitchell, ". Dissociative recombination.," *Physics Reports 430,* p. 277 – 374, 2006.

V Zhaunerchyk, "Three-Body Breakup in the Dissociative Recombination of the Covalent Triatomic Molecular Ion O3-," *Physical Review Letters PRL 98, ,* pp. 201- 223, 2007.

Kossyi IA, "Kinetic scheme of the non-equilibrium discharge in nitrogen-oxygen mixtures," *Plasma Sources Sci. Technol 1,* pp. 207-220, 1992.

J T Gudmundsson, "Electronegativity of low-pressure high-density oxygen discharges," *J. Phys. D: Appl. Phys. 34 ,* p. 1100–1109, 2001.

Phelps, "phelps database," 14 Feb 2019. [Online]. Available: www.LXcat.net.

Morgan, "Morgan Database," 14 Feb 2019. [Online]. Available: www.LXcat.net.

. S G Belostotsky, "Negative ion destruction by O(3P) atoms and O2(a1Δg) molecules in an oxygen plasma.," *Plasma Sources Sci. Technol. 14,* p. 532–542, 2005.

. J. Joseph K. Lefkowitz, " Species and temperature measurements of methane oxidation in a nanosecond repetitively pulsed discharge,," *Phil.Trans.R.Soc.A373,* p. 333, 2014.

M. T. Leu, "Temperature and Third-Body Dependence of the Rate Constant for the Reaction O + O2 + M → O3 + M.," *International Journal of Chemical Kinetics, Vol. 14,* pp. 417-434, 1982.

H. Valeriy N. Azyazov, "O2(a1Δ) quenching in the O/O2/O3 system.," *Chemical Physics Letters 482 ,* p. 56–61, 2009.

Anthony Midey, "Temperature Dependences for the Reactions of O- and O2- with O2(a1Δg) from 200 to 700 K," *J. Phys. Chem. A , 112, ,* pp. 3040-3045, 2008.

Dieter Braun, "Two-dimensional modelling of the Dielectric barrier discharge in air.," *Plasma Sources Sci. Technol. 7 ,* pp. 166-174, 1992.

Chapter V:

DBD modelling in nitrogen-oxygen mixture and ozone generation investigation

1. Introduction:

Electrical discharges occurring in the air give rise to particularly rich and complex chemical kinetics. In a relatively comprehensive model, Kossyi et al. (Kossyi IA (1992)) describe up to 140 species and more than 450 reactions. For obvious reasons, the use of such a model is not possible during numerical simulations and the identification of a reduced system of predominant reactions is necessary. Ionization by electron impact and electronic attachment are the first reactions to consider. Indeed, ionization is at the origin of the electronic avalanche phenomenon necessary to the discharge ignition while the attachment accounts for the electronegative nature of the dioxygen present in the air and allows the creation of negative ions. The reactions of recombination of electrons and negative ions with positive ions are generally taken into account. These reactions allow the number of positive and negative ions to decrease. Beyond these reactions, the role of metastable oxygen molecules in the dynamics of the discharge has also been the subject of several studies. Their ability to detach electrons from negative ions by collision was put forward by Lowke (J.Lowke, (1992)) and then by Morrow (Morrow, (1997)) as a predominant mechanism in the development of streamers. Following on from this work, Degond et al. (P. Degond, 2005)also stressed their importance for the long-time development of a discharge in the presence of a flow.

2. Differences between DBD in Oxygen and Nitrogen Gas:

In this section, Atmospheric pressure dielectric barrier discharge in nitrogen and oxygen gas is simulated based on fluid model, investigating the influence of gas electronegativity.

2.1. Discharge currant and electron density:

Figure V-1 and Figure V-2 show the waveform of discharge current and electron density near to anode varying with time.

Nitrogen discharge current only has one discharge peak, and oxygen discharge current appears two discharge peaks, which also illustrate nitrogen discharge is more uniform than oxygen. A large number of electrons are accumulated around the transient anode in both nitrogen and oxygen discharge.

This is due to the existence of dielectric plate, which prevent electrons from vanishing to anode. Therefore, electrons moving against the direction of electrical field accumulate on the surface of the dielectric. However, electrons distribution is more uniform in higher electron

density area of nitrogen discharge. There is an obvious darker area in oxygen discharge. These might indicate that nitrogen discharge is more like Townsend discharge, whereas during oxygen discharge there has a stream channel.

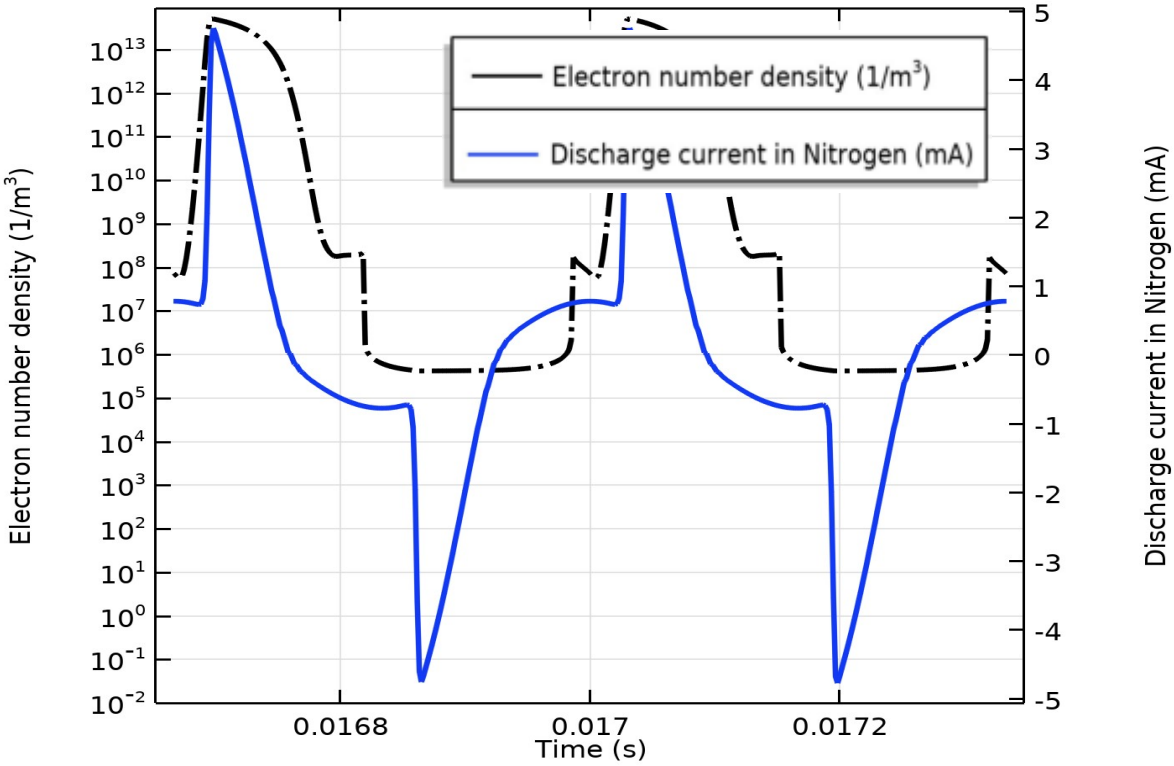

Fig. V-1: Electron density and discharge currant in Nitrogen

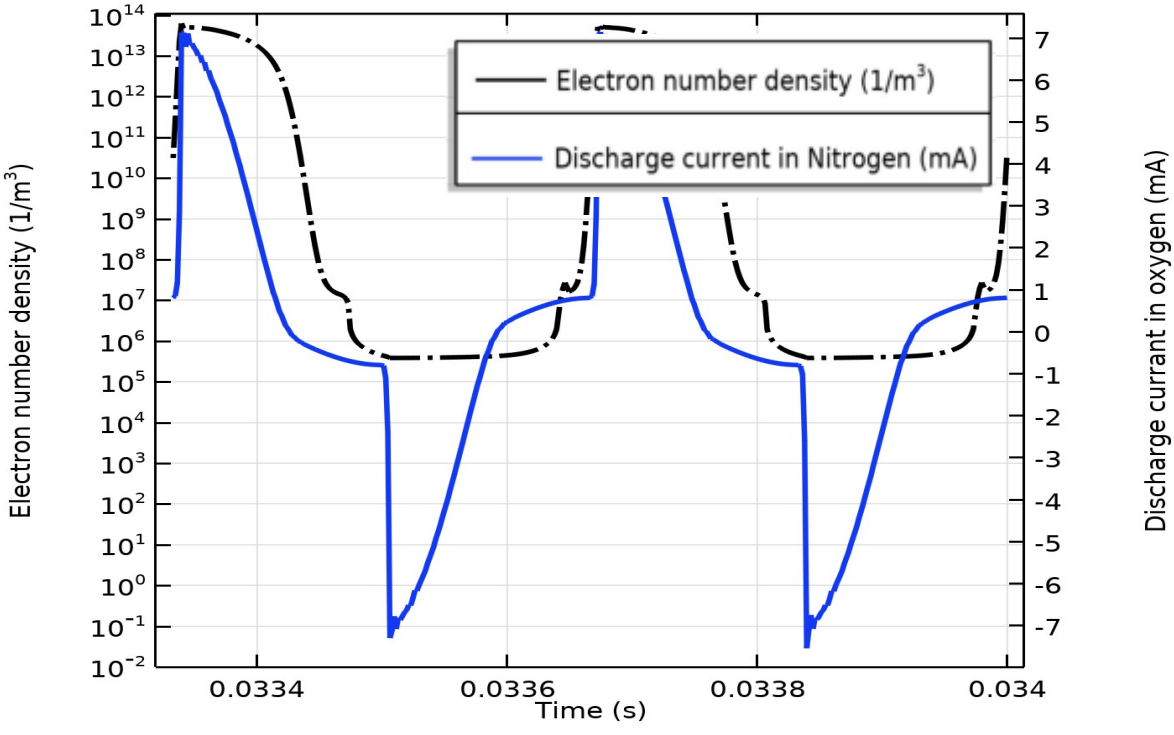

Fig. V-2: Electron density and discharge currant in oxygen

Look carefully at discharge current at nitrogen and oxygen environment, it is easy to find discharge asymmetry phenomenon. And it is more serious in nitrogen discharge. Two discharges in one period are asymmetry either the discharge interval or discharge current peak value. Nevertheless, all the simulation conditions are symmetry.

For nitrogen, only positive ions exist during the discharge, so the electrical field established by positive ions and electrons on the surface of dielectric plates is in the same direction as the electrical field established by negative applied voltage. However, there are both positive and negative ions in oxygen discharge.

During the first discharge, the number of negative ions accumulated in the positive dielectric plate and the positive ions accumulated in the negative dielectric plate are not much different, and the negative ions are slightly larger than the positive ions. The built-in electrical field extinguishes the discharge is primarily establishes by electrons, whose diffusion velocity is much faster than ions.

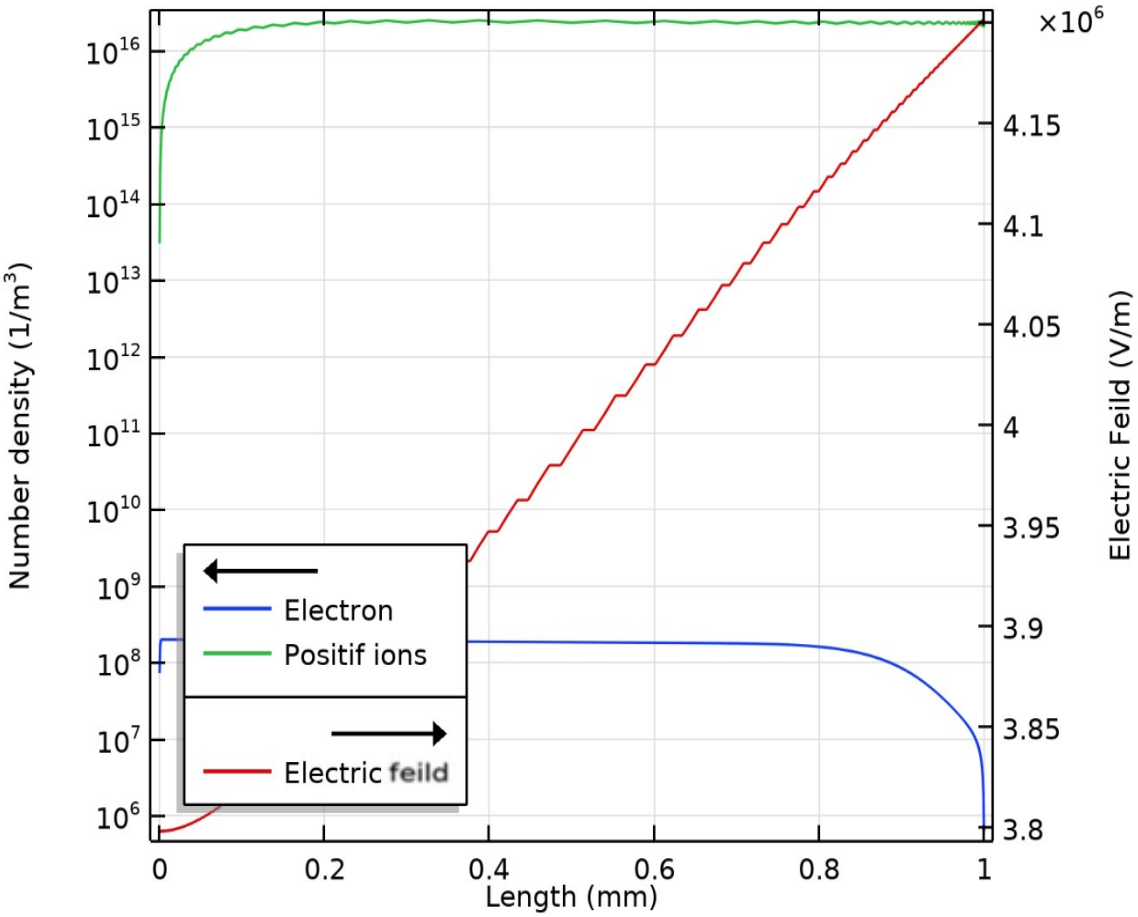

Fig. V-3 : Electrons and ions density and gap electrical field at positive half-cycle maximal current in nitrogen

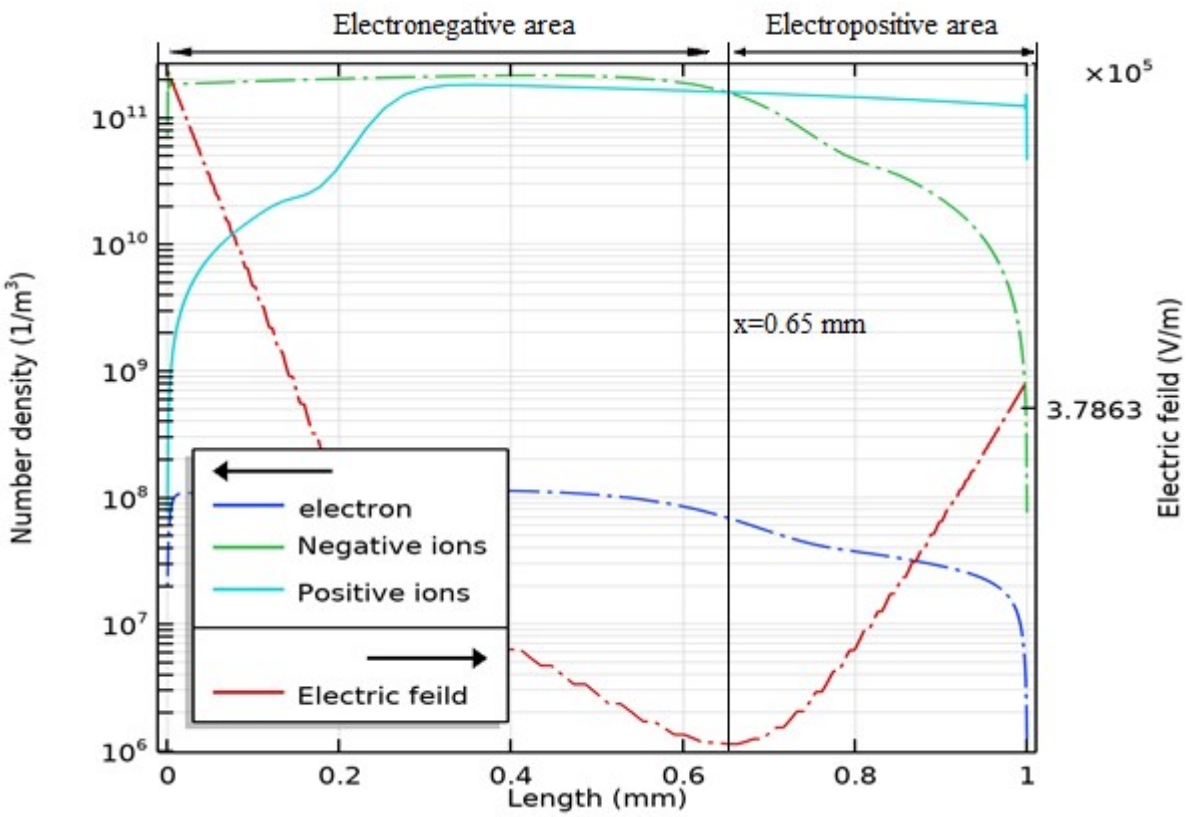

Fig. V-4: Electrons and ions density and gap electrical field at positive half-cycle maximal current in oxygen

Electrons and ions density and discharge gap electrical field at maximal current are investigated, depicted in figure V-3 for nitrogen and in figure V-4 for oxygen. Particularly, positive half-cycle maximal current has been chosen. Nitrogen discharge is at t=0.0167 s, and oxygen discharge is at t=0.0333 s. Electron's density is smaller in both nitrogen and oxygen discharge. And it almost three orders of magnitude lower than ions density. Moreover, the electron density of nitrogen discharge is larger than which of oxygen discharge, resulting from part of electrons form negative ions with oxygen molecule by attachment reaction.

It is found that the electron density of nitrogen discharge shows a certain liner growth from the cathode to the anode. Presumably, an electrons avalanche initiated near the cathode and progressed towards the anode. In other words, the nitrogen discharge manifests as Townsend discharge. As for oxygen discharge, electrons density is evenly distribution over a large area of the discharge gap. It could be a stream in this area, or a filament discharge channel.

The electrical field between the discharge gap is significantly different. In the nitrogen discharge, the electrical field curve has a knee-point, which locate at x=0.16 mm nearby. Before the knee-point, the electrical field almost unchanged. And behind the knee-point, the electrical

field intensity increases linearly, resulting from high density of positive spatial charge in this area. For oxygen discharge, the electrical field curve appears an obvious minimum point located at x=0.6508 mm, and its corresponding electrical field intensity is about 378.36 kV/m. In addition, this point lies on the same position of the intersection of positive and negative density curve. The electrical field intensity changes linearly before and after this point. According to this point, the discharge gap is divided into two regions. From the anode to this point, the negative spatial charge is greater than positive spatial charge, resulting in an electronegative region. Meanwhile, the negative spatial charge is less than positive spatial charge from this point to the cathode, bring about an electropositive region.

This section is a preliminary work for the next section which is a simulation of atmospheric pressure air DBD that indicates to perform a simulation under mixture nitrogen and oxygen gas.

3. DBD modelling in N_2/O_2 mixture at atmospheric pressure:

3.1. Chemical kinetics model of the mixture:

The chemical kinetics of the plasma in the N_2/O_2 mixture used in this thesis is extremely complex: it involves all nitrogen model reactions which sited in Table V-1 and oxygen model reactions that sited in Table V-2, plus 64 new reactions between atoms and molecules oxygen and nitrogen, and 38 species, are summarized below:

Table V-1: The species considered for air plasma

Electrons	e
Neutral species	N, N_2, O, O_2, O_3, NO, N_2O, NO_2, NO_3
Positive species	N^+, O^+, N_2^+, N_3^+, N_4^+, O_2^+, O_3^+, O_4^+, NO^+, N_2O^+, NO_2^+
Negative species	O_2^-, O^-, O_3^-, O_4^-, NO^-, NO_2^-
Exited species	$N_2(A^3\sum_u^+)$, $N_2(B^3\prod g)$, $N_2(C^3\prod u)$, $N_2(a'^1\sum_u^-)$, N(P), N(D), $O_2(a'^1\Delta)$, $O_2(a'^1\sum)$, $O_2(b^1\sum)$, O_2(4.5eV), O(^{1}D), O(^{1}S)

Several theoretical and experimental models have been carried out by many researchers in order to analyze the discharge behavior in the N_2/O_2 mixture (Kossyi IA, 1992), (M.

CAPITELLI, 2000), (Y. MIROKIN, 1998) and others. Take into account electrons, neutral, excited and positively and negatively charged species.

The objective of this model is to describe the fundamental chemistry and physics governing the discharge behavior, and to predict the ozone generation under various operating conditions. In non-equilibrium discharges, chemically active species are produced by collisions of gas molecules with electrons and the rate constants of electron- molecule reactions depend strongly on the reduced electric field. The efficiency of the production of ozone by electric discharge depends, above all, on the intensity of the micro discharges (which is influenced by a number of factors such as the width of the space; the pressure of the gas; the type of the electrodes' 'metal and dielectric'; power supply, and moisture). A large portion of the electrical energy used in an electrical discharge is dissipated primarily as heat and a small portion as light. The generators produce ozone at concentrations of 1-5% by weight of air and up to 14% by weight of pure oxygen. If compressed air is used as a feed gas, it must be very dry (Yanallah K, 2006). During discharges in dry air, the main mechanisms of primary species production relate to electronic impacts on O2 and N_2 molecules. All these species are very reactive reaction intermediates which react with the other neutral molecules present and lead to the formation of the final discharge products observed at the outlet of the reactor. Among these stable species are various forms of nitrogen oxides (NO, NO2, ...), and ozone (O3). In an electrical discharge ozone is produced in two stages (Milan Šimek, 2002):

- Oxygen atoms are produced by the direct dissociation of molecular oxygen:

$$e + O_2 \rightarrow O + O + e$$

- Ozone is produced through a process of three bodies:

$$O + O_2 + M \rightarrow O_3 + M \ (M = O_2, N_2)$$

- The production of oxygen atoms leads to the disappearance of O_3 by the following reaction:

$$O + O_3 \rightarrow 2\ O_2$$

- For the treatment of NOx ozone is largely responsible for the oxidation of NO to NO_2 and NO_3:

$$NO + O_3 \rightarrow NO_2 + O_2$$

$$NO_2 + O_3 \rightarrow NO_3 + O_2$$

The set of reaction processes and their reaction rate coefficients used in N_2/O_2 discharge model work is shown in table V-2.

Table V-2: additional reaction set for air DBD model

No.	Reaction	Rate coefficient [m^3/s.mol or m^6/s.mol(*) or 1/s(**)]
1	$e + NO \rightarrow e + NO$	Cross section
2	$e + NO \rightarrow e + NO$	Cross section
3	$e + NO \rightarrow e + NO$	Cross section
4	$e + NO \rightarrow e + NO$	Cross section
5	$e + NO \rightarrow e + NO$	Cross section
6	$e + NO \rightarrow e + NO$	Cross section
7	$e + NO \rightarrow e + NO$	Cross section
8	$e + NO \rightarrow e + NO$	Cross section
9	$e + NO \rightarrow e + NO$	Cross section
10	$e + NO \rightarrow e + e + NO^+$	Cross section
11	$e + N_2O \rightarrow e + N_2O$	Cross section
12	$e + N_2O \rightarrow e + N_2O$	Cross section
13	$e + N_2O \rightarrow e + N_2O$	Cross section
14	$e + N_2O \rightarrow e + N_2O$	Cross section
15	$e + N_2O \rightarrow e + N_2O$	Cross section
16	$e + N_2O \rightarrow e + N_2O$	Cross section
17	$e + N_2O \rightarrow e + N_2O$	Cross section
18	$e + N_2O \rightarrow e + e + N_2O^+$	Cross section
19	$O_2^- + N_2 \rightarrow e + N_2 + O_2$	$1.9e\text{-}18*(T/300)^{0.5}*\exp(-4990/T)$
20	$O_2^- + N_2(A^3\sum_u^+) \rightarrow e + N_2 + O_2$	2.1e-15
21	$O_2^- + N_2(B^3\prod g) \rightarrow e + N_2 + O_2$	2.5e-16
22	$O_2^- + N_2(B^3\prod g) \rightarrow e + N_2 + O$	1.9e-15
23	$O_2^- + N_2(A^3\sum_u^+) \rightarrow e + N_2 + O$	2.2e-15
24	$O^- + N \rightarrow NO + e$	2.6e-16
25	$N + O_3 \rightarrow NO + O_2$	2e-22
26	$O + N2(A^3\sum_u^+) \rightarrow O + N(D)$	7e-18
27	$NO + N_2(B_3\prod g) \rightarrow NO + N_2(A^3\sum_u^+)$	2.4e-16
28	$NO + O_2(a'^1\Delta) \rightarrow NO + O_2$	2.5e-17
29	$N + O_2(a'^1\Delta) \rightarrow NO + O$	$2e\text{-}20*\exp(-600/T)$
30	$N_2 + O_2(b^1\sum) \rightarrow N_2 + O_2(a^1\Delta)$	$4.9e\text{-}21*\exp(-253/T)$
31	$NO + O_2(b^1\sum) \rightarrow NO + O_2(a^1\Delta)$	4e-19
32	$N(D) + O_2 \rightarrow NO + O^1(D)$	$6e\text{-}18*\exp(T/300)^{0.5}$
33	$N(D) + O_2 \rightarrow NO + O$	2.6e-18
34	$N(P) + NO \rightarrow N_2(A^3\sum_u^+) + O$	3.4e-17
35	$N^+ + O_2 \rightarrow NO^+ + O$	2.5e-16
36	$N^+ + O \rightarrow N + O^+$	1e-18
37	$N^+ + O_2 \rightarrow NO + O^+$	2.8e-17
38	$O^+ + N(D) \rightarrow N^+ + O$	1.3e-16
39	$NO_2^+ + e \rightarrow NO + O$	$2e\text{-}13*(300/T\_e)^{0.5}$
40	$N_2O^+ + e \rightarrow N_2 + O$	$2e\text{-}13*(300/T\_e)^{0.5}$
41	$NO^+ + e \rightarrow N + O$	$4e\text{-}13*(300/T\_e)^{1.5}$

42	$NO^+ + e \rightarrow N(D) + O$	3e-13*(300/Te)
43	$e + NO_2 \rightarrow O^- + NO$	1e-17
44	$O^- + NO \rightarrow NO_2 + e$	2.6e-16
45	$N + NO \rightarrow N_2 + O$	$1.05e\text{-}18*T^{0.5}$
46	$N + NO_2 \rightarrow N_2 + O_2$	7e-19
47	$N + NO_2 \rightarrow N_2 + O + O$	9.1e-19
48	$N + NO_2 \rightarrow N_2O + O$	3e-18
49	$N + NO_2 \rightarrow NO + NO$	2.3e-18
50	$O + NO_2 \rightarrow NO + O_2$	$1.3e\text{-}17*\exp(T/1000)^{0.18}$
51	$NO + O_3 \rightarrow O_2 + NO_2$	$4.3e\text{-}18*\exp(-1560/T)^{0.18}$
52	$N_2(A^3\sum_u^+) + N_2O \rightarrow N_2 + N + NO$	1e-17
53	$O^1(D) + N_2O \rightarrow NO + NO$	7.2e-17
54	$N^+ + O_3 \rightarrow NO^+ + O_2$	5e-16
55	$N^+ + NO \rightarrow N + NO^+$	8e-16
56	$N^+ + NO \rightarrow N_2^+ + O$	3e-18
57	$N^+ + NO \rightarrow O^+ + N_2$	1e-18
58	$N^+ + N_2O \rightarrow NO^+ + N_2$	5.5e-16
59	$O^+ + N_2 \rightarrow NO^+ + N$	3e-18*exp(-0.0031*T)
60	$O^+ + NO \rightarrow NO^+ + O$	2.4e-18
61	$O^+ + NO \rightarrow O_2^+ + N$	3e-18
62	$O^+ + NO_2 \rightarrow NO_2^+ + O$	1.6e-15
63	$O^+ + N_2O \rightarrow N_2O^+ + O$	4e-15
64	$O^+ + N_2O \rightarrow O_2^+ + N_2$	2e-17
65	$N_2^+ + NO \rightarrow NO^+ + N_2$	3.3e-16
66	$N_2^+ + N_2O \rightarrow NO^+ + N_2 + N$	4e-16
67	N_2^++N_2 O→ $N_2O^+ + N_2$	5e-16
68	$O_2^+ + N \rightarrow NO^+ + O$	1.2e-16
69	$O_2^+ + NO \rightarrow O^+ + O_2$	4.4e-16
70	$O_2^+ + NO_2 \rightarrow NO^+ + O_3$	1e-17
71	$O_2^+ + NO_2 \rightarrow NO_2^+ + O_2$	6.6e-16
72	$N_3^+ + O_2 \rightarrow O_2^+ + N + N_2$	2.3e-17
73	$N_3^+ + O_2 \rightarrow NO_2^+ + N_2$	4.4e-17
74	$N_3^+ + NO \rightarrow NO^+ + N + N_2$	7e-17
75	$N_3^+ + NO \rightarrow N_2O^+ + N_2$	7e-17
76	$N_2O^+ + NO \rightarrow NO^+ + N_2O$	2.9e-16
77	$N_2O^+ + NO \rightarrow NO^+ + N_2O$	2.9e-16
78	$N_4^+ + O_2 \rightarrow O_2^+ + N_2 + N_2$	2.5e-16
79	$O_4^+ + NO \rightarrow NO^+ + O_2 + O_2$	1e-16
80	$O_2^- + NO_2 \rightarrow NO_2^- + O_2$	8e-16
81	$O^- + NO_2 \rightarrow NO_2^- + O$	1.2e-13
82	$O^- + N_2O \rightarrow NO^- + NO$	2e-16
83	$O_3^- + NO_2 \rightarrow O_3 + NO_2^-$	7e-16
84	$NO^- + O_2 \rightarrow O_2^- + NO$	5e-16

These 84 reactions sited in table V-2 are from previous works of air DBD models as (Kossyi IA, 1992) (Lazarou C, 2015) (Massines F, 2003) and the cross section reactions of electron impact with NO and N_2O are from (phelps, 2019).

3.2. Results and discussion:

This part consists of the presentation of our results concerning the modeling of a dielectric barrier discharge in gas mixtures composed of 80% N_2 and 20% O_2 (dry air) at atmospheric pressure for the production of ozone O_3.

3.2.1 Time evolution of electrical parameters:

The energetic characterization of the discharge is an important step in evaluating the performance of the generator-reactor coupling. The simulation of the temporal evolution of the voltage and current signals is essential to be able to calculate the instantaneous power in the circuit and the energy injected into the discharge. Figure V-5 and Figure V-6 represent the profile of the electrical characteristics of the discharge used in our work.

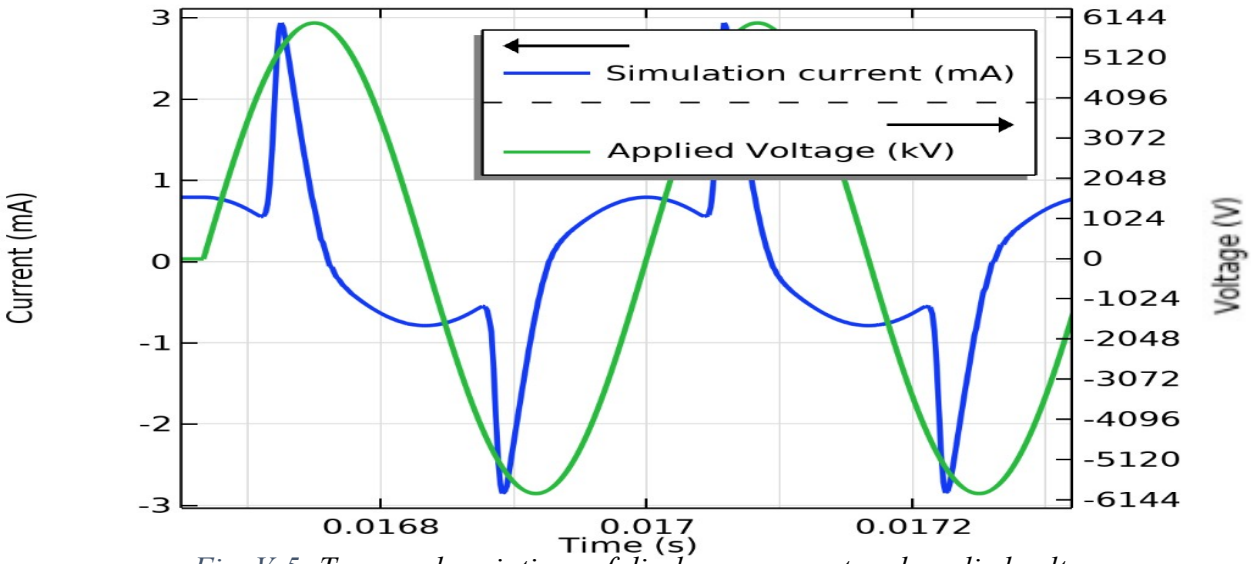

Fig. V-5: Temporal variations of discharge current and applied voltage

Figure V-5 shows the evolution of the discharge current and the applied voltage from 12 kV peak to peak as a function of time. From this figure, it is seen in that the current changed smoothly and the value of current density is nonzero for all phase of discharge. In addition, we notice a peak of 2.9354 mA at 16.7 ms. This growth is due to the increase in electron multiplication during the drift of particles under the effect of the electric field. The current then decreases rapidly going towards negative values at the negative half cycle of the voltage. The decrease in current is due to charged particles (electrons and ions) produced in volume of plasma

which reduces the voltage. In Figure V-6, the total current is shown with its electrons and ions conduction currents as well as displacement current. Ions conduction current is higher than that of the electrons, which is characteristic of Townsend discharge.

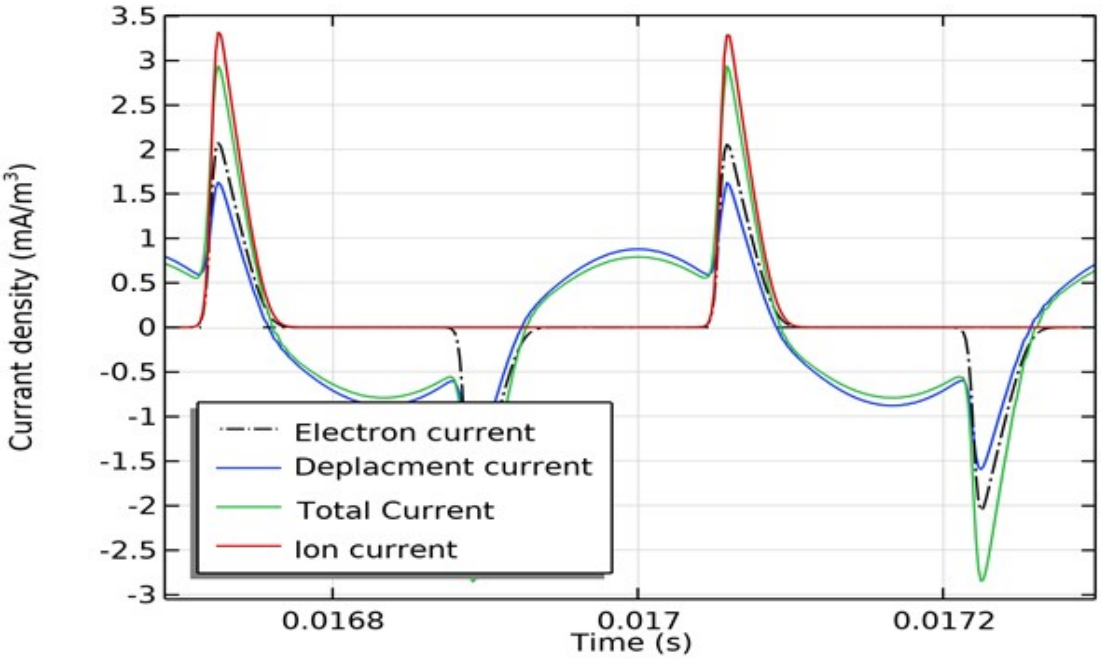

Fig. V-6: Parts of total discharge current

In Figure V-7, the electric field has a maximum value initially equal to 28Td. The field begins to increase with the same form of the applied voltage until it reaches a maximum value of 264Td. in the following negative half-wave, the electric field reduced to its maximum value of 275Td.

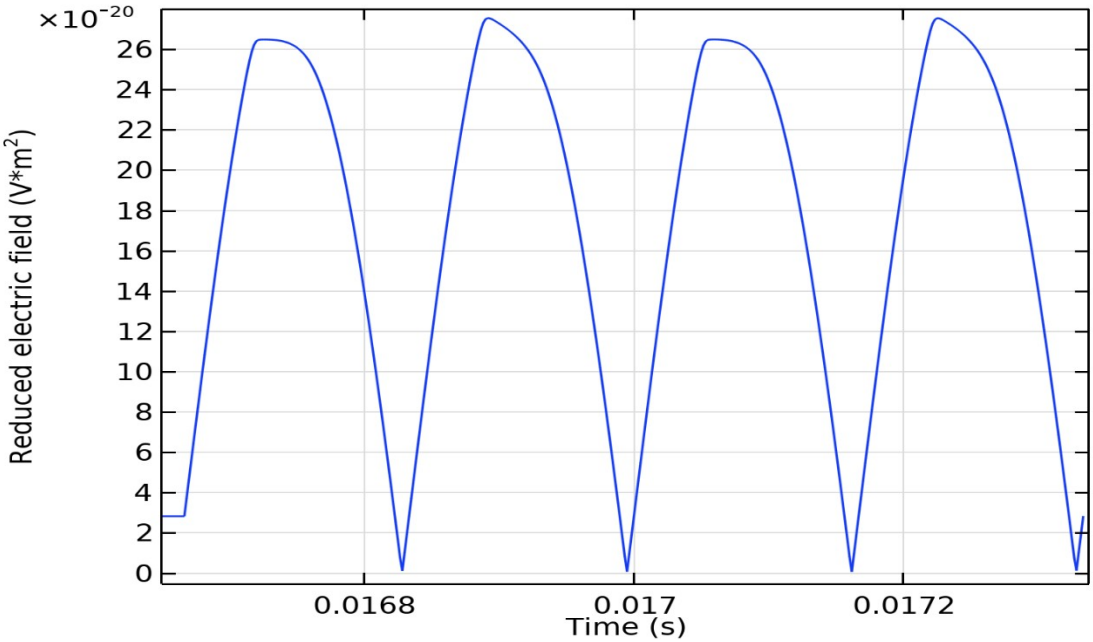

Fig. V-7:The temporal variation of the reduced electric field

3.2.2. Temporal variation of charged species densities:

We have shown in figure V-8 the temporal evolution of the density of the positively charged species. We observe a decrease in the densities of these species more or less important according to the evolutionary phases of the discharge. This decrease is due to the fact that these species which are created during the phase of discharge by electronic impacts will be used to produce other species (O_3, NO_2, NO) and that no additional creation of these species is expected during their evolution. The electron density reaches a maximum value of about $3.2449\times10^{13}m^{-3}$ and decreases as a result of recombination and electronic attachment processes.

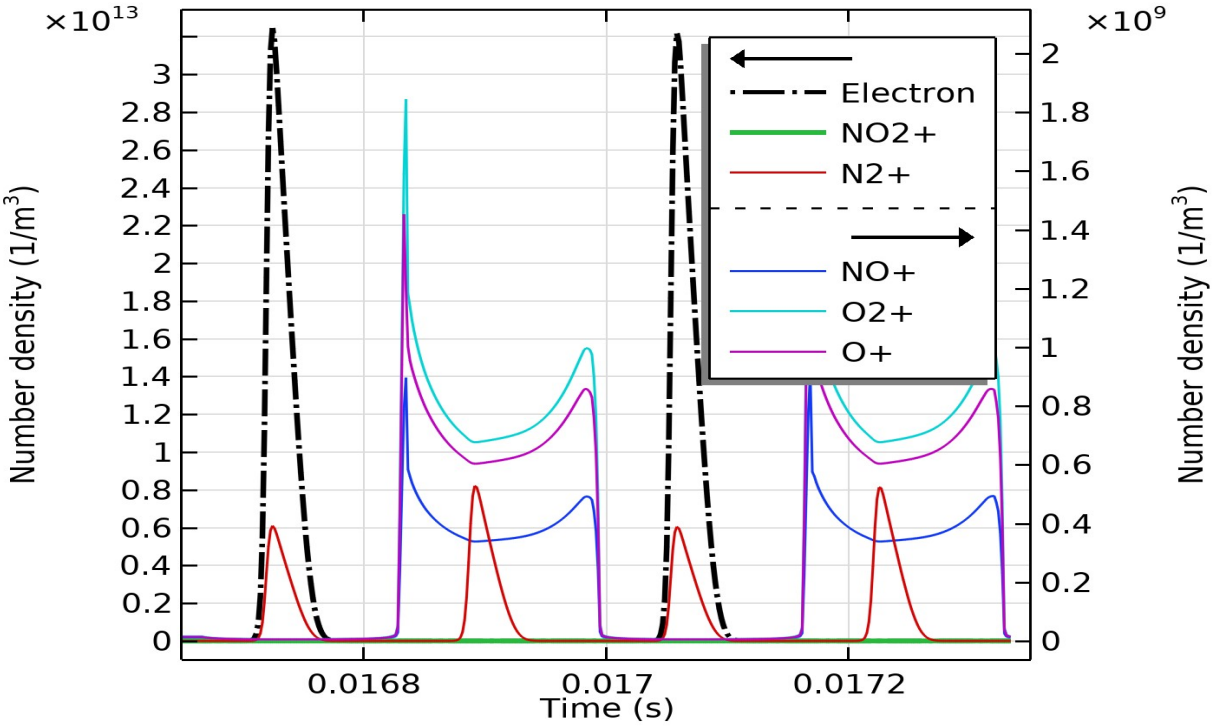

Fig. V-8: Temporal variations of the densities of positive charged species and electron

We clearly observe that the concentration of O_2^+ reaches the maximum value of $1.8441\times10^{9}m^{-3}$ which is mainly due to the direct collision with the electrons:

$e + O_2 \rightarrow O_2^+ + 2e$ (Table V-2)

Then, we observe a decrease in density following several reactions:

$O_2^+ + NO \rightarrow NO^+ + O_2$ (Table V-2)

$O_2^+ + NO_2 \rightarrow NO_2^+ + O_2$ (Table V-2)

And concerning the N_2 ions we observe as previously that the density evolves by electronic collision according to the following reaction:

$e + N_2 \rightarrow N_2^+ + 2e$ (Table III-1)

Then we observe a decrease in density which proceeds as follows:

$N_2^+ + NO \rightarrow NO^+ + N_2$ (Table V-2)

$N_2^+ + NO_2 \rightarrow NO_2^+ + N_2$ (Table V-2)

$N_2^+ + NO_2 \rightarrow NO^+ + N_2O$ (Table V-2)

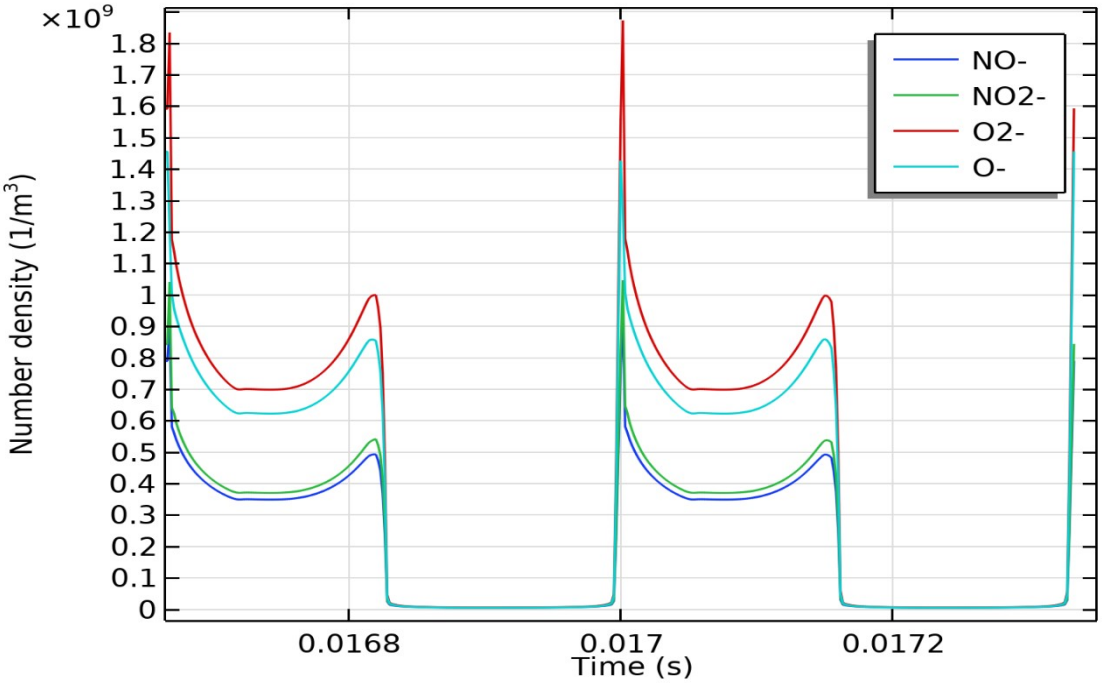

Fig. V-9 :Temporal variation of the density of the negative charged species

The major negative ion in the discharge is O_2^-. At t=0.017 s the O_2^- concentrations are approximately 1.8716×10^{19} m^{-3}. Oxygen molecules need less energy to become ionized unlike nitrogen molecules and therefore the majority of ionized species in the N_2/O_2 mixture is due to the dissociation of oxygen.

3.2.3. Temporal variation of exited species:

The temporal evolution of the concentrations of the exited species is presented in figure V-10 This process is associated with an elevated ionization rate inducing a rapid growth of the densities of the excited species, as shown in figure V-10 which illustrates the variation of the excited species. These new species are chemically active and therefore lead to the formation of new stable compounds such as ozone and NOx.

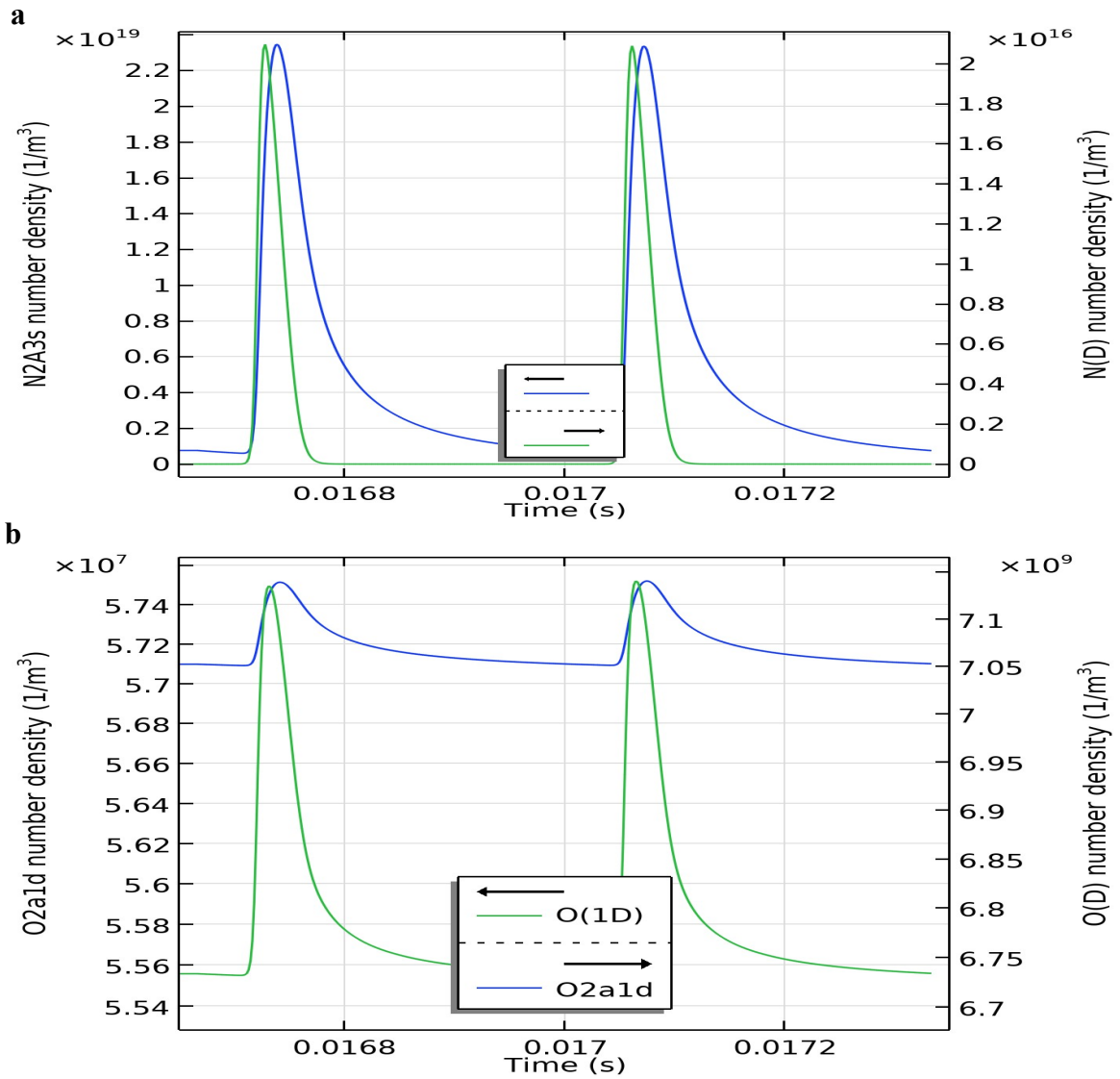

Fig. V-10: Temporal evolution of the density of exited species

3.2.4. Temporal variation of neutral species:

Figure V-11 shows that the concentration of O_3 gradually increases over time, until saturation takes place, which is approximately 17×10^{12} m^{-3} . Ozone production in N_2/O_2 mixture is more complicated than the production of ozone in pure oxygen, due to the presence of the ionic species (N^+, N_2^+) and the presence of excited nitrogen molecules. Despite this, the added amount of nitrogen changes the average electron energy which leads to the production of another atomic oxygen. Then, it leads to the production of ozone, but it is for a specific ratio of N_2/O_2 mixture. Therefore, nitrogen can have a catalytic effect on ozone production in our DBD model. In addition, we notice in the figure the ozone concentration reaches a maximum of $[O_3] = 17 \times 10^{12}$ m^{-3} cm, once the ozone is formed it collides with an atom oxygen or nitrogen oxide that has been formed to dissociate it.

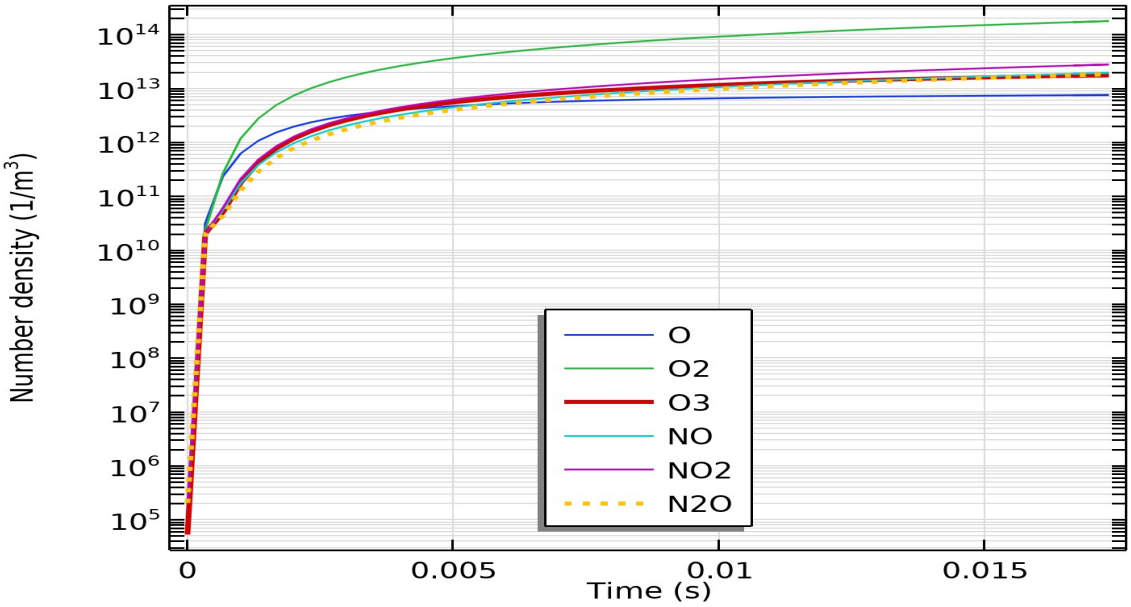

Fig. V-11: Temporal evolution of the density of Temporal variations of the densities of positively charged species and electron

3.3. Air temperature effect on Ozone production:

Figure V-12 shows the variation of ozone over time at atmospheric pressure for two gas temperatures: 300 and 400 K. The ozone concentration increases over time. An increase in the temperature of the gas leads to a decrease in the ozone concentration. At approximately 0.0167s the ozone concentration drops from 2×10^{13} m^{-3} for T = 300K to $1.72 \times 10^{13} m^{-3}$ for T = 400K. This figure clearly shows that ozone production is efficient at low gas temperature. The figure verifies the findings of (Pignolett, 1990) (Fig. V-13). Note also that (Elliasson, 1987) have shown that the density of ozone decreases by about half when the temperature increases from 350 to 400 K.

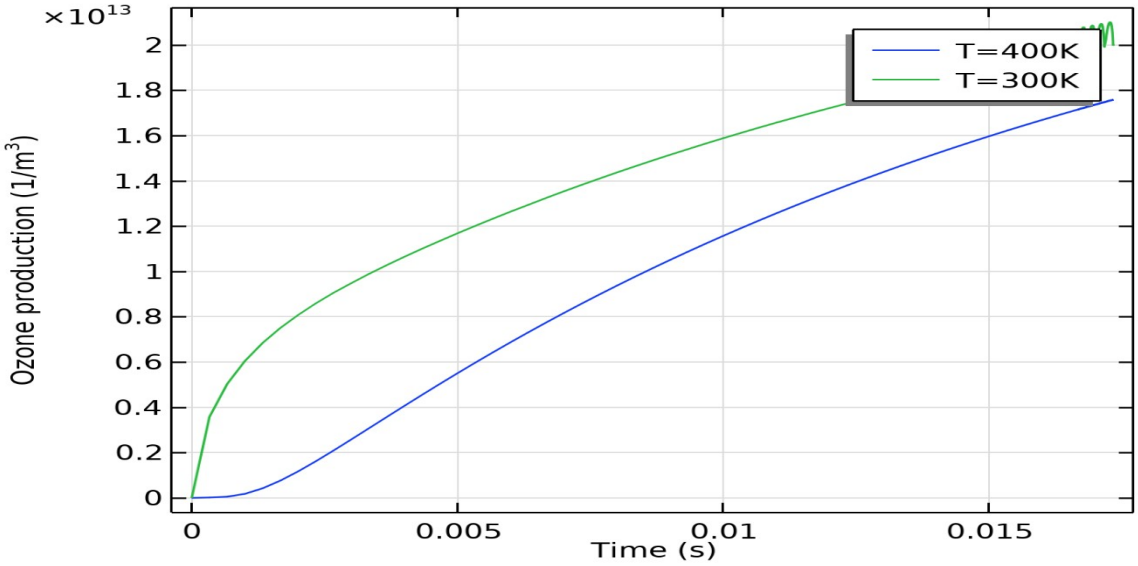

Fig. V-12: Gas temperature effect ozone production

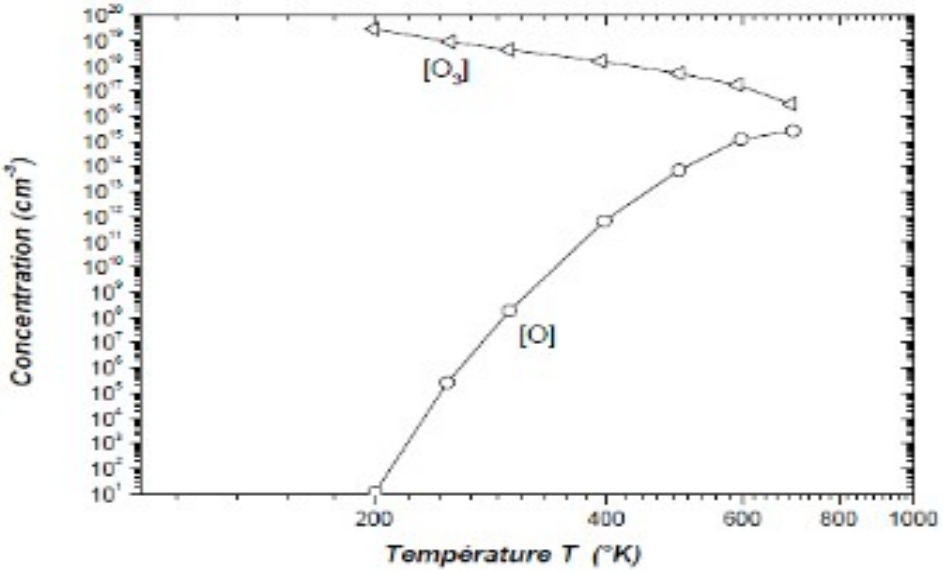

Fig. V-13: The variation of ozone and atomic oxygen densities as a function of the temperature of the gas (Pignolett, 1990)

3.4. Applied voltage effect on ozone production:

It is well known that when the applied voltage is increased, a higher fraction of the power deposition enters the process of producing excitation and ionization. We have studied three values of the applied voltage (6, 8 and 10 kilovolts). The temporal variation of the current for these three values of the applied voltage is shown in figure V-14. It clearly shows the increase in peak current, when there is more power deposited in the discharge.

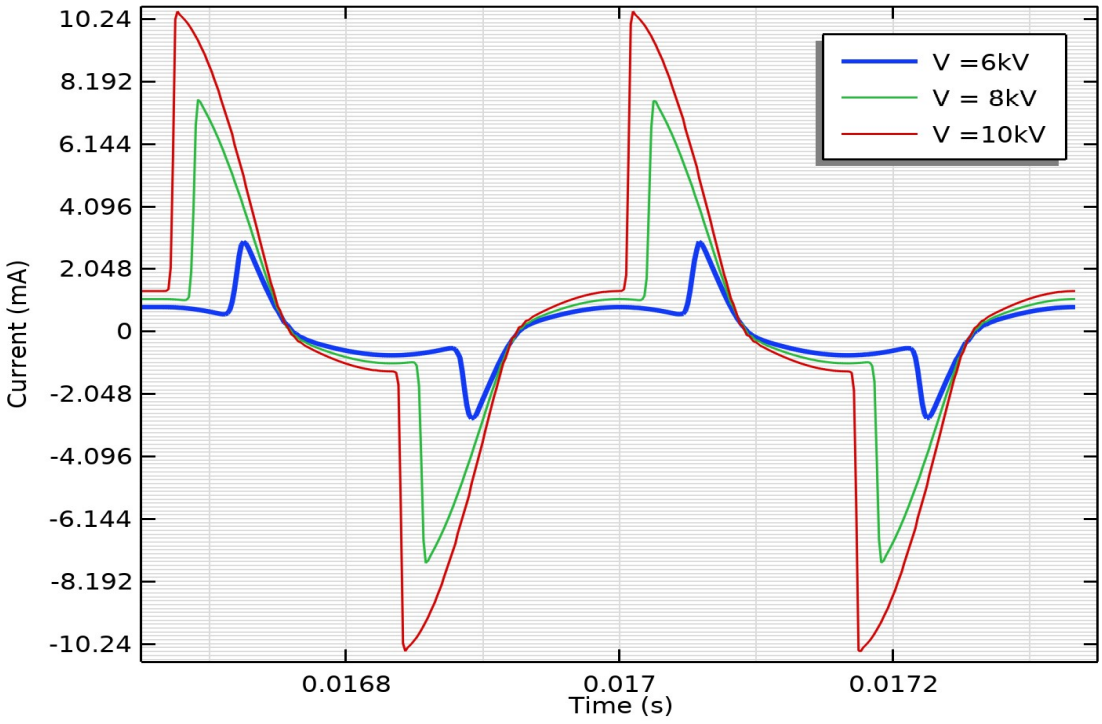

Fig. V-14: Applied voltage effect on discharge current

The effect of the applied voltage on ozone production is reported in figure V-15. The results clearly confirm that the concentration of ozone increases as the applied voltage increases.

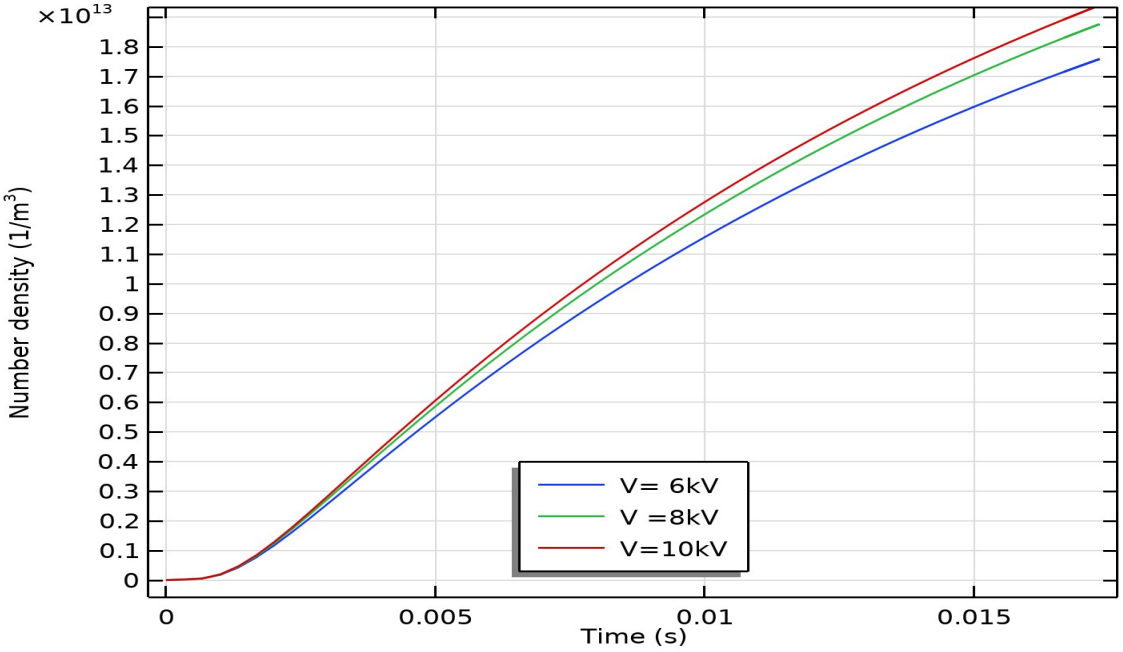

Fig. V-15: Applied voltage effect on ozone production

It should be noted that the rates of electron-impact reactions depend on the density and kinetic energy of the electrons in the discharge. However, the increase in electron density at high voltage induces a large dissociation of O_2 by electron impact and then the concentration of atomic oxygen will increase (see figure V-16) to contribute significantly to the generation of ozone.

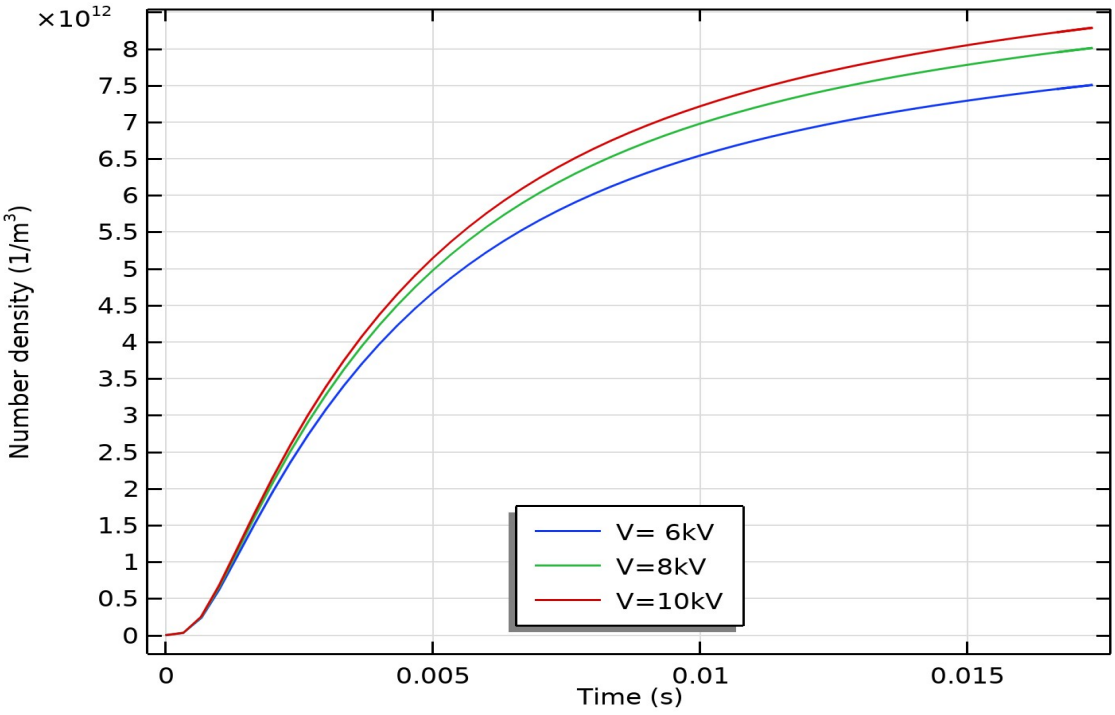

Fig. V-16: Applied voltage effect on density of oxygen Atomic

4. Conclusion:

In this chapter we have presented a numerical study of ozone generation in a gas mixture of 20% oxygen and 80% nitrogen (dry air) at atmospheric pressure. The calculations of this model are in agreement with the experimental and theoretical results available in the literature, the primary conclusion drawn in this thesis as follows.

- Firstly, compared with oxygen, electro-negative gas, nitrogen discharge is more likely to evolve into asymmetry discharge. This asymmetry is mainly reflected in the time interval of adjacent discharge current peak and peak value of discharge current. This phenomenon could be attributed to different surface charge accumulated on the dielectric barriers, which delay the inverse of built-in electrical field.
- Furthermore, in different position of discharge gap at the maximal current of positive semi-period, the electrical field curve of nitrogen differs from oxygen clearly. In nitrogen discharge, there is a knee-point in the electrical field curve, where electrical field remains a certain value before and increases linearly after. Whereas, the electrical field curve of oxygen discharge presents a shape of letter V, meaning there is a minimum point of electrical field inside the discharge gap. According to this point, the discharge gap is divided into two regions in electronegative gas, owing to negative ions and positive ions uneven distribution in the gap. Therefore, the electrical field curve is selected to be the characteristic parameter for distinguishing electropositive or electronegative gas discharge.
- It is also found that the electronegative gas leads to greater electron density gradient, higher discharge power and less uniform discharge.

In this chapter we also presented a parametric study by changing the temperature and the applied voltage. The results obtained show the following points:

- The major negative ion in the discharge is O_2^- and the major positive ion in the discharge is O_2^+.
- Ozone production is efficient at low gas temperature.
- It is obvious that the concentration of ozone increases when the applied voltage increases.

Bibliography

J.Lowke, «Theory of electrical breakdown in air: the role of metastable oxygen,» *J. Phys. D: Appl. Phys 25,* pp. 202-210, (1992).

R. Morrow, «The theory of positive glow corona,» *J. Phys. D: Appl. Phys., 30, ,* pp. 3099,3114, (1997).

F. P. Degond, «Asymptotic analysis of simple ionisation kinetics of air flows at atmospheric pressure,» *J. Phys. D : Appl. Phys., 38,* pp. 1371-1382, 2005.

Yanallah K, «Numerical modeling of ozone production in direct current corona discharge,» *Journal of Molecular Structure: THEOCHEM,Volume 777, Issues 1–3,* pp. 125-129, 2006.

Milan Šimek, «Efficiency of ozone production by pulsed positive corona discharge in synthetic air,» *J.Phys. D: Appl.Phys.35 ,* pp. 1171-1175, 2002.

Tsai H, «Numerical Simulation of Downstream Kinetics of an Atmospheric-Pressure Nitrogen Plasma Jet.,» *IEEE Transactions on Plasma Science ,* 2010.

Prevosto L, «Modelling of an Atmospheric Pressure Nitrogen Glow Discharge Operating in High-Gas Temperature Regimes,» . *Plasma Chem Plasma Process ,* 2016.

Choi YH, «One-dimensional discharge simulation of nitrogen DBD atmospheric pressure plasma,» *Thin Solid Films ,* p. 506 – 507 , 2006; .

phelps, «SIGLO Database,» 14 february 2019. [En ligne]. Available: LXCat.net.

Bacri J, «Electron diatomic molecule weighted total cross section calculation,» *Physica ,* pp. 101-l 18, 1982.

Cheng KW, «Fluid Modeling of a Nitrogen Atmospheric-Pressure Planar Dielectric Barrier Discharge Driven by a Realistic Distorted Sinusoidal Alternating Current Power Source.,» *Japanese Journal of Applied Physics ,* 2012.

Lazarou C, «Numerical modeling of the effect of the level of nitrogen impurities in a helium parallele plate dielectric barrier discharge,» *Plasma Sources Sci. Technol 24 ,* p. 13, 2015.

Massines F, «Physics and chemistry in a glow dielectric barrier discharge at atmospheric pressure: diagnostics and modelling.,» *Surface and Coatings Technology,* p. 174 – 175, 2003.

Panousis E, «Numerical modelling of an atmospheric pressure dielectric barrier discharge in nitrogen: electrical and kinetic description.,» *J. Phys. D: Appl. Phys ,* p. 4168–4180, 2007.

Kossyi IA, «Kinetic scheme of the non-equilibrium discharge in nitrogen-oxygen mixtures.,» *Plasma Sources Sci. Technol 1,* pp. 207-220, 1992.

C. C. Pignolett, «Ozone Generation by Point to Plane Corona Discharge,» *J. Phys.D: Appl. Phys. 23(8),* p. 1069–1072, 1990.

B. Elliasson, «Ozone Synthesis From Oxygen In Dielectric Barrier Discharges,» *J Phys. D: Appl.Phys.,* 1987.

M. CAPITELLI, «Plasma Kinetics in Atmospheric Gases,» *Springer,* 2000.

Y. MIROKIN, «The NIST Chemical Kinetics Database-Version 2q98,» 1998.

General Conclusion

General Conclusion

Non-thermal plasma technologies at atmospheric pressure have shown their effectiveness in fields as varied as pollution control, surface treatment, sterilization and ozone production. These technologies can provide simple and robust solutions for the implementation of innovative processes.

In the first chapter, we made some reminders on electric discharge and cold plasmas out of thermal equilibrium. There are in particular reminders on dielectric barrier discharges and their physicochemical characteristics and industrial applications.

The second chapter a presentation of mathematical model used in this work has been made, and there is also an overview on the different models (kinetic, particulate, fluid and hybrid) to characterize the out-of-equilibrium discharges that interest us. We used the fluid model which describes the coupling between the phenomena of transport of charged particles, and the electric field. The interaction between charged particles and electrode is also considered. In a discharge at atmospheric pressure the breakdown and ensured by the electrons, accelerated by the electric field of the cladding, ionize the gas and deposit their energy (ionization, excitation) in the plasma of the negative glow. Also, in this chapter we define model's geometry and the simulation conditions.

In the third chapter, characteristics of pure nitrogen discharges at atmospheric pressure are simulated theoretically. Simulation results show that the discharge structure in nitrogen DBD atmospheric pressure plasma has the characteristics similar to the Townsend discharge. The discharge behaviors are studied by varying external parameters such as the amplitude and frequency of external voltages, and properties of dielectric barrier materials. Higher plasma densities can be obtained by increasing both amplitude and frequency of the applied voltage with available power generator as long as arcing and dielectric barrier problems are avoided.

The developed model of DBD in with pure oxygen has been successfully simulated using physicochemical model that include both neutral and charged species. This simulation has allowed us to elucidate the role played by the excited molecule $O_2(^1\sum_g^+)$ and the interplay between charged and neutral species. The results of this model showed that the interaction between charged and neutral species occurs mainly via the electron density distribution, since most of neutral species are strongly correlated with the electrons. The increase of the electric field shifts the electron density distribution towards the anode, and this modification is then

translated to the spatial distribution of neutrals. However, since ozone distribution is nearly constant, it is very little affected by this change.

Chapter five present a comparison between DBD in nitrogen and DBD in oxygen as a first part of this chapter. The results showed that compared with nitrogen, the discharge current in oxygen displayed more symmetric waveform, which indicated simultaneous existence of positive ions and negative ions owing to the gas electronegativity. And at the maximal discharge current, there is obvious minimum point of electrical field curve in oxygen discharge, owing to the density difference of positive and negative ions at different position of discharge gap. It also proves that the gas electronegative could lead to greater electron density gradients, higher discharge power and less uniform discharge. The electrical field curve at the moment of maximal current is selected as the characteristic parameter to distinguish gas property, electro-positivity or electro-negativity gas. The electrical field appear a minimum point in discharge gap, presented the shape of letter V, in electronegative gas discharge. According the mentioned characteristic curve, it is useful to determine the electronegativity of working gas.

The second part presents a model which allowed us to study the production of ozone in a dielectric barrier discharge for plasma of the N_2/ O_2 mixture at atmospheric pressure. Based on several pieces of research, the full set of processes considered is grouped into 286 reactions involving 38 atomic and molecular species. The results obtained allow us to see the temporal evolution of the electrical parameters (electric current, electronic current and total ionic current) and kinetics (densities of ionized and excited particles).

In the third part of our work, we approached a parametric study of a dielectric barrier discharge for the contribution to the improvement of ozone production. When the voltage applied in the discharge is increased, the gas takes less time to become a conductor, so it bursts quickly and the value of the power dissipated by the electrons in the discharge gap increases, this has a great effect on the creation of the metastable.

We observed in this study the influence of gas heating and the inhomogeneity of the electronic pre-ionization density on the spatiotemporal evolution of ozone and NOx in the gas mixture 20% O_2 – 80% N_2 in a DBD discharge of plane - plane geometry.

From the results obtained it was found that:

- The electrical characteristics of the discharge can be influenced by the temperature of the gas and obviously by the voltage applied.
- Ozone production is effective at ambient temperature 300 k.